NASA MEMO 6-5-59A

NASA

MEMORANDUM

WIND-TUNNEL INVESTIGATION AT SUBSONIC AND SUPERSONIC SPEEDS OF THE STATIC AND DYNAMIC STABILITY DERIVATIVES OF AN AIRPLANE MODEL WITH AN UNSWEPT WING AND A HIGH HORIZONTAL TAIL

By Henry C. Lessing and James K. Butler

Ames Research Center
Moffett Field, Calif.

Declassified July 17, 1962

June 1959

NATIONAL AERONAUTICS AND SPACE ADMINISTRATION

MEMORANDUM 6-5-59A

WIND-TUNNEL INVESTIGATION AT SUBSONIC AND SUPERSONIC SPEEDS OF THE STATIC AND DYNAMIC STABILITY DERIVATIVES OF AN AIRPLANE MODEL WITH AN UNSWEPT WING AND A HIGH HORIZONTAL TAIL

By Henry C. Lessing and James K. Butler

SUMMARY

Results are presented of a wind-tunnel investigation to evaluate the static and dynamic stability derivatives of a model with a low-aspect-ratio unswept wing and a high horizontal tail. In addition to results for the complete model, results were also obtained of the body alone, body and wing, and body and tail. Data were obtained in the Mach number range from 0.65 to 2.2, at a Reynolds number of 2 million based on the wing mean aerodynamic chord. The angle-of-attack range for most of the data was -11.5° to 18°. A limited amount of data was obtained with fixed transition.

A correspondence between the damping in pitch and the static stability, previously noted in other investigations, was also observed in the present results. The effect observed was that a decrease (or increase) in the static stability was accompanied by an increase (or decrease) in the damping in pitch. A similar correspondence was observed between the damping in yaw and the static-directional stability.

Results from similar tests of the same model configuration in two other facilities over different speed ranges are presented for comparison. It was found that most of the results from the three investigations correlated reasonably well.

Estimates of the rotary derivatives were made using available procedures. Comparison with the experimental results indicates the need for development of more precise estimation procedures.

INTRODUCTION

The field of dynamic stability of aircraft has in recent years become one of major importance. Advances in the fields of propulsion, structure, and aerodynamics have each lead to such a reduction in dynamic stability that, at least for highly maneuverable types of aircraft, the dynamic stability of the configuration must be considered in the design from its inception.

In keeping with the growing importance of this field, added emphasis has been put on theoretical and experimental methods for obtaining those quantities which determine the principal aerodynamic contribution to the stability of an aircraft, the dynamic stability derivatives. Exact solutions for most dynamic stability derivatives are extremely difficult to obtain, primarily because of the complicated interference effects between the various components of a given configuration. For this reason experimental results and empirical estimation procedures provide the major source of dynamic stability derivatives for new configurations. At the Ames Research Center, equipment now exists for measuring the dynamic stability derivatives in several wind tunnels whose combined speed range provides effectively a continuous Mach number spectrum from 0.25 to 3.5 inclusive.

References 1 and 2 present results of such investigations for the configuration of the present report in the Mach number ranges 0.25 to 0.94 and 2.5 to 3.5. The purpose of the present investigation was to obtain data in the Mach number range between these two sets of results to determine the degree of correlation of data obtained in the various facilities, to compare the experimental results with available estimation procedures, and to contribute to the store of experimental results which must be assembled if more accurate empirical estimation procedures are to be developed in the future.

NOTATION

Definitions of the symbols used in the report are as follows. Symbols used only in the appendix are defined in the appendix.

A wing aspect ratio, $\frac{b^2}{S}$

b wing span

$\bar{c}$ wing mean aerodynamic chord

C_1 distance from body nose to oscillation axis

C_D drag coefficient, $\frac{\text{drag}}{\frac{1}{2}\rho V^2 S}$

C_L lift coefficient, $\frac{\text{lift}}{\frac{1}{2}\rho V^2 S}$

C_l rolling-moment coefficient, $\frac{\text{rolling moment}}{\frac{1}{2}\rho V^2 S b}$

C_m pitching-moment coefficient, $\frac{\text{pitching moment}}{\frac{1}{2}\rho V^2 S \bar{c}}$

C_N normal-force coefficient, $\frac{\text{normal force}}{\frac{1}{2}\rho V^2 S}$

C_n yawing-moment coefficient, $\frac{\text{yawing moment}}{\frac{1}{2}\rho V^2 S b}$

C_Y side-force coefficient, $\frac{\text{side force}}{\frac{1}{2}\rho V^2 S}$

$C_{m_\delta}, C_{m_\alpha}, C_{N_\alpha}, C_{l_\beta}, C_{n_\beta}, C_{y_\beta}$ derivatives with respect to subscript

$C_{N_q}, C_{N_{\dot{\alpha}}}, C_{m_q}, C_{m_{\dot{\alpha}}}$ derivatives with respect to $\frac{\bar{c}}{2V} \times$ subscript

$C_{l_r}, C_{l_{\dot{\beta}}}, C_{l_p}, C_{n_r}, C_{n_{\dot{\beta}}}, C_{n_p}, C_{y_r}, C_{y_{\dot{\beta}}}$ derivatives with respect to $\frac{b}{2V} \times$ subscript

f oscillation frequency, cycles per unit time

l body length

l_H horizontal-tail length

l_V vertical-tail length

M Mach number

p rolling velocity

q pitching velocity

R Reynolds number

r yawing velocity

S wing area

S_b body cross-sectional area at base

S_m mean cross-sectional area of body

V velocity

X_O distance from wing apex to moment center, positive for moment center behind wing apex

Z_V height of center of pressure of vertical tail above x axis

α angle of attack, radians unless noted otherwise

β angle of sideslip, radians unless noted otherwise

Γ dihedral angle, positive for tip chord above root chord, deg

δ horizontal-tail deflection, deg

ϵ effective angle of downwash at horizontal tail, radians unless otherwise noted

Λ wing leading-edge-sweep angle, positive for sweepback, deg

λ wing taper ratio, $\frac{\text{tip chord}}{\text{root chord}}$

ρ air density

σ effective angle of sidewash at vertical tail, positive for velocity component along negative Y axis, radians unless otherwise noted

ω circular frequency of oscillation, $2\pi f$, radians per unit time

$(\dot{})$ $\frac{d(\ )}{dt}$

Subscripts attached to a coefficient in parentheses indicate the contribution to that coefficient by the component indicated, as follows:

B body

W wing

H horizontal tail

V vertical tail

MODEL AND APPARATUS

Description of Model

The sting-mounted model was geometrically similar to the one used in the investigation reported in references 1 and 2, and consisted of an unswept wing of aspect ratio 2.44, a horizontal tail mounted in a high position on a vertical tail, and a body with a circular cross section modified by the addition of a canopy and protuberances simulating side inlets. A photograph and a dimensional sketch of the model are shown in figures 1 and 2. The airfoil sections for the wing, vertical tail, and horizontal tail were elliptical over the forward 50 percent of the chord and biconvex over the rear 50 percent. The forward 2.5 percent of the elliptical wing cross section was modified to form a sharp leading edge. Thickness ratio of the wing was 3.4 percent, of the horizontal tail 5 percent, and of the vertical tail 5 percent at the root tapering to 3.4 percent at the tip.

Except for the brackets which attached the horizontal tail to the vertical tail, the entire model was constructed of magnesium. The brackets were made of aluminum, and provided a range of tail deflections from $+6^{\circ}$ to -16° in approximately 2° increments.

In some tests the location of boundary-layer transition was fixed by means of 0.010-inch-diameter wire at the 10-percent chord of the wing and horizontal tail, and circling the body 2 inches from the nose. The wire size was selected on the basis of the results of reference 3.

Static tests were made with a 2-1/2-inch-diameter, six-component, strain-gage balance. Dynamic oscillatory tests were made with balances similar to those described in reference 4. The principal differences between the balances used in the present investigation and those described in the above reference were:

(1) A reduction in diameter from 4 inches to 2-1/2 inches.

(2) The addition of the rolling-moment gage on the inclined axis balance for the purpose of measuring the rolling moment in phase with angular velocity.

(3) The use of the accelerometers which were used to cancel electrically the output of the rolling-moment gages due to products and moments of inertia. Pictures of the dynamic balances are shown in figure 3. The oscillation axis of the disassembled balance is normal to its longitudinal axis, and the oscillation axis of the other balance is inclined at 45° to its longitudinal axis.

Test Facility

This investigation was conducted in the Ames 6- by 6-foot supersonic wind tunnel which is a closed-circuit variable-pressure type with a Mach number range continuously variable from 0.65 to 2.22. The test section has a perforated floor and ceiling and a boundary-layer-removal system to enable uniform flow to be maintained at transonic and low supersonic speeds.

TEST AND PROCEDURES

Range of Test Variables

Mach numbers of 0.65, 0.90, 0.94, 1.00, 1.10, 1.30, 1.50, 1.70, 1.90, and 2.20 were covered in the investigation. The test Reynolds number based on the mean aerodynamic chord was 2 million.

For the static tests the angle-of-attack range was from -6° to 21°; the deflection of the horizontal tail was 0.1° for tests made throughout the range. For the dynamic tests, it was necessary that the pitching moment be small in order that the balance not deflect under static loads and prevent oscillation of the model. Hence, for dynamic tests of the complete configuration, the deflection of the horizontal tail was varied in the range from -11.8° to 4.1° and tests were made at the angle of attack where the static pitching moment was approximately zero for each tail deflection. The angle of attack was always within the range from -11.5° to 18°. For the body-tail configuration, the tail deflection

was fixed at 0.1° and data were obtained only at one angle of attack at each Mach number. The various tail deflections and corresponding angles of attack used during dynamic tests of the complete configuration were also investigation during static tests of the complete configuration to permit comparison of the data obtained by the two techniques.

The oscillation amplitude of the dynamic test was 1.5°. The oscillation frequency varied from 8 to 12 cycles per second, depending on the moments of inertia and the aerodynamic restoring moments of the various configurations. The reduced frequency $\omega\bar{c}/2V$ varied from 0.008 to 0.03. The center of oscillation was at a point corresponding to either 25 or 35 percent of the wing mean aerodynamic chord, the major portion of the investigation being conducted at the forward location.

Reduction of Data

The methods and instrumentation used in obtaining the forces and moments from the oscillation measurements of the balance during the dynamic tests are completely described in reference 4. All force and moment coefficients were reduced to standard form as defined in the Notation. The two force coefficients, C_L and C_D, are referred to the wind system of axes and the remaining coefficients are referred to the body system of axes shown in figure 4. For both systems, the origin is at the center of moments at a point on the fuselage reference line corresponding to 25 percent of the wing mean aerodynamic chord.

Factors which may affect the accuracy of the wind-tunnel results and corrections made thereto in reducing these results to the coefficients presented herein are discussed below.

Stream variations.- Surveys of the stream characteristics of the Ames 6- by 6-foot supersonic wind tunnel showed that in the region of the test section, stream curvature was negligible and axial static-pressure variations were usually less than ±1 percent of the dynamic pressure. This static-pressure variation resulted in negligible longitudinal-buoyancy corrections to the drag. Therefore, no corrections for stream curvature or static-pressure variation were made in the present investigation.

From tests of various models in the normal and inverted attitudes, the stream angle in the pitch plane was found to be less than ±0.3° throughout the Mach number range, and no corrections to the data were made for these angles.

Support interference.- The effects of model support interference on the aerodynamic characteristics obtained during the static tests were considered to consist primarily of a change in the pressure at the base of the model. However, the drag data presented herein contain no base

drag component since the base pressure was measured and the drag adjusted to correspond to that in which the base pressure was equal to the free-stream static pressure. Therefore no corrections were made to take into account support interference on the static test data.

Another aspect of what might be termed support interference, which must be considered for the dynamic tests, is translation of the model center of oscillation due to operation close to the support resonance frequency. In general, such a coupling of model and support causes an apparent change in both the static aerodynamic restoring moments and the damping of the model. In anticipation of this difficulty, the dynamic apparatus was provided with a variable-length sting. A series of tests was made with systematically varied sting lengths from the one extreme of sting length sufficiently long that the support resonant frequency was close to model oscillation frequency, to the other extreme of sting length so short that support aerodynamic interference was excessive. Examination of these data enabled a sting length to be chosen such that both coupling and aerodynamic interference effects were reduced to acceptable values.

Tunnel-wall interference.- The effectiveness of the perforations in the wind-tunnel test section in preventing choking and absorbing disturbances at transonic and low supersonic speeds has been established experimentally. Unpublished data from the wind-tunnel calibrations indicate that reliable static data can be obtained throughout the Mach number range if certain restrictions are imposed on model size and attitude. The configurations and method of testing used in the present investigation conform to these restrictions so that static data obtained at transonic and low supersonic speeds are reasonably free of interference effects.

Tunnel-wall interference effects on the dynamic data are very difficult to determine. As discussed in reference 5, aerodynamic resonance can very strongly influence the results of a two-dimensional wing oscillating in a tunnel with solid walls. However, because of the three-dimensional nature of the present investigation plus the disturbance-absorbing characteristics of the tunnel-wall perforations mentioned above, it is believed that tunnel resonance effects were negligible, and no corrections to the data were made.

Internal damping of oscillation mechanism.- The damping measured by the oscillation apparatus was the sum of the aerodynamic damping of the model and the internal damping of the oscillation mechanism. Although the internal damping was always a very small quantity, its value was determined prior to each run by oscillating the model in still air with the tunnel evacuated and subtracting this value from the measured damping under test conditions.

EXPERIMENTAL RESULTS

All moment data from the static test and all force and moment data from the dynamic test are presented for a center of moments and center of oscillation corresponding to 25 percent of the mean aerodynamic chord.

Longitudinal Test Results

Static test results of angle of attack, pitching-moment coefficient, and drag coefficient are shown as a function of lift coefficient in figure 5 for each of the configurations tested. Additional data not shown in the figure were obtained for the complete configuration for a range of horizontal-tail deflection angles from $+4.1^\circ$ to -15.8°. These data were obtained for a limited range of lift coefficients near trim for each tail deflection for purposes of comparison with the data at trim conditions obtained during the dynamic tests and to calculate the downwash angle at the horizontal tail and the horizontal-tail effectiveness.

The rate of change of effective downwash angle, $d\epsilon/d\alpha$, at the horizontal tail on the complete configuration is shown in figure 6, together with the horizontal-tail effectiveness parameter C_{m_δ}. The values shown are approximate because of the limited amount of data obtained for the various tail deflections. The values of C_{m_δ} were computed by dividing the tail deflection into the pitching-moment increment trimmed by that deflection; that is,

$$C_{m_\delta} = \left\{ \frac{\left[(C_m)_{BWVH} \right]_{\delta = 0.1}}{\delta_{trim} - 0.1} \right\}_{\alpha_{trim}} \tag{1}$$

Results indicated C_{m_δ} to be independent of angle of attack. The values of ϵ were obtained as follows: The pitching-moment contribution of the horizontal tail on the complete configuration is

$$(C_m)_H = (C_m)_{BWVH} - (C_m)_{BW} = C_{m_\delta}(\alpha - \epsilon + \delta)$$

in which it is assumed that the contribution of the vertical tail is negligible. When

$$(C_m)_{BW} = (C_m)_{BWVH}$$

then

$$(C_m)_H = 0$$

and

$$\epsilon = \alpha + \delta \tag{2}$$

At trim

$$(C_m)_{BWVH} = 0$$

so that

$$(C_m)_H = -(C_m)_{BW}$$

and

$$\epsilon = \alpha + \delta + \frac{(C_m)_{BW}}{C_{m_\delta}} \tag{3}$$

Because of the approximate nature of the tail effectiveness, C_{m_δ}, the average downwash angles computed by means of equation (3) were also approximate. Wherever possible, the true average downwash angle given by equation (2) was computed, and comparison of results from the two equations showed good agreement. The available data generally restricted the use of equation (2) to the lower angles of attack, and the high angle of attack results of figure 6 were therefore obtained primarily from equation (3).

The slope of the pitching-moment curve, C_{m_α}, obtained from both the static and dynamic tests and the damping-in-pitch parameter $C_{m_q} + C_{m_{\dot{\alpha}}}$ are shown in figure 7 as a function of angle of attack and in figures 8 and 9 as a function of Mach number. The static and dynamic data are for conditions at or near trim because of the previously mentioned restrictions imposed by the oscillation technique.

The static force derivative, C_{N_α}, obtained from the dynamic tests and the dynamic force derivative, $C_{N_q} + C_{N_{\dot{\alpha}}}$, are shown for the complete configuration in figure 10. The derivative C_{N_α} was obtained by means of the transformation equation (A3) given in the appendix and the data obtained at oscillation centers at both 25 and 35 percent of the mean

aerodynamic chord. Data obtained at both oscillation centers together with equations (A2) and (A4) were used to compute $C_{N_q} + C_{N_{\dot{\alpha}}}$. These latter data may be combined in equation (A4) with the data of previous figures to compute the damping in pitch about any arbitrary center-of-gravity position.

Lateral Test Results

The static lateral-directional derivatives, C_{l_β}, C_{n_β}, C_{Y_β}, obtained from the static and dynamic tests are presented in figure 11 as a function of angle of attack. The data for the complete configuration at zero angle of attack are plotted as a function of Mach number in figure 12. The derivatives obtained from the static test are approximate in that they were computed as the coefficients at a constant sideslip angle divided by the sideslip angle. The sideslip angle was chosen to be 1° in order to eliminate as much as possible the effect of any nonlinearity of the coefficient with angle of sideslip, and thus to obtain derivatives comparable with those obtained from the dynamic test which was run at 1.5° amplitude. The dynamic test values of C_{Y_β} for the complete configuration were obtained from results at oscillation centers at both 25- and 35-percent mean aerodynamic chord using equation (A7) of the appendix.

The yawing-velocity derivatives, $C_{l_r} - C_{l_{\dot{\beta}}} \cos \alpha$ and $C_{n_r} - C_{n_{\dot{\beta}}} \cos \alpha$, are presented as a function of angle of attack in figure 13 for each of the configurations tested. These data for the complete configuration at zero angle of attack are presented as a function of Mach number in figure 14. Equations (A6) and (A8) of the appendix were applied to the damping in yaw obtained for the complete configuration oscillated at the 25- and 35-percent mean aerodynamic chord in order to compute the derivative $C_{Y_r} - C_{Y_{\dot{\beta}}} \cos \alpha$ shown in figures 13 and 14.

The rolling-velocity derivatives, $C_{l_p} + C_{l_{\dot{\beta}}} \sin \alpha$ and $C_{n_p} + C_{n_{\dot{\beta}}} \sin \alpha$, are presented as a function of Mach number for the complete configuration at zero angle of attack in figure 15. It was found that these derivatives were sensitive to the support vibration mentioned earlier, and were more affected by support aerodynamic interference for a given sting length than the longitudinal derivatives. In an attempt to eliminate these difficulties, the data shown in figure 15 were obtained by oscillating the model in the maximum stiffness plane of the support on a sting sufficiently long to eliminate aerodynamic interference; for these tests only, therefore, the model was oriented so that the wing was in the vertical plane.

ESTIMATES OF ROTARY STABILITY DERIVATIVES

The rotary derivatives were estimated by available estimation procedures where possible. For those quantities for which no published theory or estimate was available, estimates were derived.

Longitudinal Stability Derivatives

Estimate of $C_{m_q} + C_{m_{\dot{\alpha}}}$.- The damping in pitch of a body of high fineness ratio is given by slender-body theory (see, e.g., ref. 6) as

$$(C_{m_q} + C_{m_{\dot{\alpha}}})_B = - \frac{4S_b}{S\bar{c}^2} (l - c_1)^2 \tag{4}$$

The damping contributions of the wing at subsonic speeds were estimated from the following equation given in reference 1.

$$(C_{m_q})_W = - \frac{9\pi}{32} \frac{1 + \lambda^2}{[1+\lambda-(\lambda/1+\lambda)]^2} \frac{1}{\sqrt{1-M^2}} \tag{5}$$

At supersonic speeds the damping contribution was estimated from the expression for a rectangular wing given in reference 7 which, for a center-of-gravity position of 25-percent chord, becomes

$$(C_{m_q} + C_{m_{\dot{\alpha}}})_W = - \frac{7}{6\sqrt{M^2-1}} + \frac{1}{4A(M^2-1)} + \frac{5}{3(M^2-1)^{3/2}} - \frac{2(M^2+1)}{3A(M^2-1)^2} \tag{6}$$

This equation is valid for $A\sqrt{M^2-1} \geq 1$.

The damping in pitch of the horizontal tail was calculated from the expression (ref. 8)

$$(C_{m_q} + C_{m_{\dot{\alpha}}})_H = (2l_H/\bar{c})[1+(d\epsilon/d\alpha)]C_{m_\delta} \tag{7}$$

The horizontal-tail contribution to the damping in pitch of the complete configuration was estimated using the values of $d\epsilon/d\alpha$ and C_{m_δ} from figure 6. The tail contribution to the damping in pitch of the body-tail combination was estimated on the assumption that $d\epsilon/d\alpha$ was zero for this configuration at small angles of attack. The values of C_{m_δ} used in the estimate were again obtained from figure 6.

Estimate of $C_{N_q} + C_{N_{\dot{\alpha}}}$.- The normal force due to pitching velocity given by slender-body theory is (see, e.g., ref. 6)

$$(C_{N_q} + C_{N_{\dot{\alpha}}})_B = (4/S\bar{c})[(l-C_1)S_b+lS_m] \tag{8}$$

The normal-force contribution for a rectangular wing at supersonic speeds due to pitching about the quarter chord can be obtained from reference 7.

$$(C_{N_q} + C_{N_{\dot{\alpha}}})_W = \frac{2}{M^2-1} - \frac{1}{3A(M^2-1)} - \frac{4}{(M^2-1)^{3/2}} + \frac{2(M^2+1)}{3A(M^2-1)^2} \tag{9}$$

The horizontal-tail contribution to the normal force is

$$(C_{N_q} + C_{N_{\dot{\alpha}}})_H = -2[1+(d\epsilon/d\alpha)]C_{m_\delta} \tag{10}$$

Lateral Stability Derivatives

Estimate of $C_{l_r} - C_{l_{\dot{\beta}}} \cos \alpha$.- No exact theory exists for the rolling moment due to yawing velocity for a wing. Estimation procedures have been published (see, e.g., ref. 9) but none appear to be applicable at all speeds. An estimate was therefore developed, based on a strip theory assuming an elliptical span load distribution, which takes into account wing sweep, dihedral, oscillation-center position, and variation of angle of attack and dynamic pressure across the span, but neglects the effect of spanwise Mach number variations. The estimate was developed in such a manner that static test data could be incorporated. The resulting expression is, for a given angle of attack,

$$(C_{l_r})_W = \left(\frac{32e+3\pi bh}{24\pi bg}\right)(C_{N_\alpha})_W + \frac{(C_N)_W}{4} \tag{11}$$

where

e $\alpha \cos \Gamma - \sin \Lambda \sin \Gamma$

h $X_o \cos \Lambda \sin \Gamma$

g $\alpha^2(\cos^2\Gamma - \cos^2\Lambda) + \cos^2\Lambda$

The contribution of the vertical tail to the yawing velocity derivatives was estimated in a manner similar to that for the contribution of the horizontal tail to the pitching derivatives. If it is assumed that

for the angle-of-attack range of interest $\cos \alpha = 1$, the vertical-tail contribution to the rolling moment due to yawing velocity is

$$(C_{l_r} - C_{l_{\dot{\beta}}} \cos \alpha)_V = -2(Z_V/b)(l_V/b)[1-(d\sigma/d\beta)](C_{Y_\beta})_V \tag{12}$$

where $(C_{Y_\beta})_V$ is the static stability contribution of vertical tail in the absence of sidewash. It was assumed that

$$\frac{Z_V}{b} = \left[\frac{(C_{l_\beta})_V}{(C_{Y_\beta})_V}\right]_{\alpha=0}, \quad \frac{l_V}{b} = -\left[\frac{(C_{n_\beta})_V}{(C_{Y_\beta})_V}\right]_{\alpha=0}, \quad \frac{d\sigma}{d\beta} = \frac{\left[(C_{n_\beta})_V\right]_{\alpha=\alpha}}{\left[(C_{n_\beta})_V\right]_{\alpha=0}} - 1$$

which is equivalent to assuming a center of pressure independent of angle of attack, and that any apparent decrease in tail effectiveness is due to sidewash. With these assumptions equation (12) becomes

$$(C_{l_r} - C_{l_{\dot{\beta}}} \cos \alpha)_V = 2\left[\frac{(C_{l_\beta})_V}{(C_{Y_\beta})_V}\right]_{\alpha=0} \left\{2\left[(C_{n_\beta})_V\right]_{\alpha=0} - \left[(C_{n_\beta})_V\right]_{\alpha=\alpha}\right\} \tag{13}$$

The static derivatives for the vertical tail were obtained from static test results as the increment of derivative due to adding the vertical and horizontal tails to the body-wing configuration. Although the horizontal-tail contribution to $C_{l_r} - C_{l_{\dot{\beta}}} \cos \alpha$ was not accounted for explicitly, its effect is included in equation (13) in the static derivatives.

Estimate of $C_{n_r} - C_{n_{\dot{\beta}}} \cos \alpha$.- The contribution of the body to the damping in yaw was assumed to be

$$(C_{n_r} - C_{n_{\dot{\beta}}} \cos \alpha)_B = (C_{m_q} + C_{m_{\dot{\alpha}}})_B(\bar{c}/b)^2 \tag{14}$$

The yaw damping of the vertical tail was estimated in the same manner as the pitch damping of the horizontal tail. If the same assumptions noted in the estimate for $(C_{l_r} - C_{l_{\dot{\beta}}} \cos \alpha)_V$ are used, the damping of the tail is

$$(C_{n_r} - C_{n_{\dot{\beta}}} \cos \alpha)_V = 2\left[\frac{(C_{n_\beta})_V}{(C_{Y_\beta})_V}\right]_{\alpha=0} \left\{2\left[(C_{n_\beta})_V\right]_{\alpha=0} - \left[(C_{n_\beta})_V\right]_{\alpha=\alpha}\right\} \tag{15}$$

The damping contribution of the wing was estimated and found to be negligible.

Estimate of $C_{Y_r} - C_{Y_{\dot{\beta}}} \cos \alpha$.- The body contribution to the side force due to yawing velocity was assumed to be

$$(C_{Y_r} - C_{Y_{\dot{\beta}}} \cos \alpha)_B = (C_{N_q} + C_{N_{\dot{\alpha}}})_B(\bar{c}/b) \tag{16}$$

The tail contribution was computed using the same assumptions used for other yawing derivatives.

$$(C_{Y_r} - C_{Y_{\dot{\beta}}} \cos \alpha)_V = 2\left\{2\left[(C_{n_\beta})_V\right]_{\alpha=0} - \left[(C_{n_\beta})_V\right]_{\alpha=\alpha}\right\} \tag{17}$$

Estimate of $C_{l_p} + C_{l_{\dot{\beta}}} \sin \alpha$, $C_{n_p} + C_{n_{\dot{\beta}}} \sin \alpha$.- The theoretical incompressible-flow results of reference 10 were used to estimate the damping in roll due to the wing at subsonic speeds. Static test data extrapolated to zero Mach number for the body-wing configuration were used to form the compressibility correction

$$\left[(C_{l_p})_W\right]_{M=M} = \left[(C_{l_p})_W\right]_{M=0} \frac{(C_{N_\alpha})_{M=M}}{(C_{N_\alpha})_{M=0}} \tag{18}$$

The linearized theory of reference 11 was used to compute the roll damping of the wing at supersonic speeds. Although the results of this reference are not valid for the present wing at a Mach number of 1.1, they were extrapolated to that Mach number in order to aid in fairing the estimated results.

Calculations based on the method of reference 12 indicated that, at least at low subsonic speeds, the damping contribution of the vertical tail was negligibly small as a result of the rolling flow caused by the wing. This was assumed to be the case at all Mach numbers. The roll damping of the horizontal tail can be considered to be the result of the effects of the rolling wing wake, the sideslip angle generated by placement of the tail high above the roll axis, and the damping-in-roll of the tail. The first two effects were assumed to cancel, and the roll-damping contribution of the horizontal tail was estimated by scaling the wing contribution according to the relative sizes of the wing and tail.

At zero angle of attack the wing and horizontal-tail contribution to $C_{n_p} + C_{n_{\dot{\beta}}} \sin \alpha$ was assumed to be zero. The vertical-tail contribution, due to the rolling wake of the wing, was again found to be negligibly small.

DISCUSSION

Longitudinal Results

Aerodynamic characteristics.- One of the more significant features of the static longitudinal characteristics was the loss in static stability of the complete configuration at the higher angles of attack throughout the Mach number range of the investigation and the reduction in stability at low angles of attack at the high Mach numbers (figs. 5 and 8). The loss in stability at high angles of attack was due to the increase in rate of change of downwash angle with angle of attack, $d\epsilon/d\alpha$, at the horizontal tail. This downwash characteristic, shown in figure 6, was caused primarily by the vortices generated by the fuselage. The powerful effect of the vortices on the downwash at the horizontal tail, and hence the lift of the tail, is shown in figure 5 by the sharp reversal in the static stability of the body-tail configuration in contrast to the relatively constant stability of the body alone at high angles of attack. That this effect persisted even in the presence of the wing is indicated by the correspondence between the angles of attack of the complete configuration and that of the body-tail at which static instability occurred. Loss of horizontal-tail lift due to stall would also produce the observed characteristics. However, the similarity of the wing and horizontal tail would tend to indicate similar stall characteristics, and it may be observed (fig. 5) that wing stall and loss of stability occurred at widely different angles of attack.

In contrast to the stability loss at high angles of attack resulting from the body-induced flow field, the reduction in stability at low angles of attack and Mach numbers of 1.9 and 2.2 was associated with wing-tail interference. At these conditions a substantial portion of the high horizontal tail was enveloped by a flow field bounded by Mach lines from the leading and trailing edges of the wing. In this region the value of $d\epsilon/d\alpha$ was large, theoretically unity, so that the stability contribution of the horizontal tail was small. With increasing angle of attack the horizontal tail moved below the wing-induced flow field, resulting in a reduction of $d\epsilon/d\alpha$ and an increase in stability. This effect, altered at the high angles of attack by the effect of the body vortices, is seen in figures 5 and 6.

The damping in pitch for the complete configuration was stabilizing throughout the Mach number range of the investigation and varied smoothly with angle of attack for Mach numbers below 0.90 and above 1.1 (fig. 7). In the transonic speed range, however, large variations in damping occurred through the angle-of-attack range. As noted previously in references 1, 13, and 14, there is a close correspondence between damping in pitch and the static stability, C_{m_α}, wherein an increase (or decrease) in damping accompanied a decrease (or increase) in static stability. This effect is particularly pronounced at transonic speeds.

The effect of fixing transition (flagged symbols, fig. 7) was not consistent at subsonic and transonic Mach numbers. At a Mach number of 1.3 and above, the effects were negligible.

Comparison of static and dynamic test results.- In addition to the rotary derivatives, some static derivatives were also obtained during the dynamic tests, enabling a comparison of these quantities to be made for the two different test conditions. The static stability derivative C_{m_α} presented in figure 7 from the static and dynamic tests in general agrees very well. The exception is at a Mach number of 1.0 where the data obtained dynamically deviated from those obtained in the static test in a manner which tended to smooth the erratic variations exhibited by the static test data. It is believed that support aerodynamic interference on the horizontal tail was the primary reason for the deviations. Because of the oscillating-lift force tending to excite vibrations of the support structure, it was necessary to use a much shorter sting length than for the static test, and some aerodynamic interference possibly existed throughout the transonic speed range.

The comparison of C_{N_α} from the static and dynamic tests (fig. 10) shows the greatest discrepancy at transonic speeds where, as mentioned previously, some aerodynamic support interference probably existed during the dynamic tests. Because of the manner in which it was obtained from the dynamic test data, this coefficient provides a sensitive indication of such interference. At a Mach number of 1.3 and above, the agreement with the static test data is good.

Comparison of experiment and estimate.- The estimated damping of the complete configuration as calculated herein is a function of angle of attack only through the experimentally determined variation of $d\epsilon/d\alpha$ shown in figure 6. At other than transonic speeds the estimate gave approximately the correct values and trends with angle of attack (fig. 7). At Mach numbers 0.90 through 1.1, however, since $d\epsilon/d\alpha$ was a smoothly varying function of angle of attack, the estimated values also varied smoothly, rather than following the erratic variations of the experimental results. The lack of agreement between estimate and experiment at transonic speeds appears to be due to the inadequacy of the damping estimate of the wing. That the erratic variations appear to be due to the wing is evidenced by the damping for the body-wing combination also shown in figure 7. Although the data for this configuration are rather limited, they are of sufficient extent to show damping variations of the same order of magnitude as for the complete configuration. A further inadequacy of the wing estimate is shown in the lower part of figure 9, which presents the damping in pitch of the various configurations as a function of Mach number. Whereas the linearized theory for the rectangular wing indicates an unstable trend as the Mach number decreases toward 1.0, the experimental results show increasingly stable damping. The same type of discrepancy was found in reference 15 for a wing of somewhat similar plan form for an

oscillation center at 35 percent of the mean aerodynamic chord, whereas results obtained at 20 percent of the mean aerodynamic chord followed the unstable trend indicated by the theory. At Mach numbers of 1.0 and 1.1, the estimated damping values for the complete configuration are the contributions only of the body and horizontal tail, because of the lack of a suitable wing estimate.

The suggestion was made in references 13 and 14 that the correspondence between the damping in pitch and the static stability could possibly be used as a basis for damping estimates. The correspondence between the contribution of the horizontal tail to the static stability and the damping in pitch is well known. Whereas the static stability contribution of the horizontal tail when written as

$$(C_{m_\alpha})_H = C_{m_\delta}[1-(d\epsilon/d\alpha)]$$

indicates a destabilizing effect of increasing downwash with increasing angle of attack, the damping-in-pitch contribution given by equation (7) indicates a stabilizing effect. The reason for the correspondence in the case of the wing is not so clear. A simple analysis presented in reference 15 led to the conclusion that a decrease in static stability should be accompanied by a decrease in damping. Although this conclusion appeared to explain some of the results of reference 15, it contradicts the observed effect in references 13, 14, and the present results. The phenomenon evidently is not a simple one, and more investigation must be carried out in order to use it as a means of estimation.

The variation of $C_{N_q} + C_{N_{\dot\alpha}}$ with Mach number is shown in figure 10. For this derivative the negative trend of the estimate as the Mach number approaches unity, as a result of linearized rectangular-wing theory, was borne out by the experimental results.

Correlation of data with those from other facilities.- The comparison of the static stability C_{m_α} and damping in pitch $C_{m_q} + C_{m_{\dot\alpha}}$ with data from references 1 and 2 (figs. 8 and 9) tends to show the greatest discrepancies at transonic speeds. The overall agreement between the data from the three facilities is good, however.

Lateral Results

Aerodynamic characteristics.- Except for radical variations of C_{l_β} and C_{n_β} at high angles of attack at Mach numbers of 0.90 and 0.94 (fig. 11), the static derivatives varied relatively smoothly with angle of attack. In the supersonic speed range, increasing angle of attack was generally accompanied by a reduction of directional stability. The

reduction of stability with angle of attack, coupled with the reduction of stability at low angles with increasing Mach number, resulted in directional instability of the complete configuration at Mach numbers of 1.9 and 2.2 at the higher angles of attack.

There was a tendency for the damping in yaw and the static directional stability of the complete configuration to be related in the same manner described earlier for the damping in pitch and the static longitudinal stability. This can be seen from a comparison of figures 11 and 13, although the absence of large fluctuations makes the correspondence less striking than for the longitudinal data.

Comparison of static and dynamic test results.- The agreement between the static and dynamic test data shown in figure 11 is fair. Some of the discrepancies between the static and dynamic test results can probably be attributed to inaccuracies in the static test data because of the small sideslip angle used. Aerodynamic support interference effects in the dynamic test data are believed to be negligible since they were obtained with the maximum sting length available. It is also possible that some sting vibration existed during these tests, although none was observed. At Mach numbers of 0.90 and 0.94 the extreme fluctuations noted in the static test data made it impossible to test dynamically the winged configurations at the higher angles of attack. The side-force derivative C_{Y_β}, which was computed from dynamic data obtained at two oscillation positions, agrees reasonably well with static test results. However, the scatter in some of these data indicate that the distance between oscillation centers should be greater in order to obtain more consistent results.

Comparison of experiment and estimate.- The experimental and estimated results are compared in figures 13, 14, and 15. Each of the estimates is deficient in one respect or another, and the indications are that the estimate of the tail contribution is the primary cause. The greatest discrepancies appear in the side-force derivative $C_{Y_r} - C_{Y_{\dot\beta}} \cos \alpha$ shown in figures 13 and 14, and in the yawing-moment derivatives $C_{n_p} + C_{n_{\dot\beta}} \sin \alpha$ shown in figure 15. In the case of the side-force derivative, the erratic variations with angle of attack make the accuracy of the data suspect. However, although the absolute values may be somewhat in error, the similarity between the variation of this derivative with Mach number (fig. 14) and that of $C_{N_q} + C_{N_{\dot\alpha}}$ shown in figure 10 indicates the trend of the data to be correct. The vertical tail provides the primary contribution to the side-force derivative, and the type of tail estimate commonly used is inadequate to predict the behavior exhibited by the experimental results. More sophisticated estimates utilizing wing theory are evidently needed.

The yawing-moment derivative $C_{n_p} + C_{n_{\dot{\beta}}} \sin \alpha$ (fig. 15) is also caused primarily by the vertical tail. In addition to the spanwise variation of angle of attack due to rolling, the vertical tail is also subjected to the flow field from the rolling wing, and up to the present time no estimate of these effects suitable throughout the speed range has been developed.

Correlation of data with those from other facilities.- Results of the present investigation and those of references 1 and 2 presented in figures 8 and 9 have shown good correlation. This is also true of the static derivatives compared in figure 12. In figure 14 the values of $C_{l_r} - C_{l_{\dot{\beta}}} \cos \alpha$ obtained in the present investigation varied relatively slowly with Mach number. This characteristic is confirmed also by the data of reference 1, whereas the data of reference 2 indicate a sizable change between a Mach number of 2.2 and 2.5, as well as a reversal in sign. The reason for such a change is not known. There may be some question as to the accuracy of the Mach number 2.5 data inasmuch as the Mach number 3.0 and 3.5 data of reference 2 appear to follow the trend of a gradually decreasing value of $C_{l_r} - C_{l_{\dot{\beta}}} \cos \alpha$ with increasing Mach number.

In figure 15 the comparison of $C_{l_p} + C_{l_{\dot{\beta}}} \sin \alpha$ with the data of references 1 and 2 is fair, although the trend of the present results at low Mach numbers appears less reasonable than the data of reference 1, and maintains too large a value at high Mach numbers to fair smoothly with the results of reference 2. The present results for $C_{n_p} + C_{n_{\dot{\beta}}} \sin \alpha$ show good agreement with those of reference 1 at a Mach number of 0.65 but depart considerably at transonic speeds, even though the trend of the data is the same. The comparison at high Mach numbers is very poor, the results of the present investigation and those of reference 2 exhibiting a similar trend with Mach number which, in conjunction with the opposite signs of the derivative at Mach numbers of 2.2 and 2.5, makes the two sets of data appear incompatible. It seems probable, since the maximum variation appears to be in the transonic and low supersonic speed ranges and small almost everywhere else, that the two data points in question are in error, and that above a Mach number of 1.5 the value of the derivative is essentially zero.

CONCLUSIONS

This report presents results of static and dynamic wind-tunnel measurements of a model with a low-aspect-ratio unswept wing and a high horizontal tail. The results of the investigation showed that:

1. A correspondence between the damping in pitch and the static stability, previously noted in other investigations, was also observed in the present results. The effect observed was that a decrease (or increase) in the static stability was accompanied by an increase (or decrease) in the damping in pitch. A similar correspondence was observed between the damping in yaw and the static-directional stability.

2. Comparison of estimated and experimental results in general showed inconsistent agreement, indicating the need to develop more precise estimation procedures.

3. Comparison of the data from the present investigation with similar results from investigations of the same model configuration in two other facilities in general showed good agreement.

Ames Research Center
National Aeronautics and Space Administration
Moffett Field, Calif., Mar. 12, 1959

APPENDIX

TRANSFORMATION OF STABILITY DERIVATIVES FROM ONE CENTER OF OSCILLATION TO ANOTHER

Oscillation center "1" is the axis about which the original derivatives were measured. They will be transferred to a new oscillation center "2" which is $\bar{x}$ feet forward of position "1."

Longitudinal

$$C_{N_{\alpha_2}} = C_{N_{\alpha_1}} \tag{A1}$$

$$(C_{N_q} + C_{N_{\dot{\alpha}}})_2 = (C_{N_q} + C_{N_{\dot{\alpha}}})_1 + C_{N_\alpha} \frac{2\bar{x}}{\bar{c}} \tag{A2}$$

$$C_{m_{\alpha_2}} = C_{m_{\alpha_1}} - C_{N_\alpha} \frac{\bar{x}}{\bar{c}} \tag{A3}$$

$$(C_{m_q} + C_{m_{\dot{\alpha}}})_2 = (C_{m_q} + C_{m_{\dot{\alpha}}})_1 - (C_{N_q} + C_{N_{\dot{\alpha}}})_1 \frac{\bar{x}}{\bar{c}} + C_{m_{\alpha_1}} \frac{2\bar{x}}{\bar{c}} - C_{N_\alpha} \frac{2(\bar{x})^2}{(\bar{c})^2} \tag{A4}$$

Lateral

$$C_{Y_{\beta_2}} = C_{Y_{\beta_1}} \tag{A5}$$

$$(C_{Y_r} - C_{Y_{\dot{\beta}}} \cos \alpha)_2 = (C_{Y_r} - C_{Y_{\dot{\beta}}} \cos \alpha)_1 - C_{Y_\beta} \frac{2\bar{x}}{b} \tag{A6}$$

$$C_{n_{\beta_2}} = C_{n_{\beta_1}} - C_{Y_\beta} \frac{\bar{x}}{b} \tag{A7}$$

$$(C_{n_r} - C_{n_{\dot{\beta}}} \cos \alpha)_2 = (C_{n_r} - C_{n_{\dot{\beta}}} \cos \alpha)_1 - (C_{Y_r} - C_{Y_{\dot{\beta}}} \cos \alpha)_1 \frac{\bar{x}}{b} - C_{n_{\beta_1}} \frac{2\bar{x}}{b} + C_{Y_\beta} \frac{2(\bar{x})^2}{b} \tag{A8}$$

$$C_{l_{\beta_2}} = C_{l_{\beta_1}} \tag{A9}$$

$$(C_{l_r} - C_{l_{\dot{\beta}}} \cos \alpha)_2 = (C_{l_r} - C_{l_{\dot{\beta}}} \cos \alpha)_1 - C_{l_\beta} \frac{2\bar{x}}{b} \tag{A10}$$

$$(C_{l_p} + C_{l_{\dot{\beta}}} \sin \alpha)_2 = (C_{l_p} + C_{l_{\dot{\beta}}} \sin \alpha)_1 \tag{A11}$$

$$(C_{Y_p} + C_{Y_{\dot{\beta}}} \sin \alpha)_2 = (C_{Y_p} + C_{Y_{\dot{\beta}}} \sin \alpha)_1 \tag{A12}$$

$$(C_{n_p} + C_{n_{\dot{\beta}}} \sin \alpha)_2 = (C_{n_p} + C_{n_{\dot{\beta}}} \sin \alpha)_1 - (C_{Y_p} + C_{Y_{\dot{\beta}}} \sin \alpha)_1 \frac{\bar{x}}{b} \tag{A13}$$

REFERENCES

1. Buell, Donald A., Reed, Verlin D., and Lopez, Armando E.: The Static and Dynamic-Rotary Stability Derivatives at Subsonic Speeds of an Airplane Model With an Unswept Wing and a High Horizontal Tail. NACA RM A56I04, 1956.

2. Lampkin, Bedford A., and Tunnell, Phillips J.: Static and Dynamic-Rotary Stability Derivatives of an Airplane Model With an Unswept Wing and a High Horizontal Tail at Mach Numbers of 2.5, 3.0, and 3.5. NACA RM A58F17, 1958.

3. Winter, K. G., Scott-Wilson, J. B., and Davies, F. V.: Methods of Determination and of Fixing Boundary Layer Transition on Wind Tunnel Models at Supersonic Speeds. R.A.E. TN Aero. 2341, British, Sept., 1954. (Also ARC Rep. 17,416 and CP 212, 1955; and AGARD Rep. AG17/P7, 1954)

4. Beam, Benjamin H.: A Wind-Tunnel Test Technique for Measuring the Dynamic Rotary Stability Derivatives at Subsonic and Supersonic Speeds. NACA Rep. 1258, 1956. (Supersedes NACA TN 3347)

5. Runyan, Harry L., Woolston, Donald S., and Rainey, A. Gerald: Theoretical and Experimental Investigation of the Effect of Tunnel Walls on the Forces on an Oscillating Airfoil in Two-Dimensional Subsonic Compressible Flow. NACA Rep. 1262, 1956. (Supersedes NACA TN 3416)

6. Sacks, Alvin H.: Aerodynamic Forces, Moments, and Stability Derivatives for Slender Bodies of General Cross Section. NACA TN 3283, 1954.

7. Miles, John W.: The Application of Unsteady Flow Theory to the Calculation of Dynamic Stability Derivatives. North American Aviation Rep. AL-957, 1950.

8. Perkins, Courtland D., and Hage, Robert E.: Airplane Performance, Stability and Control. John Wiley and Sons, Inc., New York, 1949.

9. Campbell, John P., and Goodman, Alex: A Semiempirical Method for Estimating the Rolling Moment Due to Yawing of Airplanes. NACA TN 1984, 1949.

10. Bird, John D.: Some Theoretical Low-Speed Span Loading Characteristics of Swept Wings in Roll and Sideslip. NACA Rep. 969, 1950. (Supersedes NACA TN 1839)

11. Harmon, Sidney M., and Jeffreys, Isabella: Theoretical Lift and Damping in Roll of Thin Wings With Arbitrary Sweep and Taper at Supersonic Speeds - Supersonic Leading and Trailing Edges. NACA TN 2114, 1950.

12. Michael, William H., Jr.: Analysis of the Effects of Wing Interference on the Tail Contributions to the Rolling Derivatives. NACA Rep. 1086, 1952. (Supersedes NACA TN 2332)

13. Kemp, William B., Jr., and Becht, Robert E.: Damping-In-Pitch Characteristics at High Subsonic and Transonic Speeds of Four 35° Sweptback Wings. NACA RM L53G29a, 1953.

14. Beam, Benjamin H., Reed, Verlin D., and Lopez, Armando E.: Wind-Tunnel Measurements at Subsonic Speeds of the Static and Dynamic-Rotary Stability Derivatives of a Triangular-Wing Airplane Model Having a Triangular Vertical Tail. NACA RM A55A28, 1955.

15. Tobak, Murray: Damping in Pitch of Low-Aspect-Ratio Wings at Subsonic and Supersonic Speeds. NACA RM A52L04a, 1953.

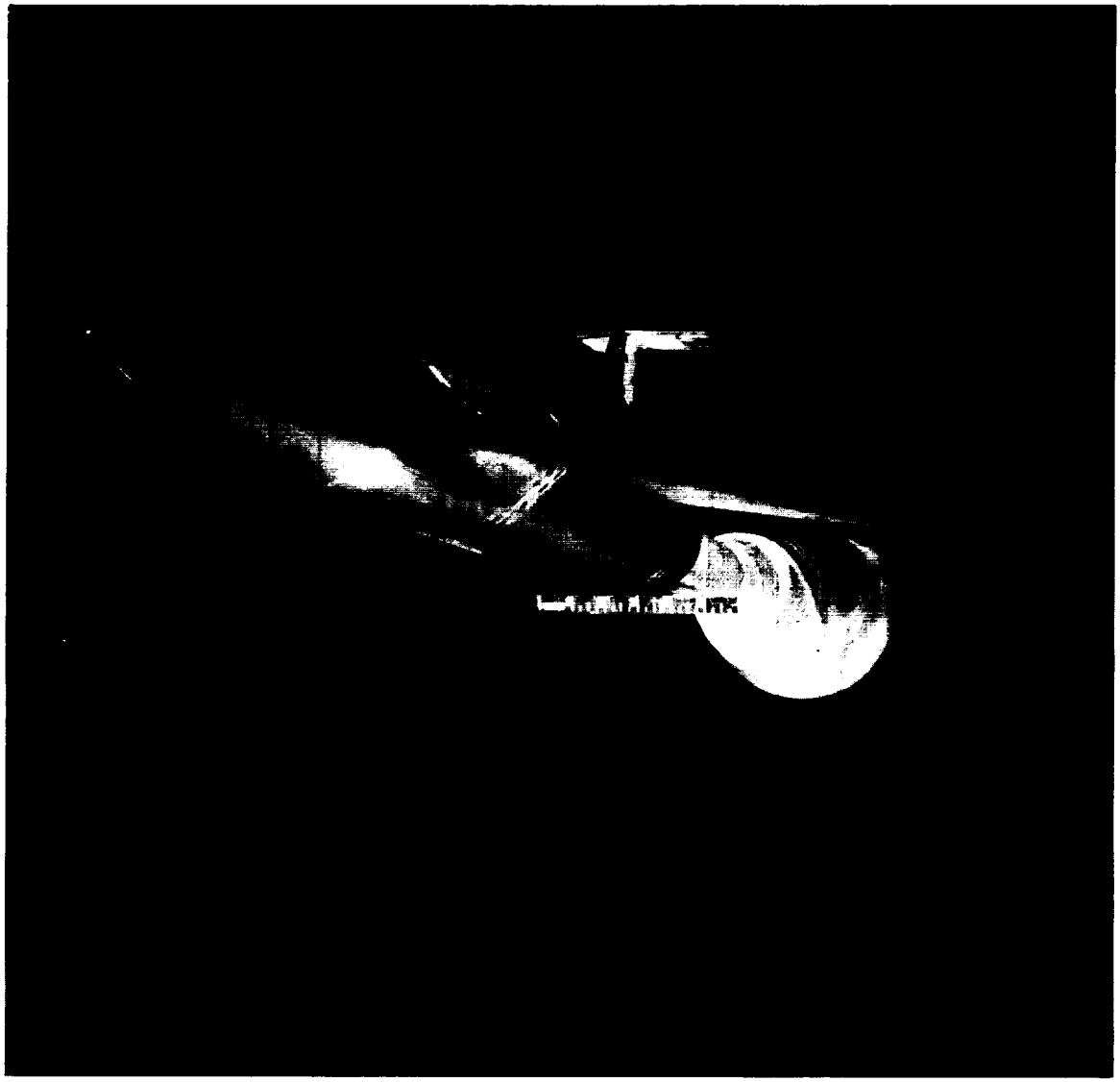

A-23975

Figure 1.- Photograph of model mounted in wind tunnel.

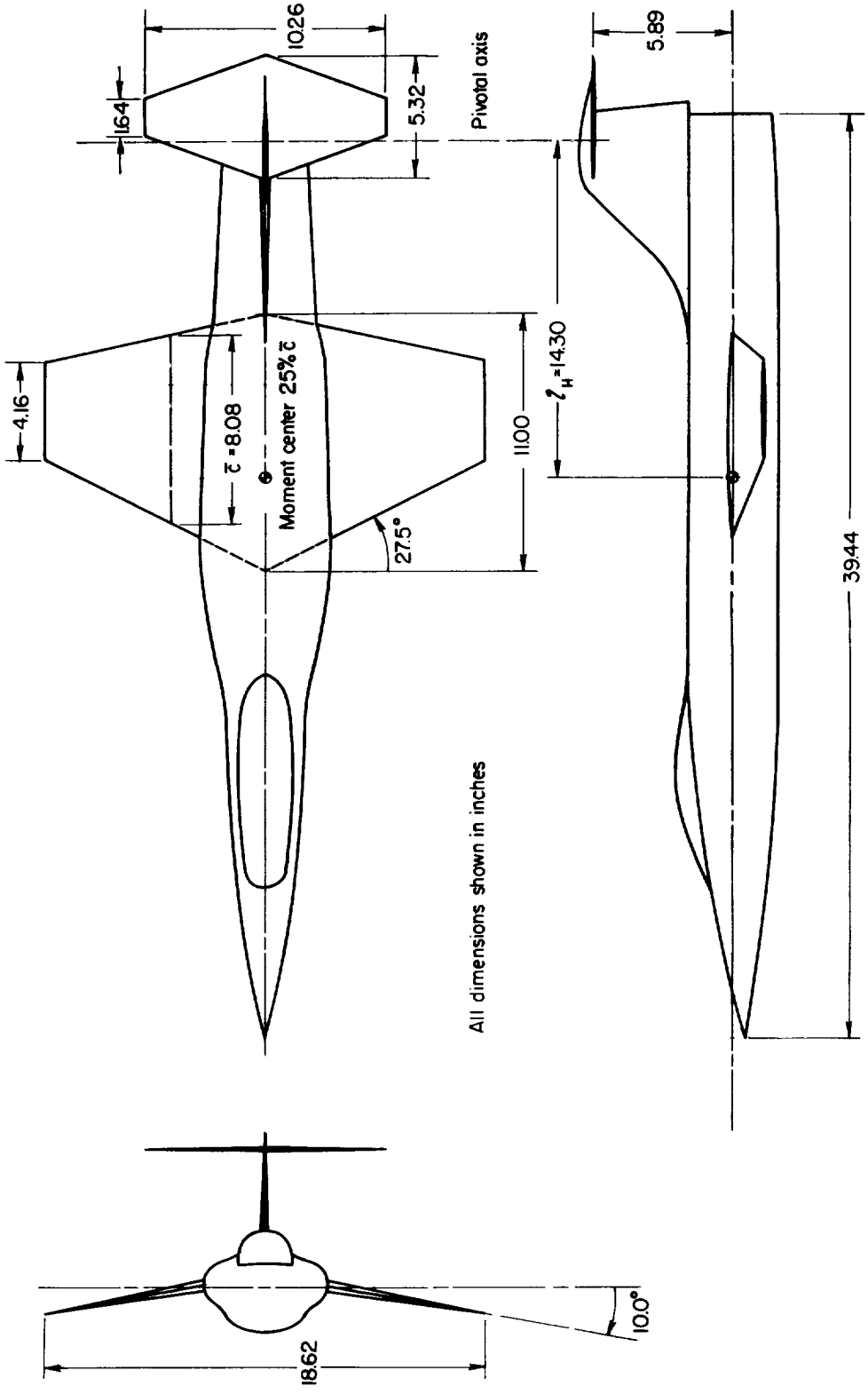

Figure 2.- Three-view drawing of model.

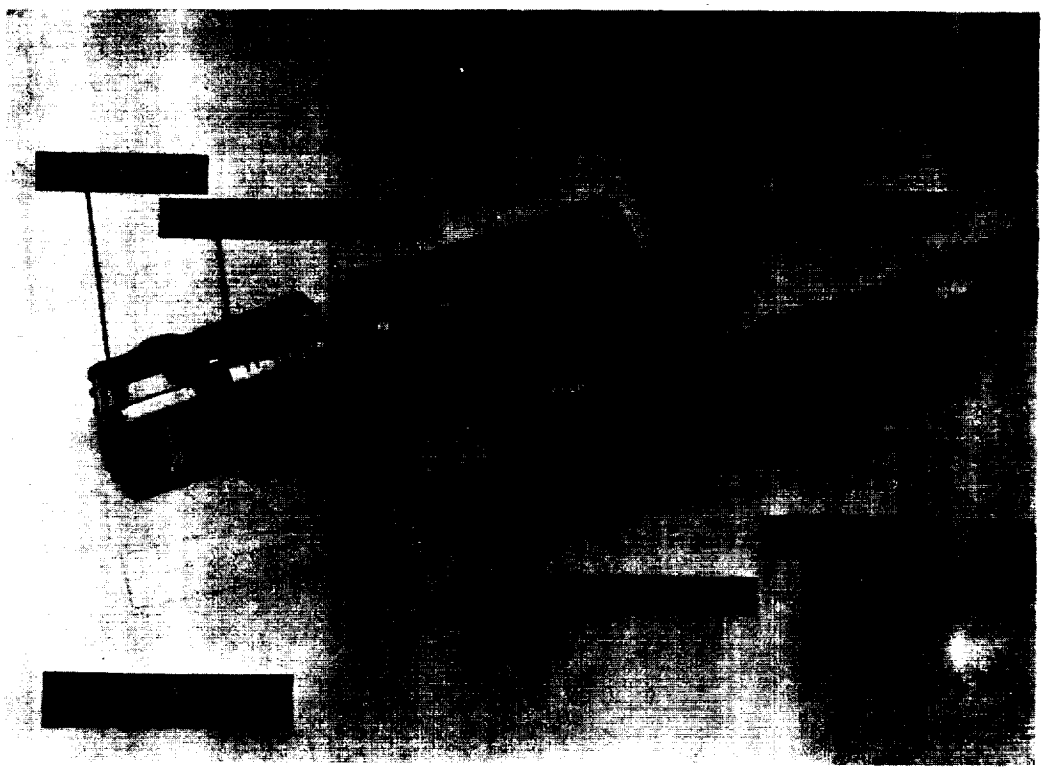

A-24168.1

A-24169.1

Figure 3.- Photographs of dynamic balances.

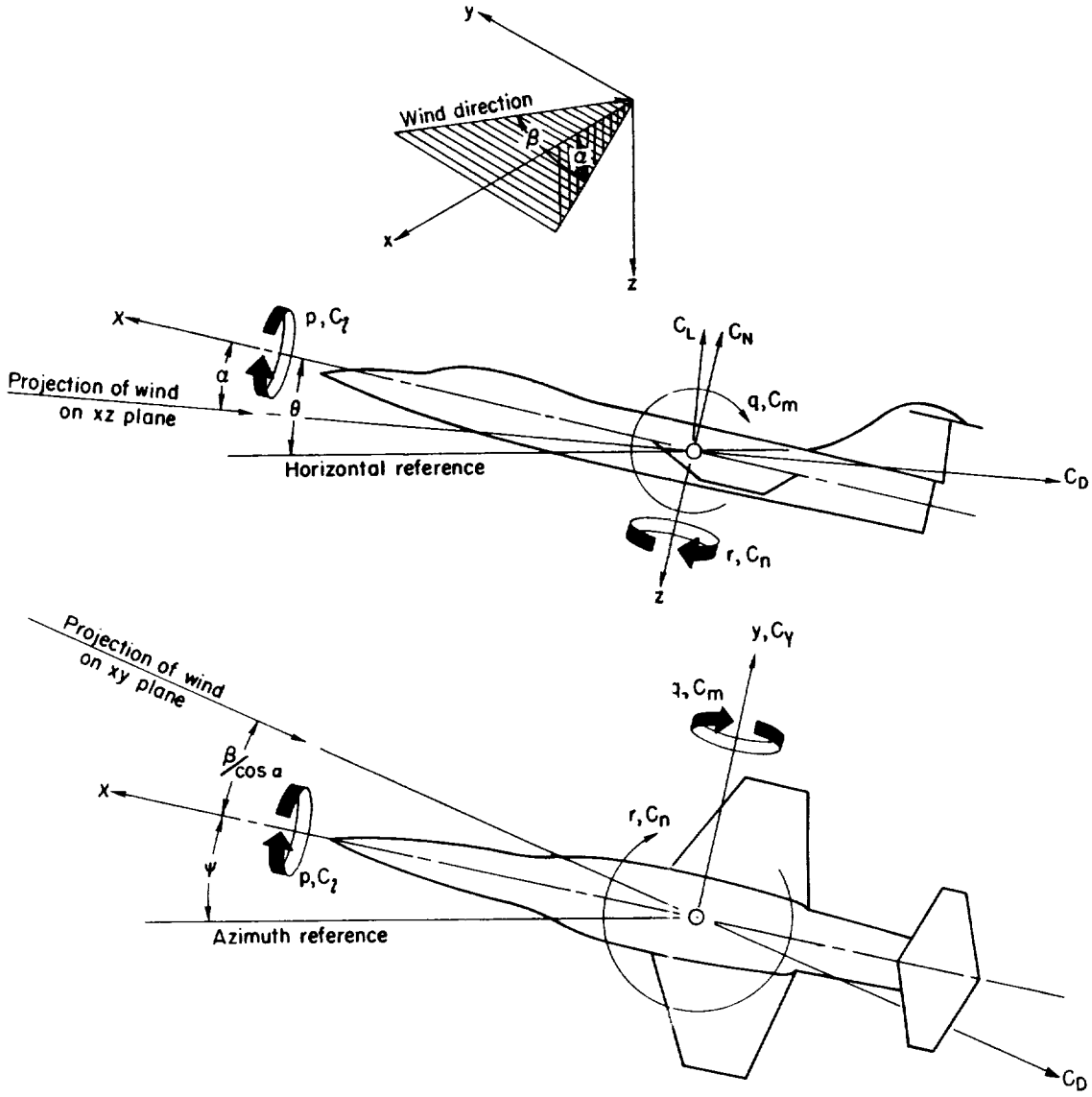

Figure 4.- The body system of axes. All moments, forces, angles, and angular velocities are shown in the positive sense.

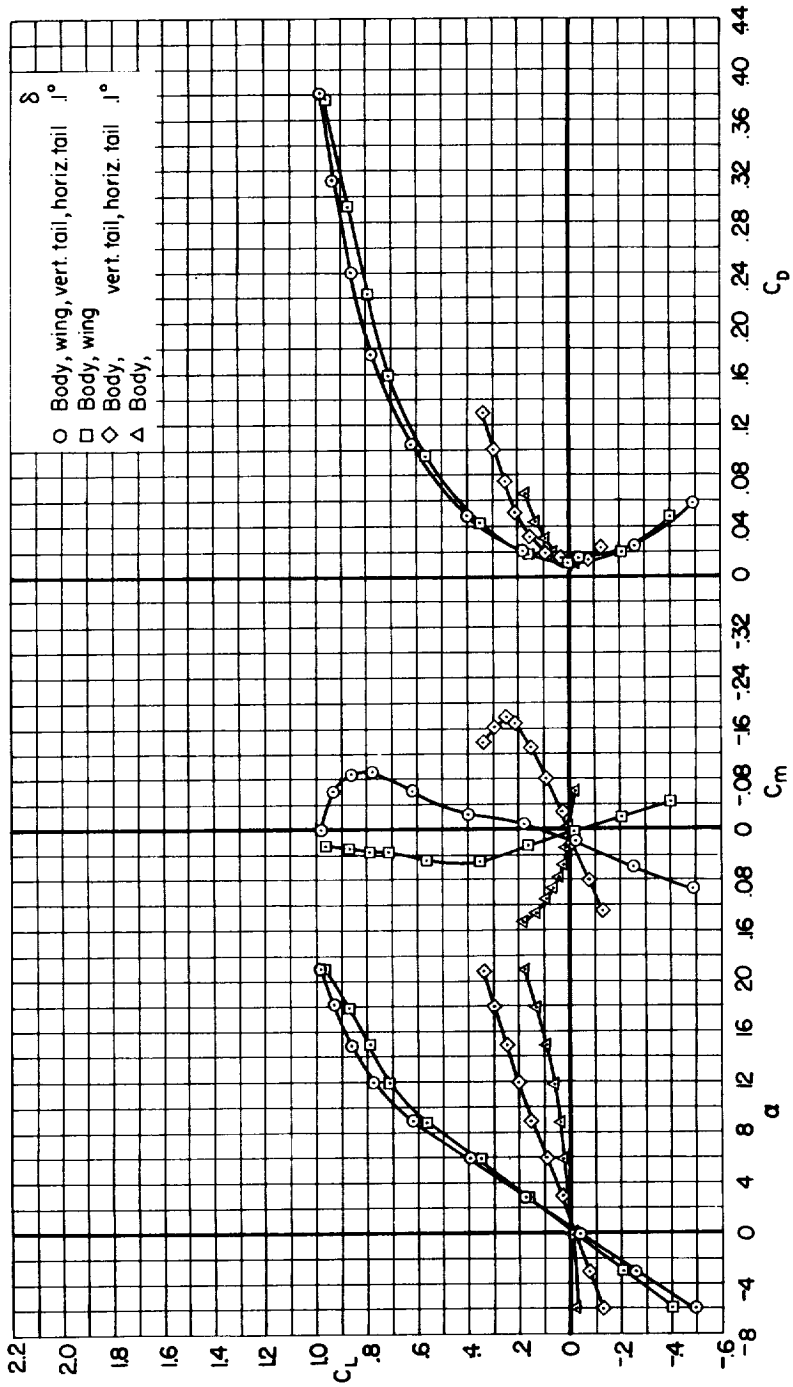

(a) M = 0.65

Figure 5.- The static longitudinal characteristics for the complete model and various component combinations

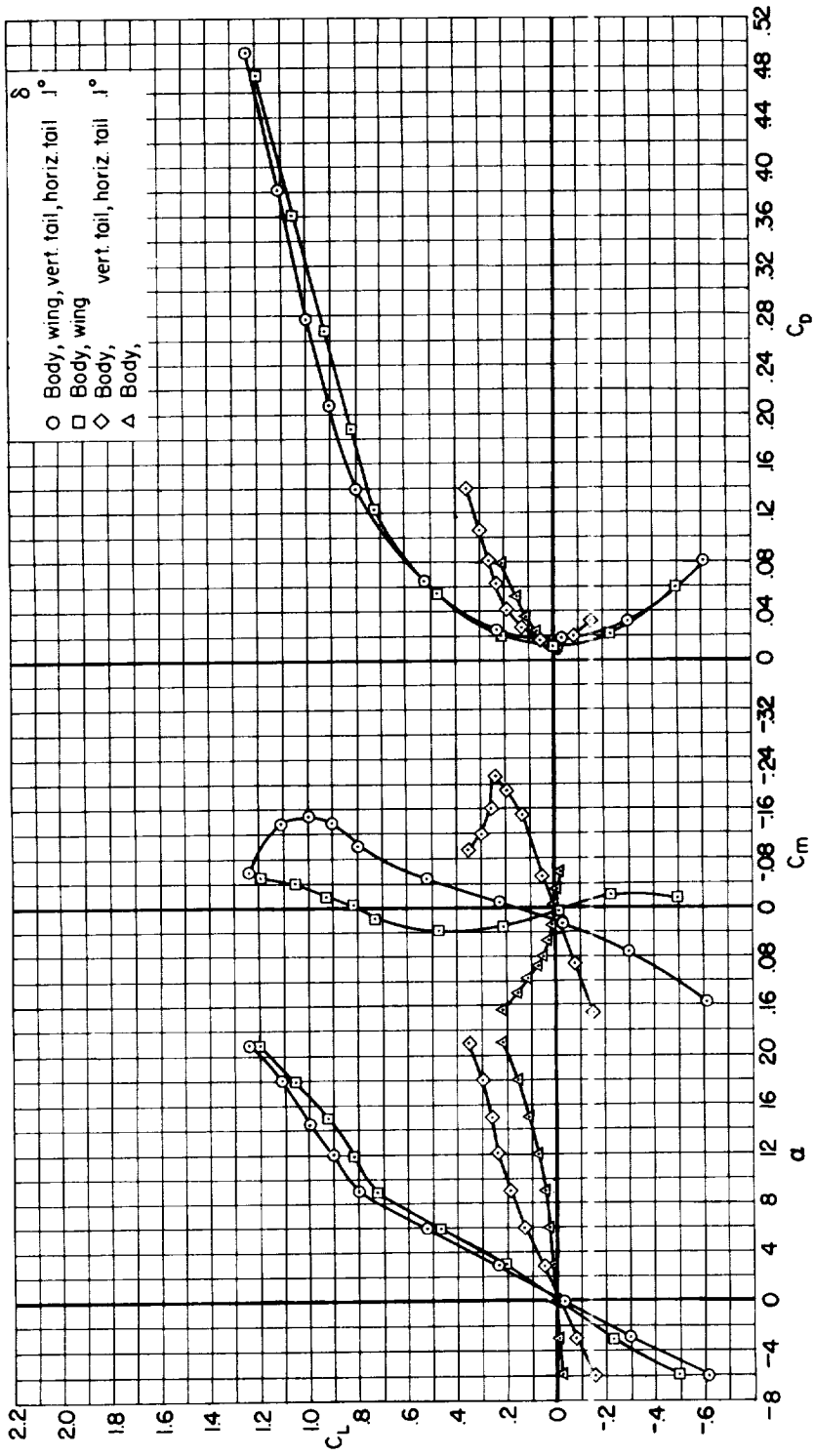

(b) M = 0.90

Figure 5.- Continued.

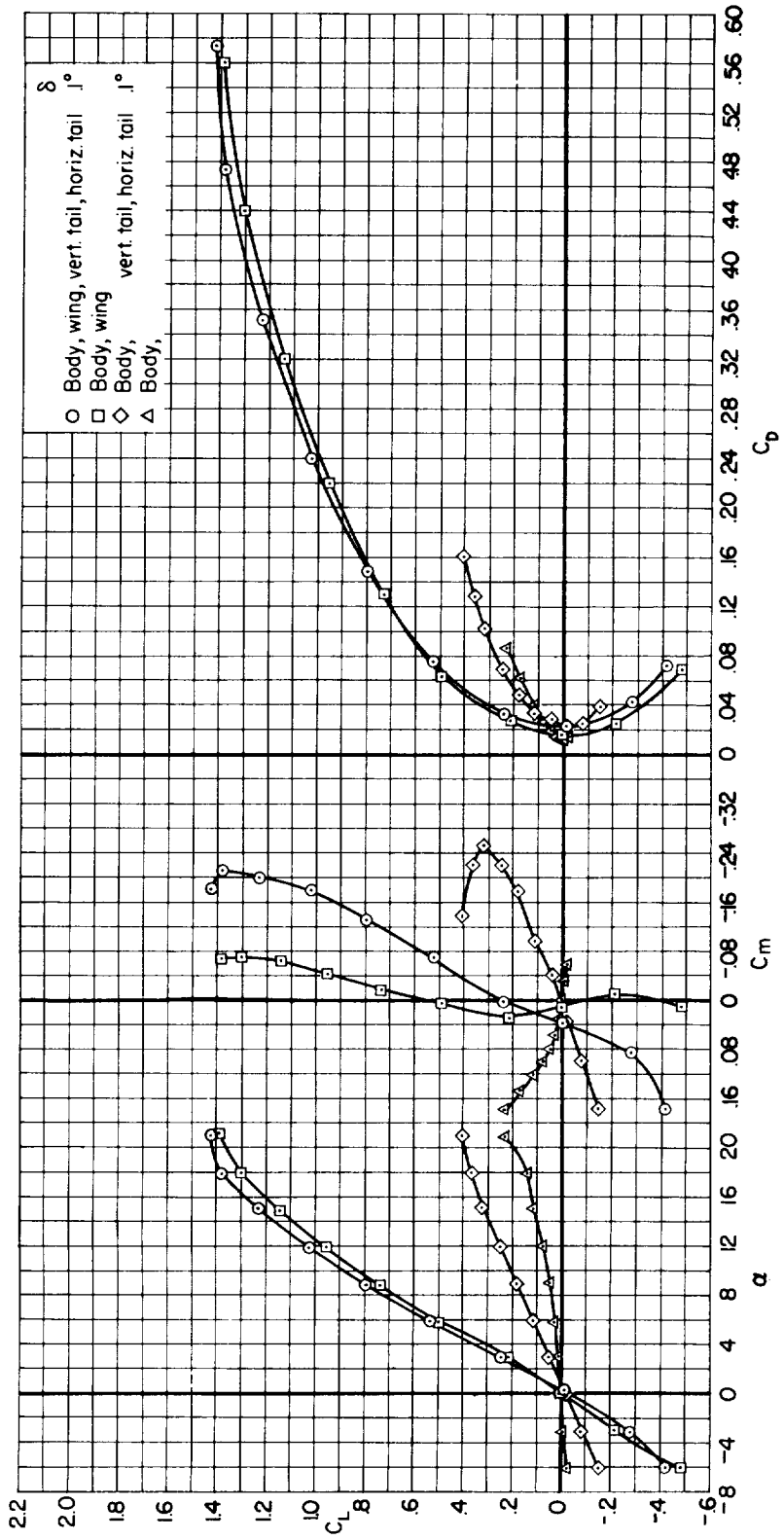

(c) M = 0.94

Figure 5.- Continued.

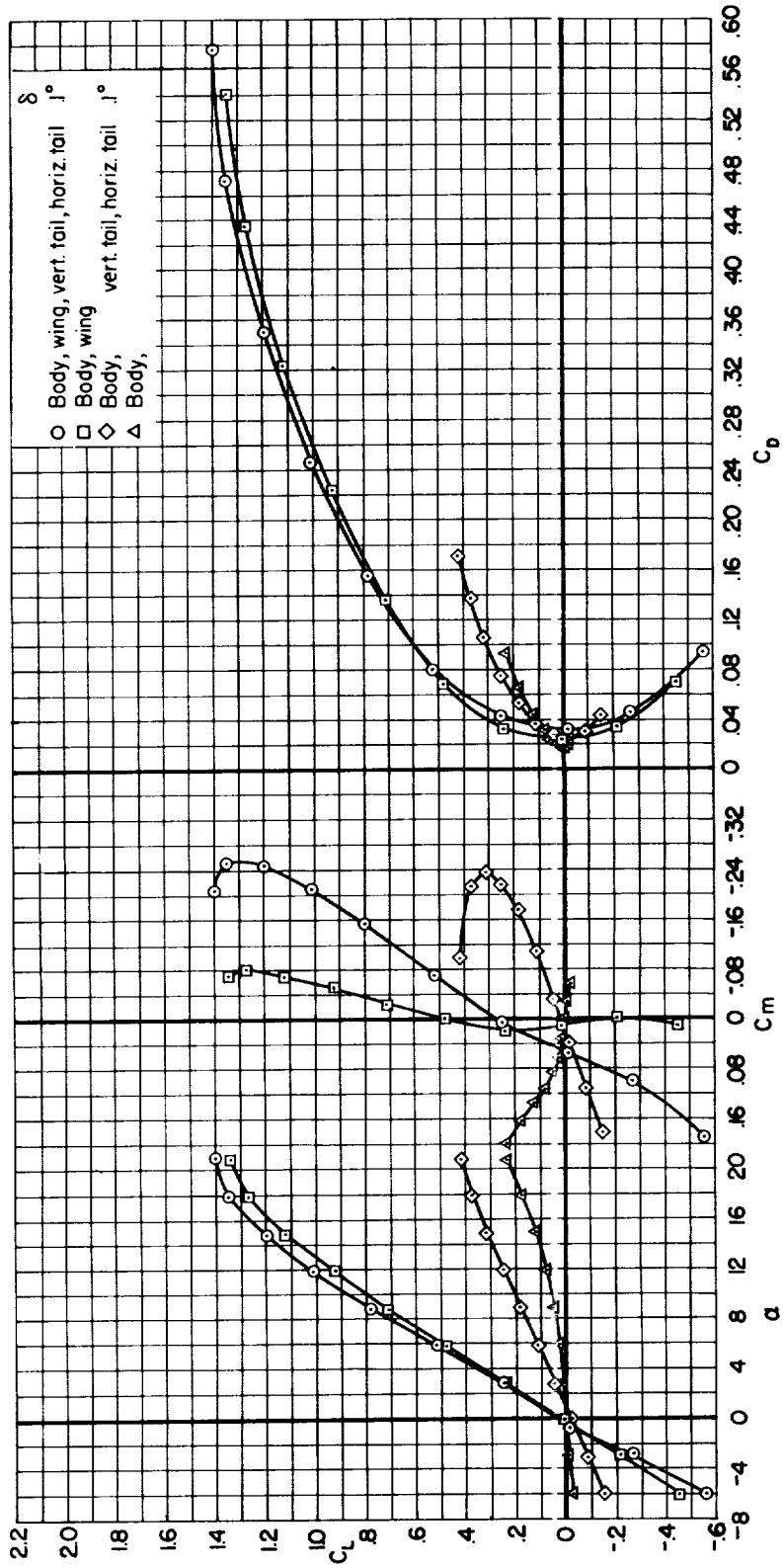

(d) M = 1.0

Figure 5.- Continued.

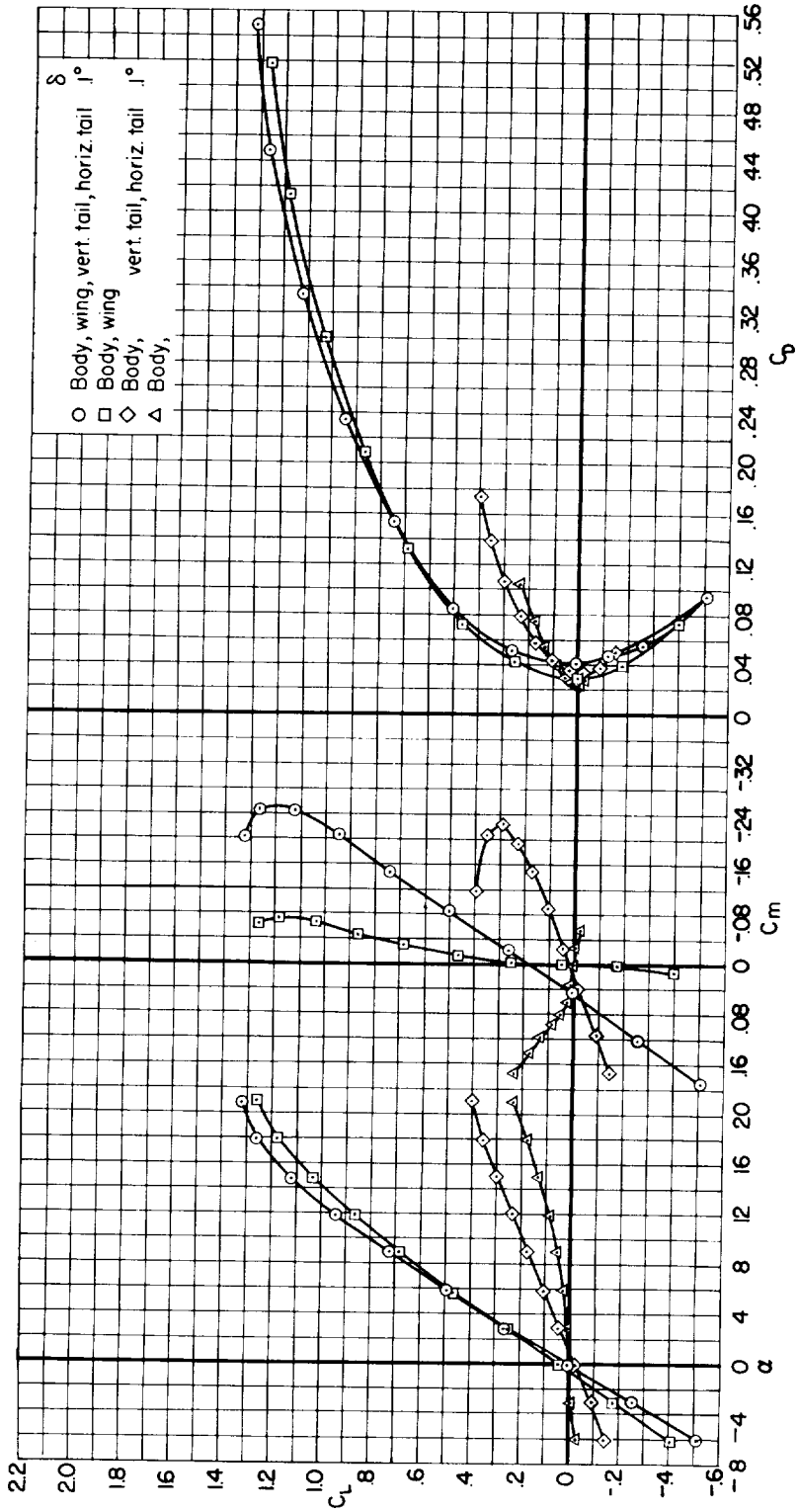

(e) M = 1.1

Figure 5.- Continued.

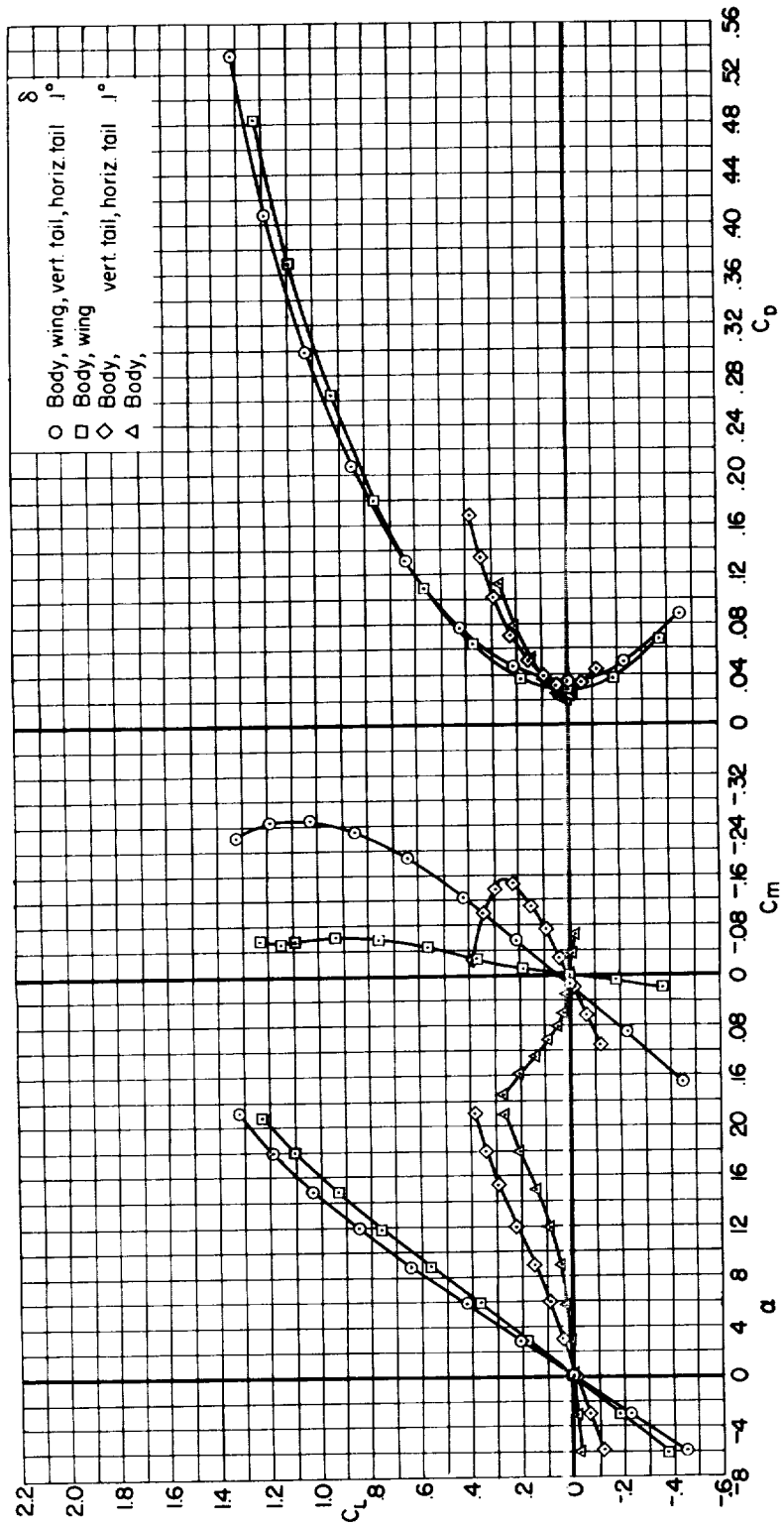

(f) M = 1.3

Figure 5.- Continued.

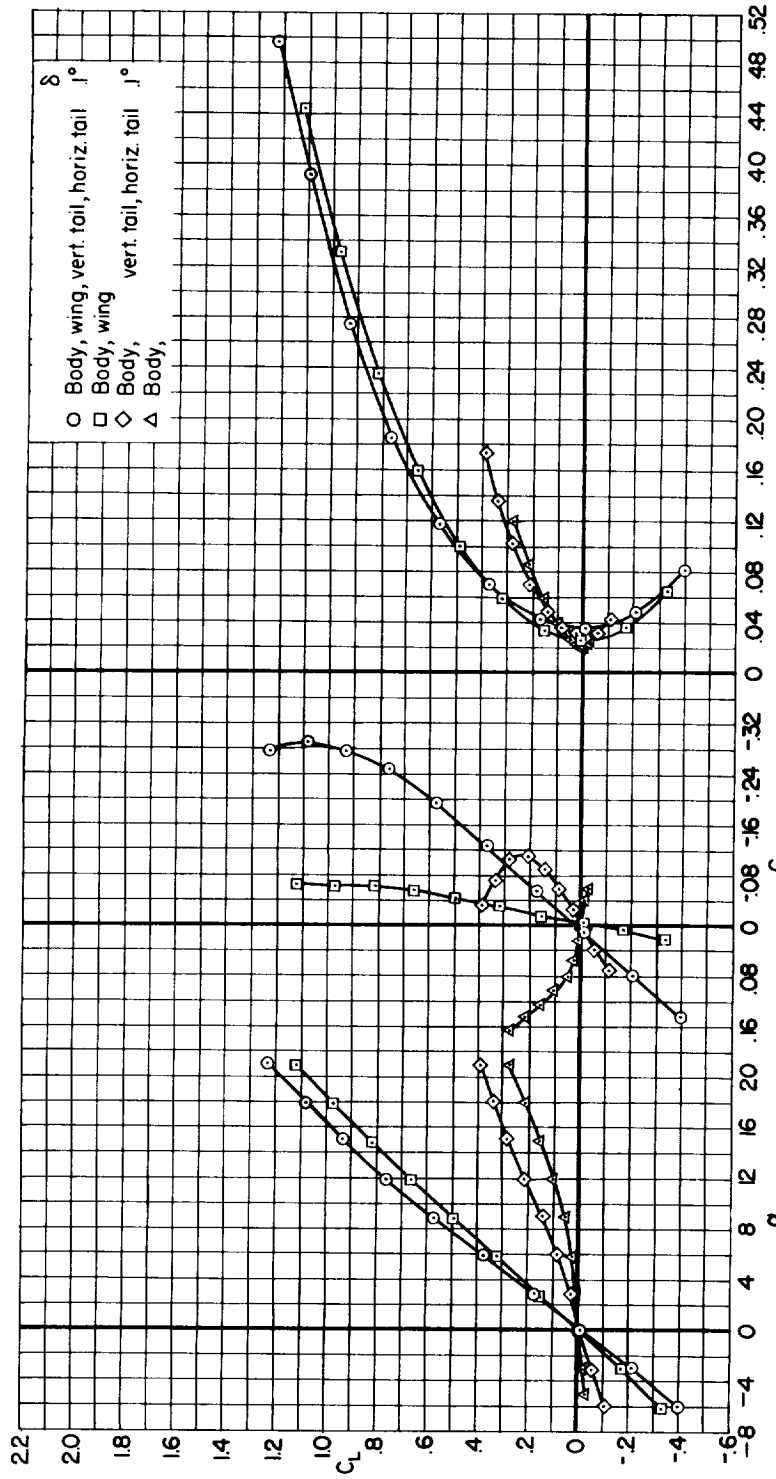

(g) M = 1.5

Figure 5.- Continued.

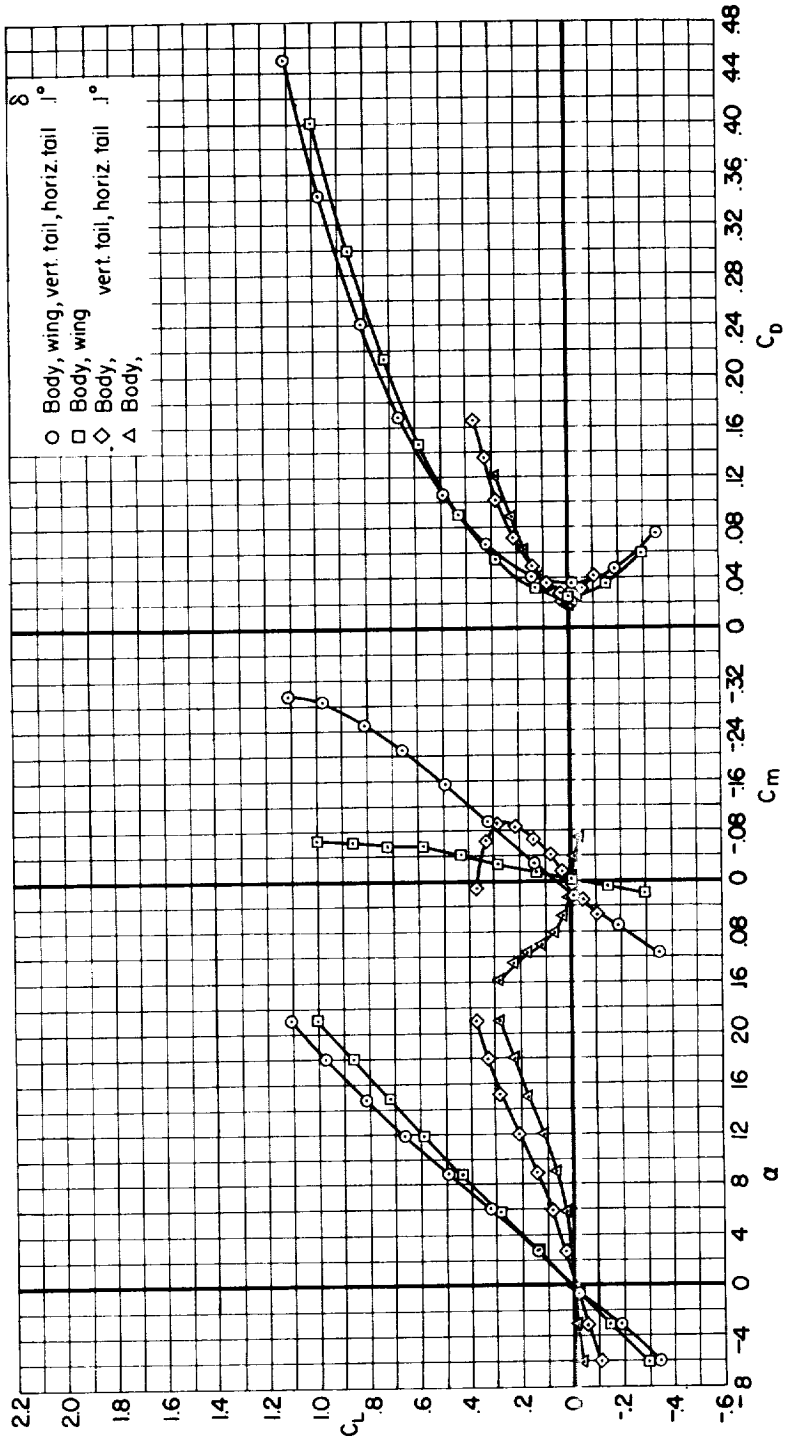

(h) M = 1.7

Figure 5.- Continued.

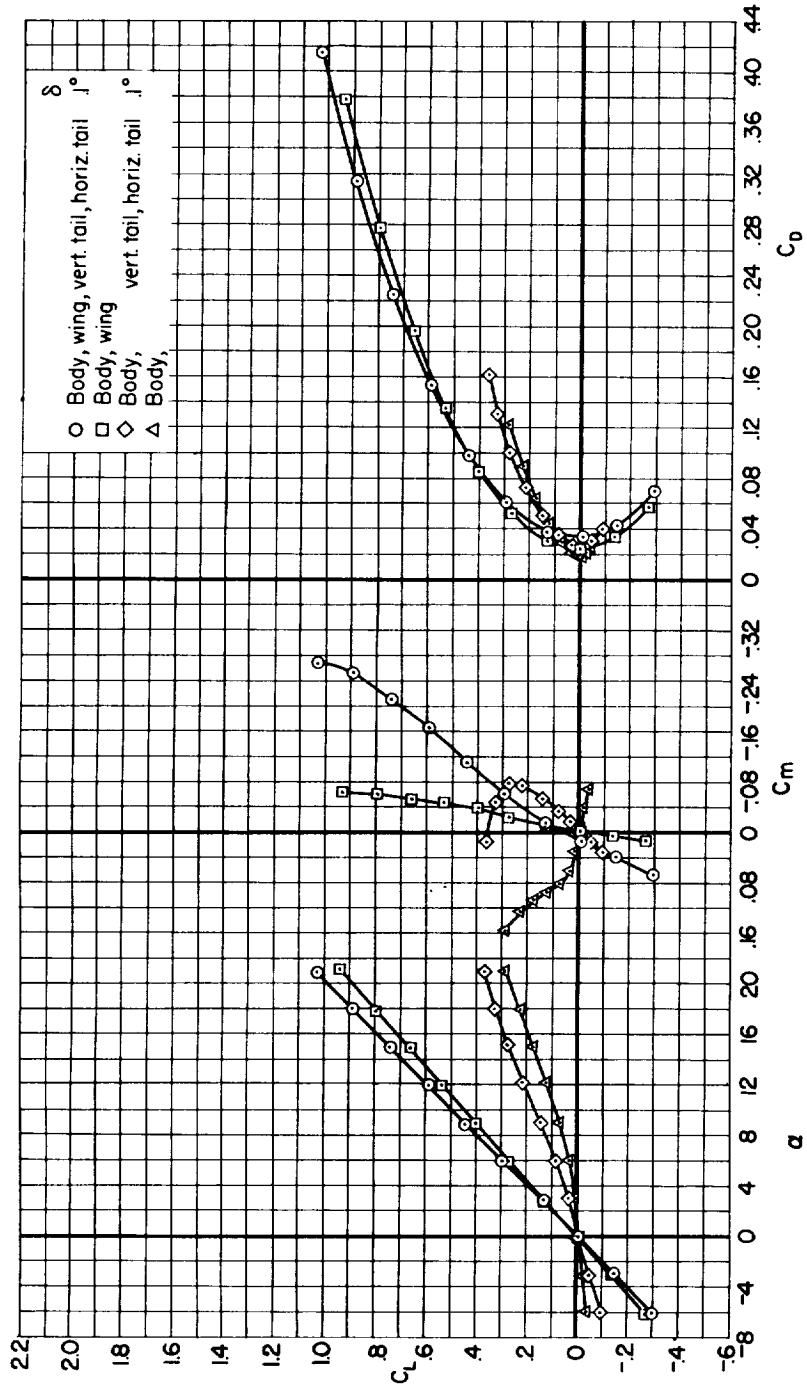

(i) M = 1.9

Figure 5.- Continued.

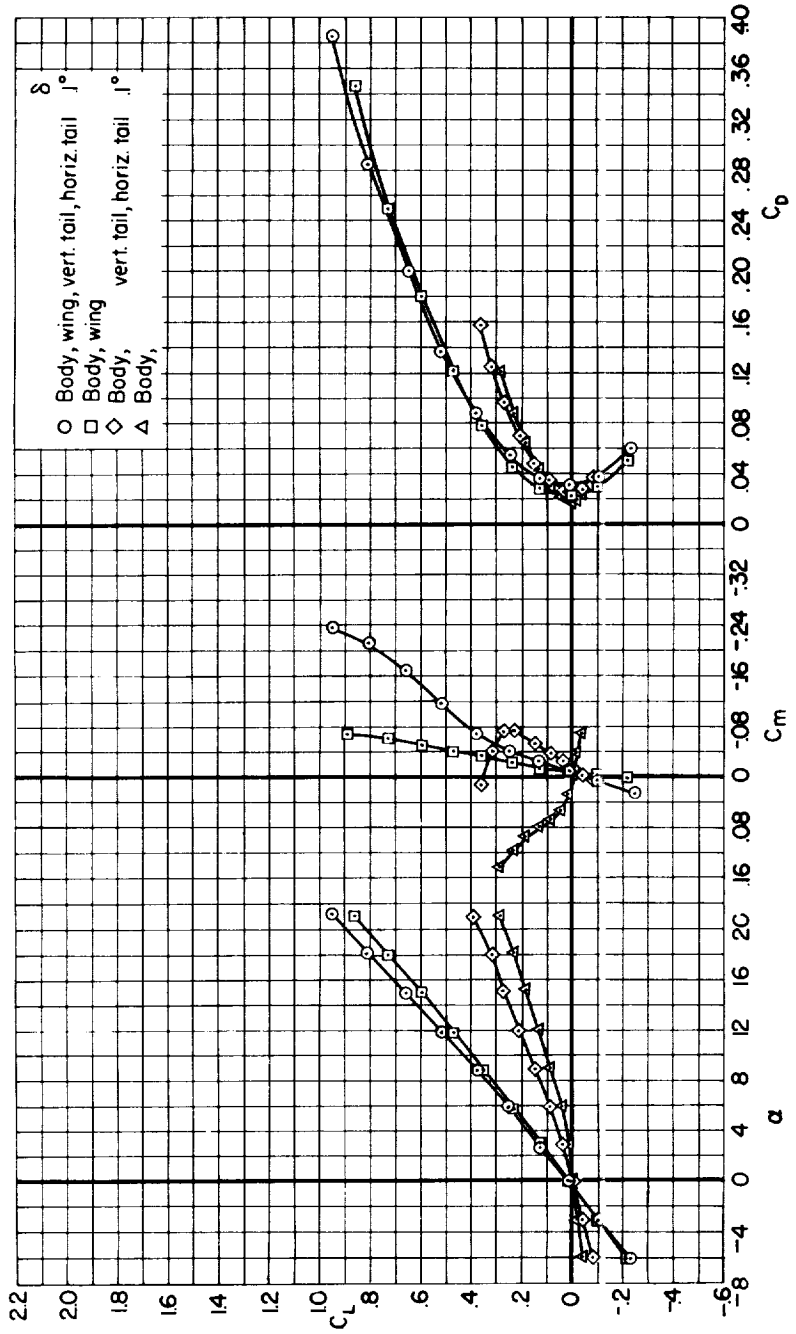

(j) M = 2.2

Figure 5.- Concluded.

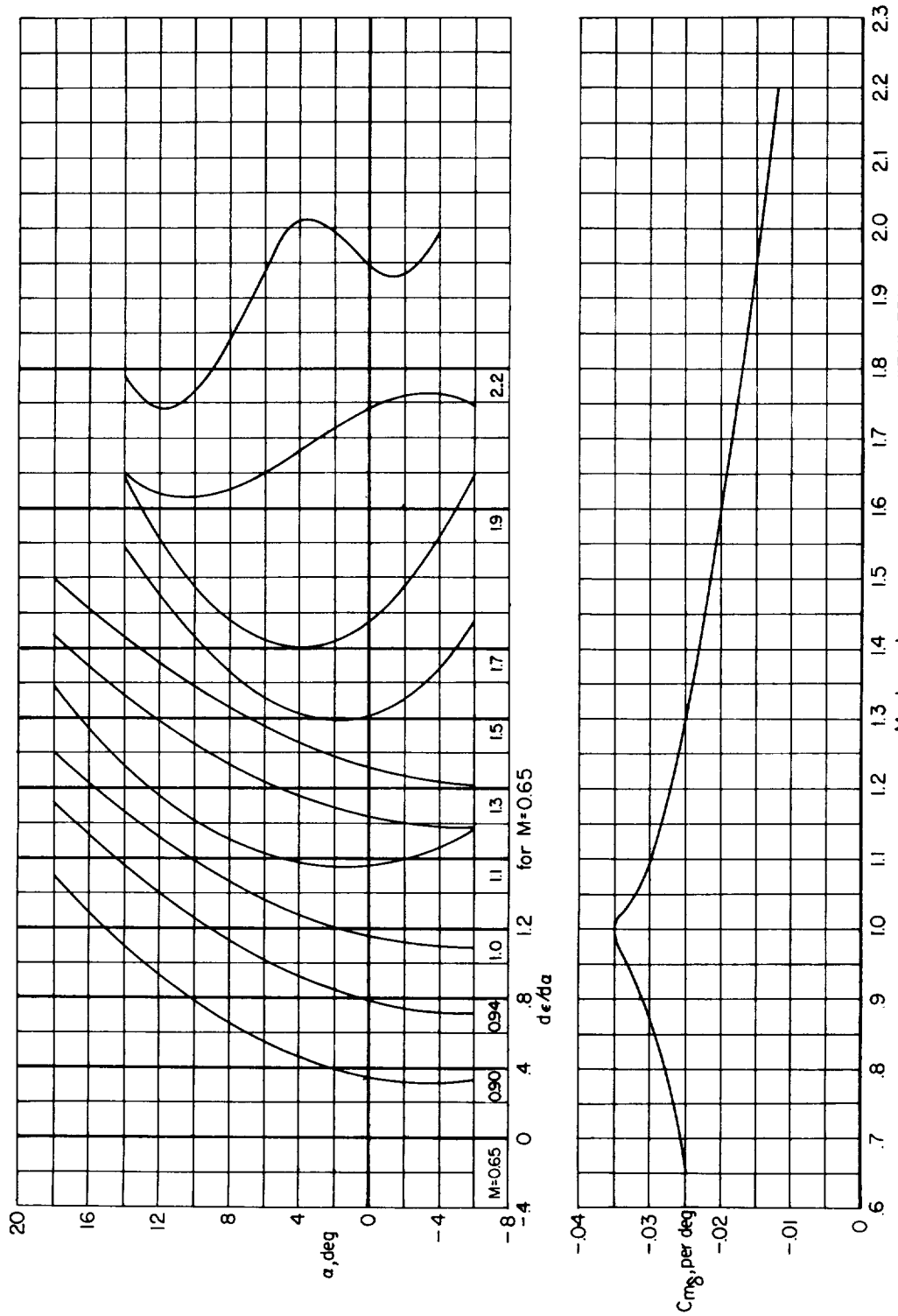

Figure 6.- The variation of $d\epsilon/d\alpha$ with angle of attack, and the variation of C_{m_δ} with Mach number.

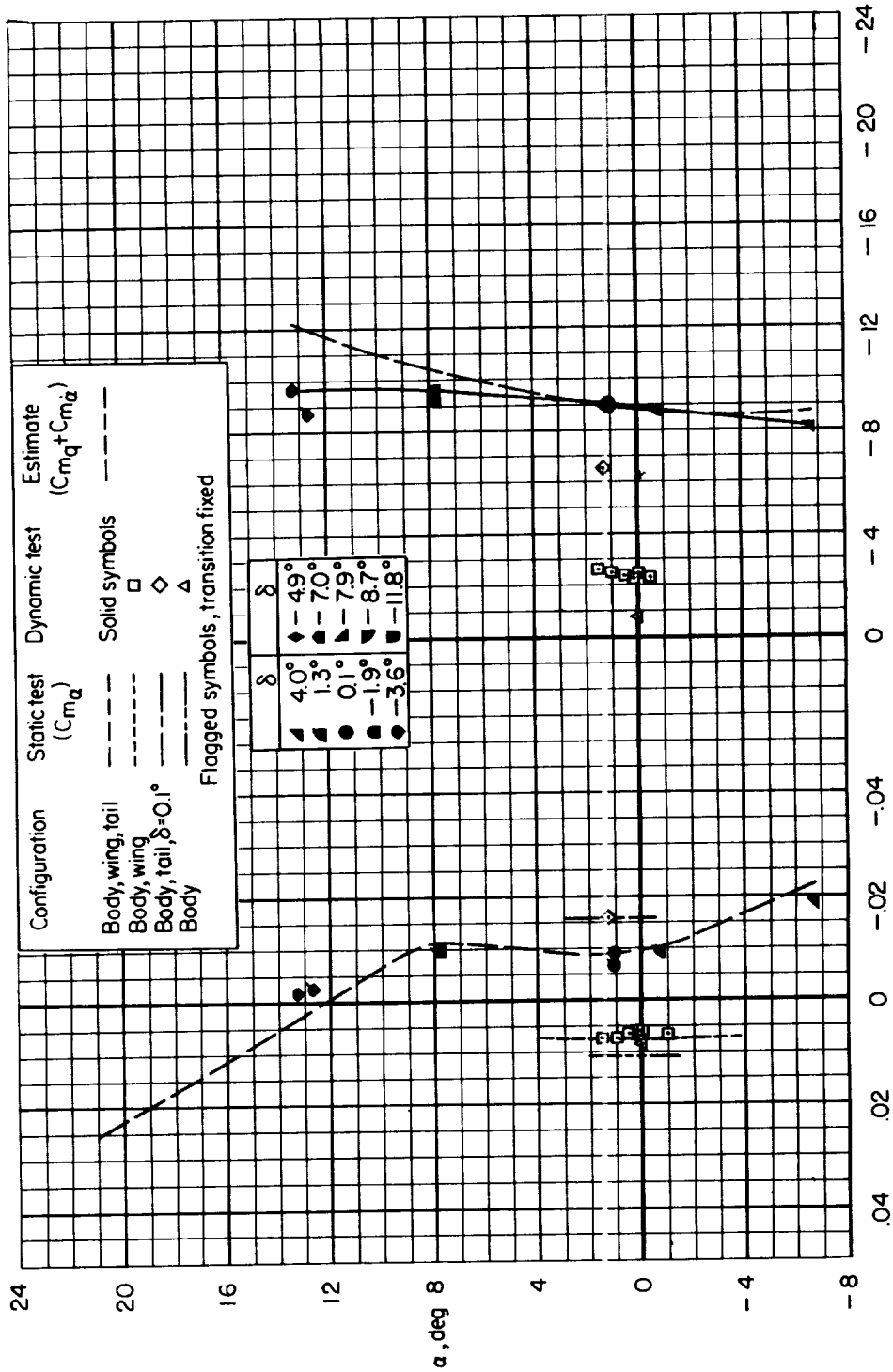

(a) M = 0.65

Figure 7.- The variation of C_{m_α} and $C_{m_q} + C_{m_{\dot\alpha}}$ with angle of attack.

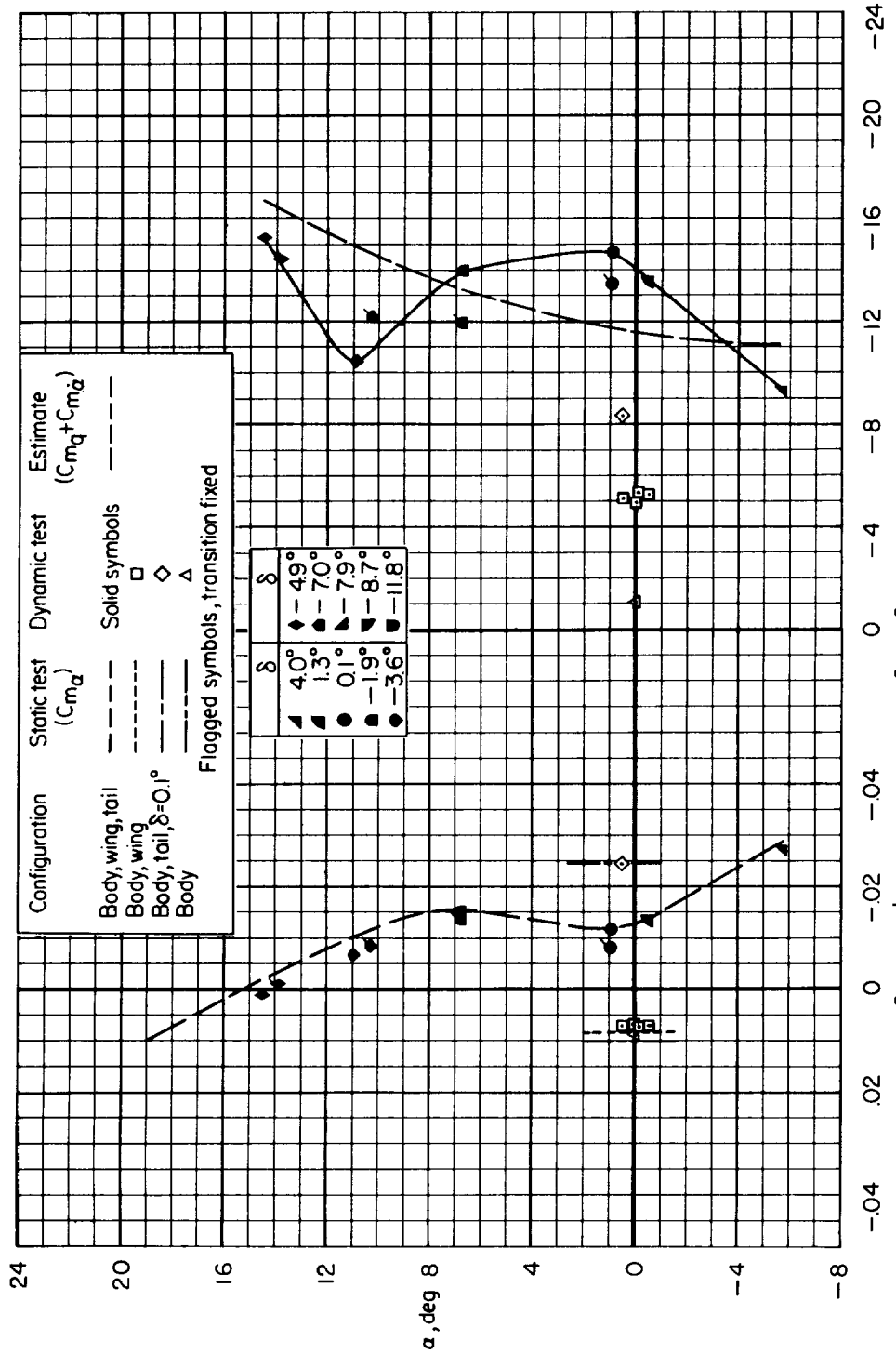

(b) M = 0.90

Figure 7.- Continued.

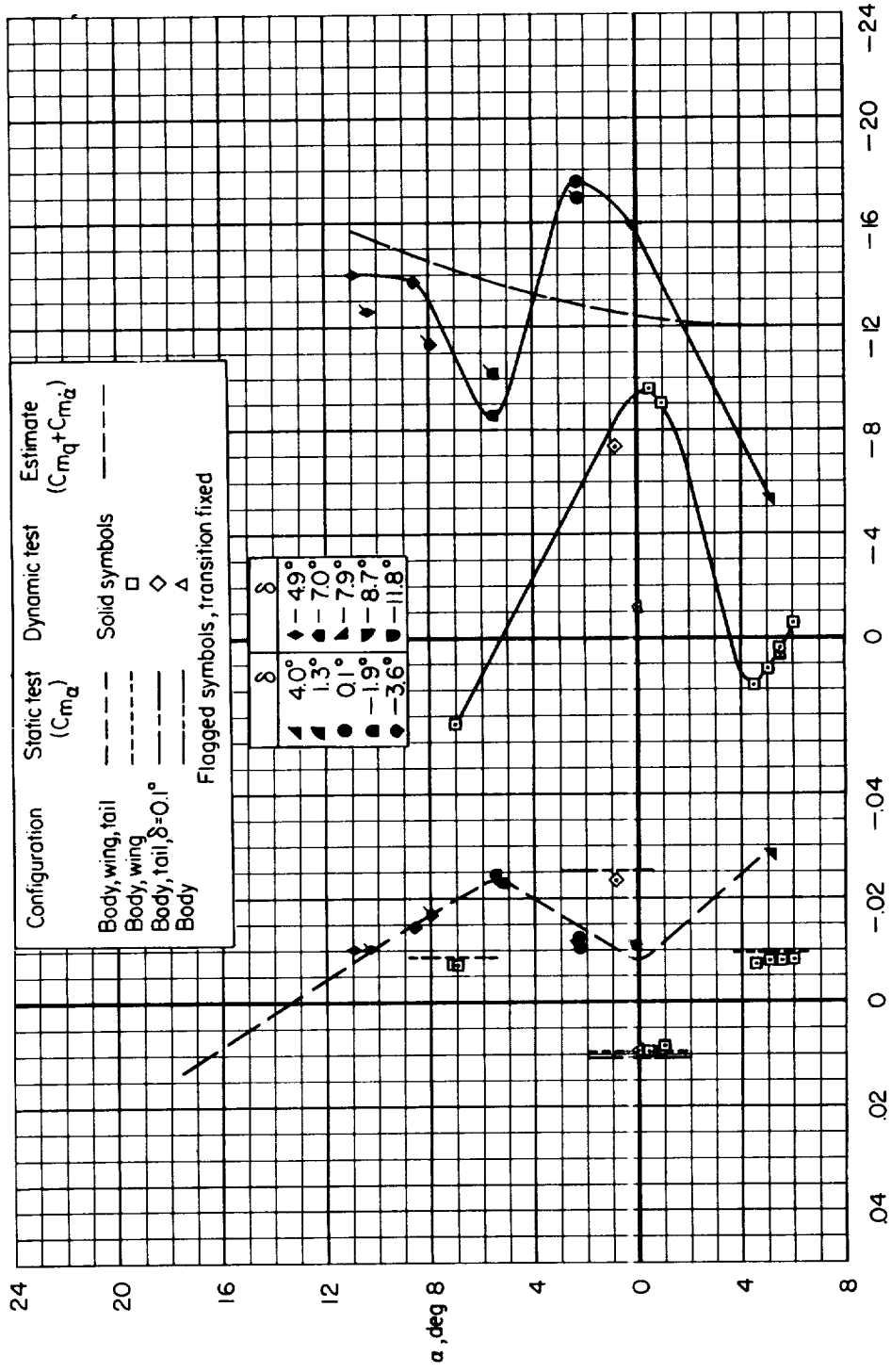

(c) M = 0.94

Figure 7.- Continued.

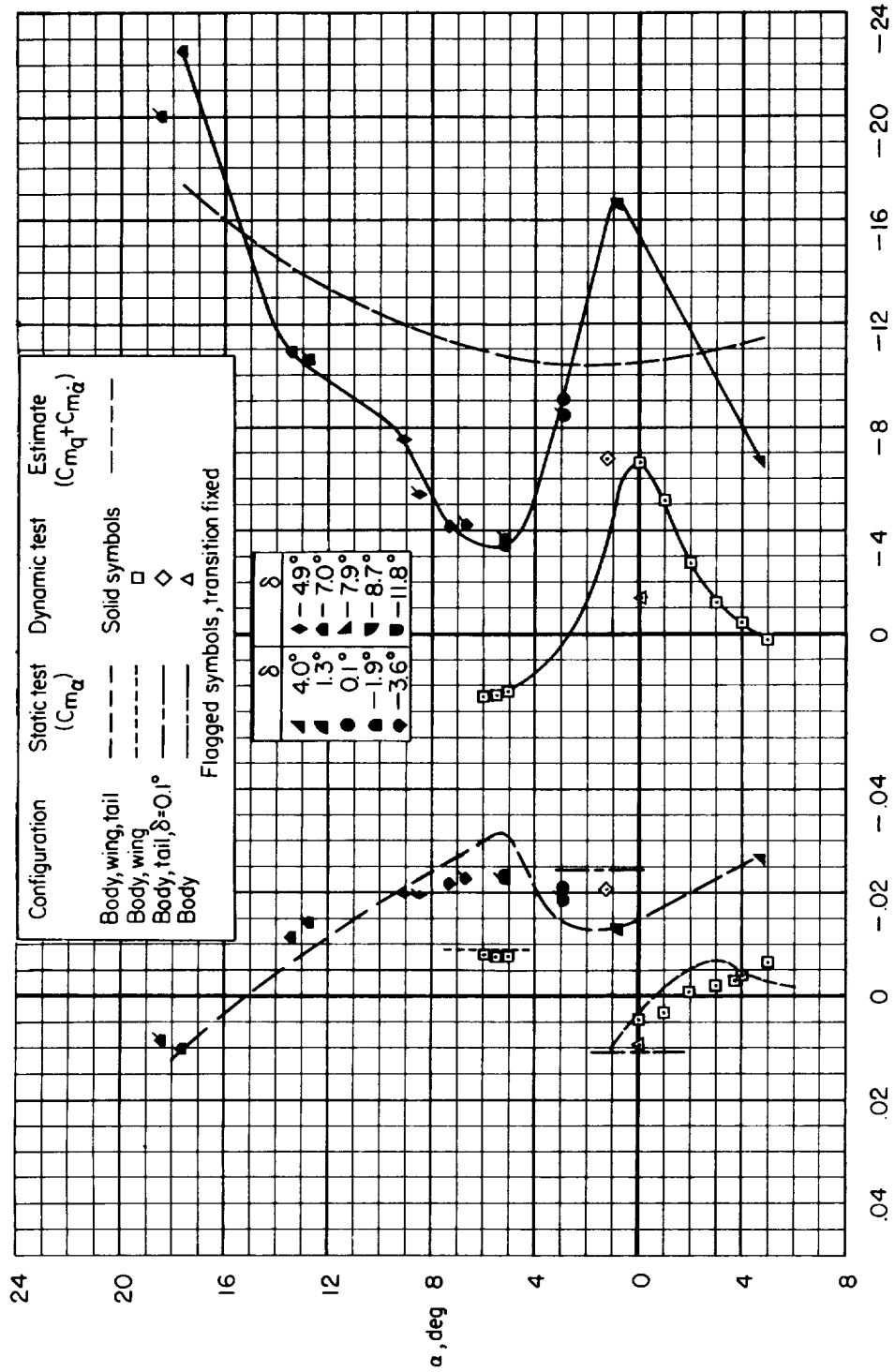

(d) M = 1.0

Figure 7.- Continued.

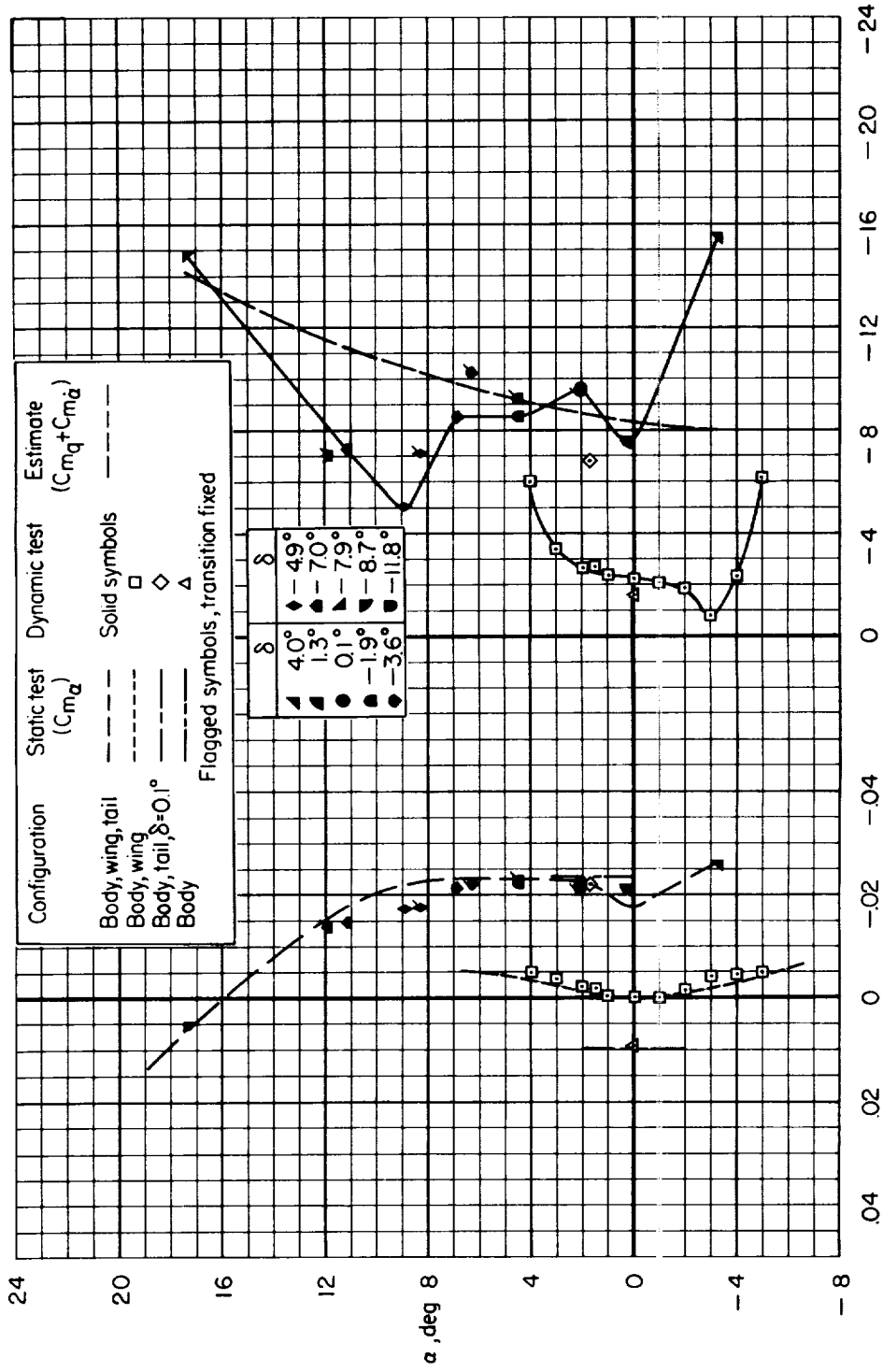

(e) M = 1.1

Figure 7.- Continued.

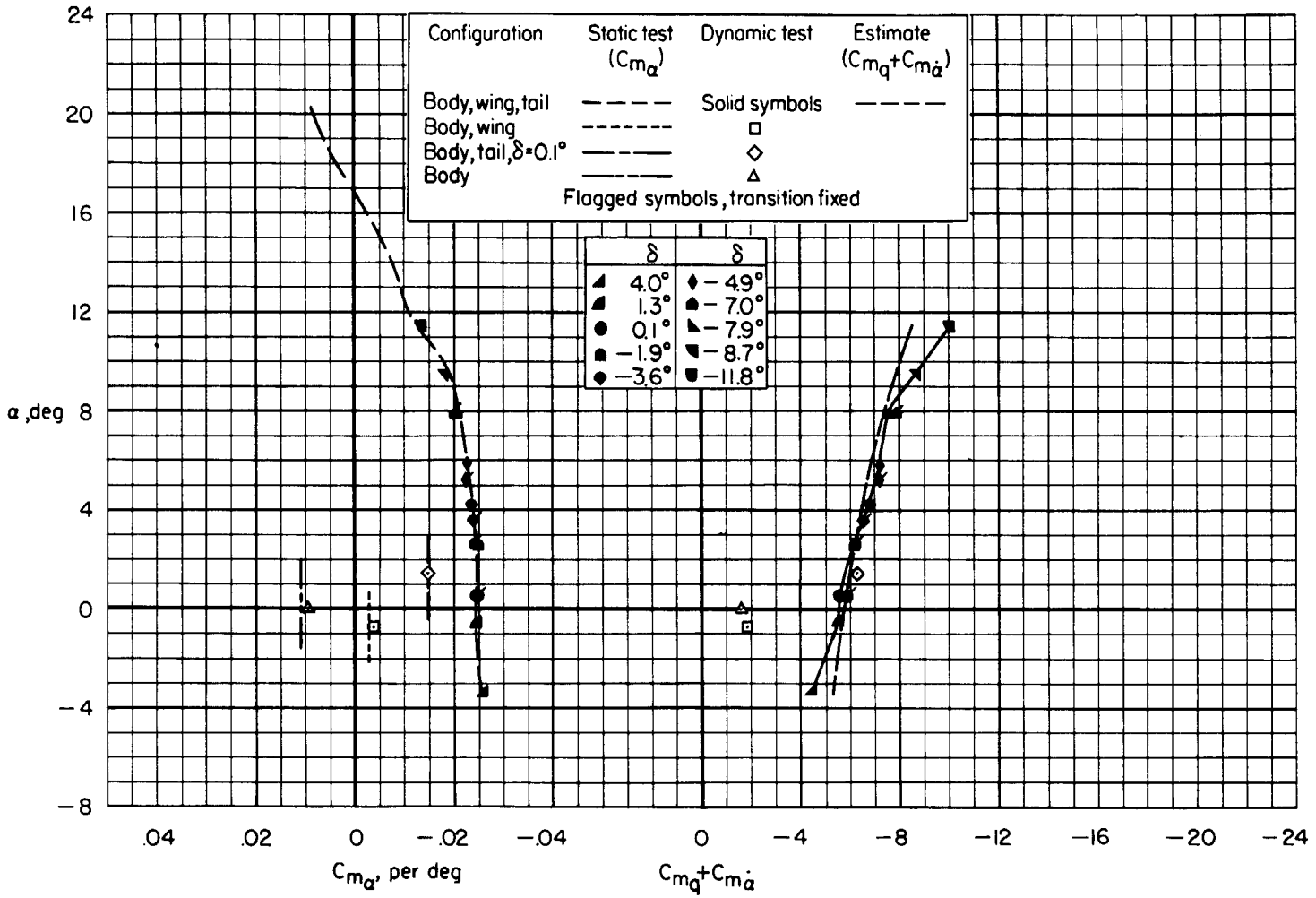

(f) M = 1.3

Figure 7.- Continued.

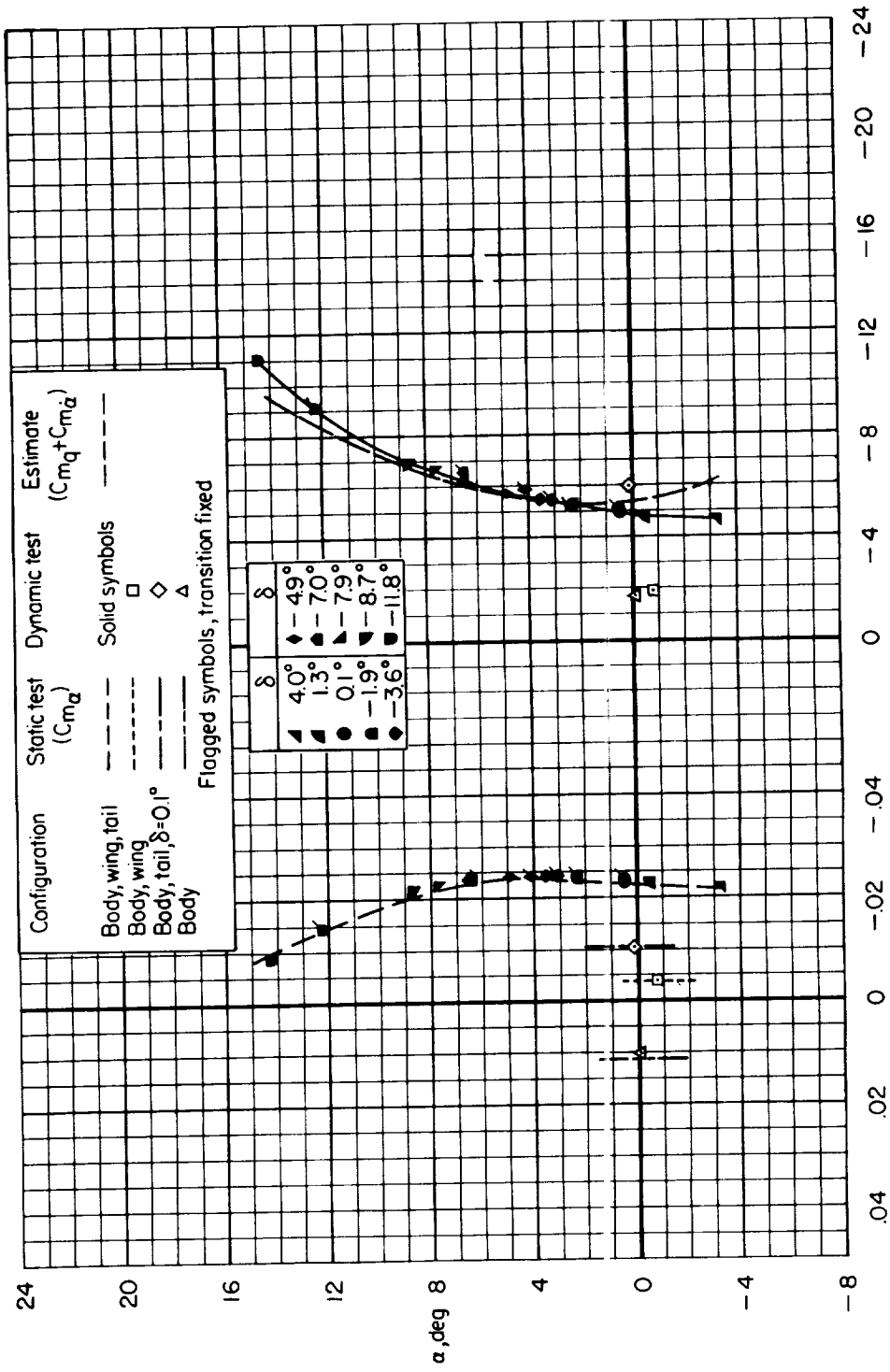

(g) M = 1.5

Figure 7.- Continued.

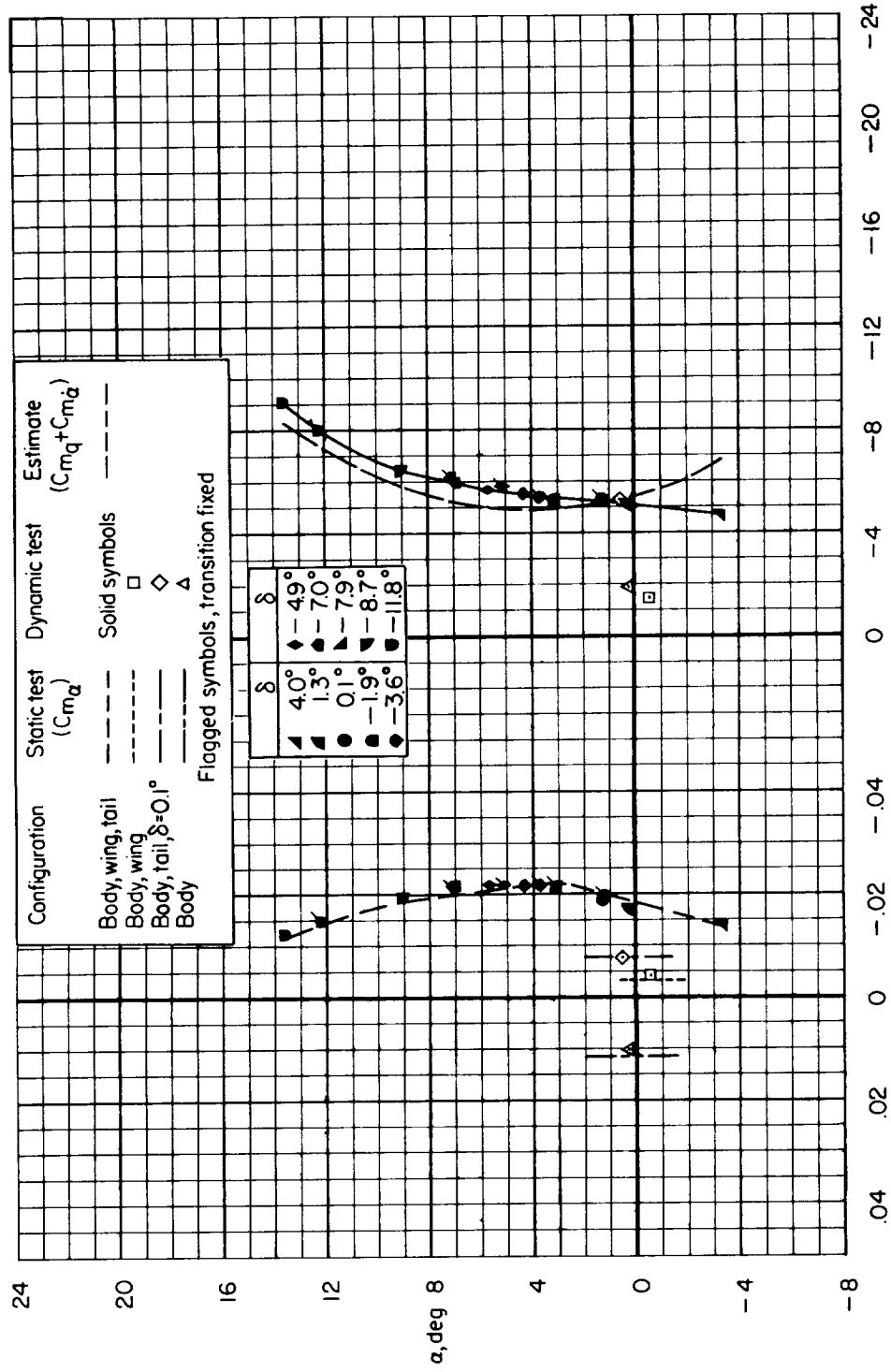

(h) M = 1.7

Figure 7.- Continued.

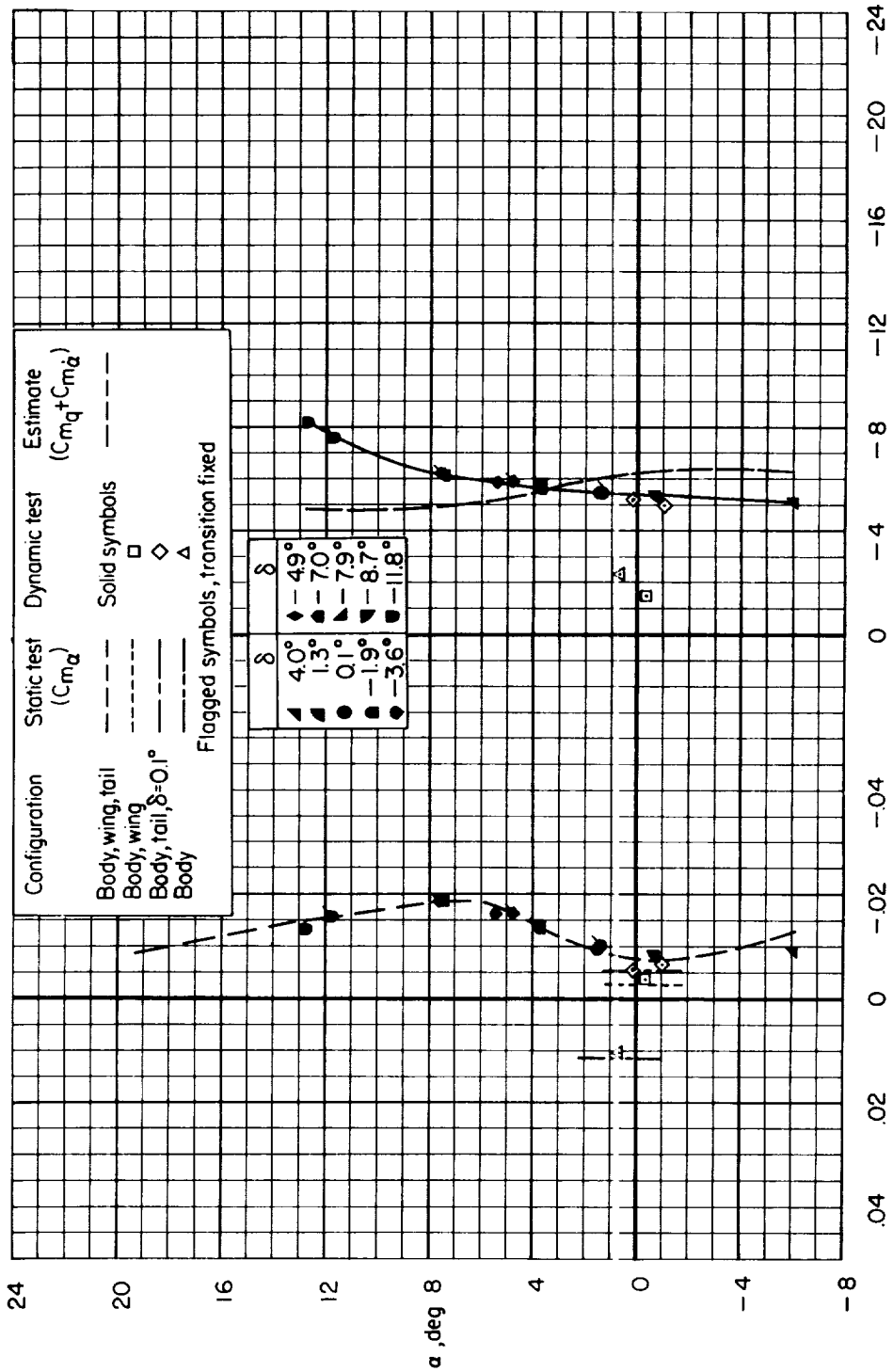

Figure 7.- Continued.

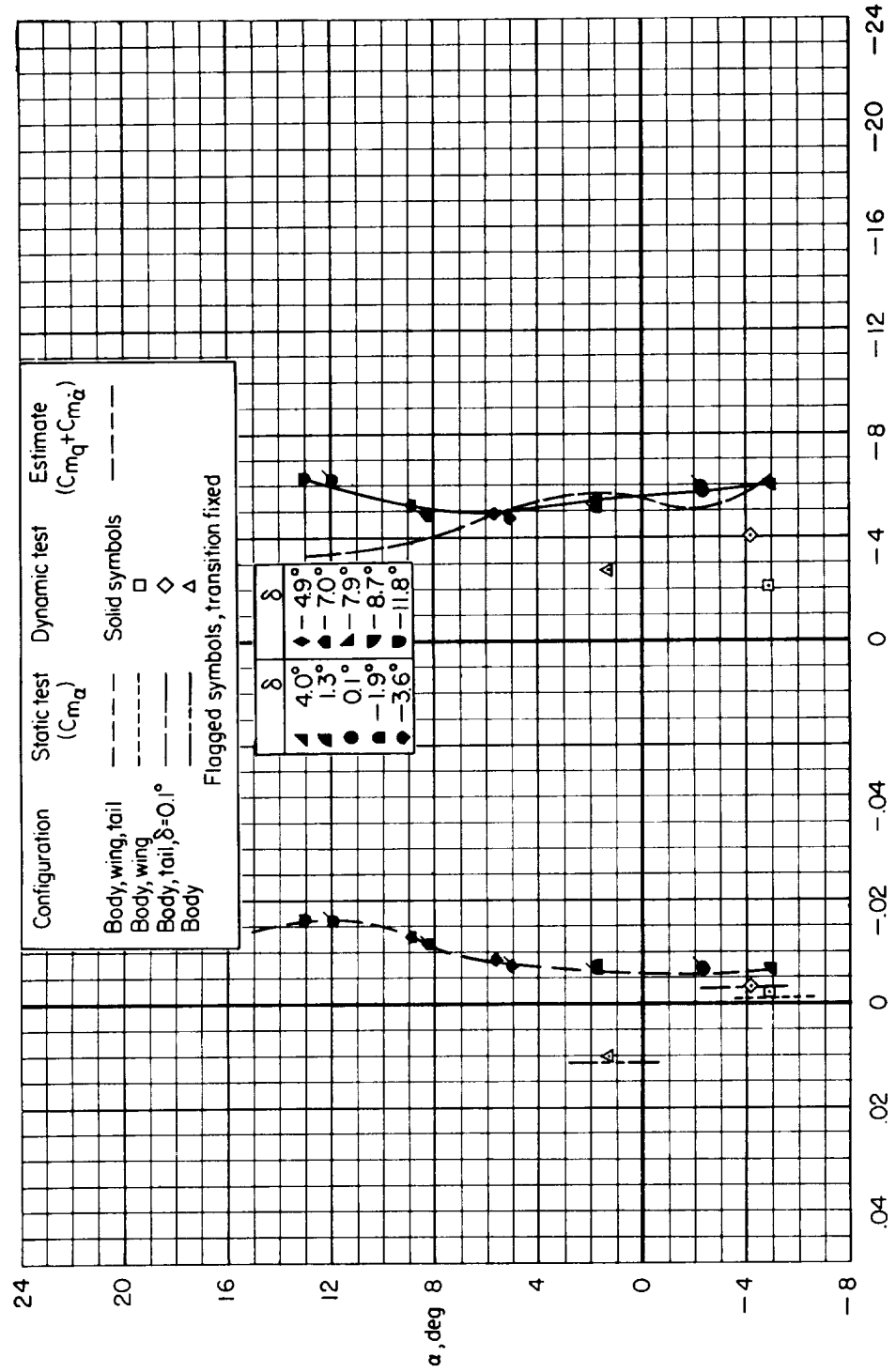

(j) M = 2.2

Figure 7.- Concluded.

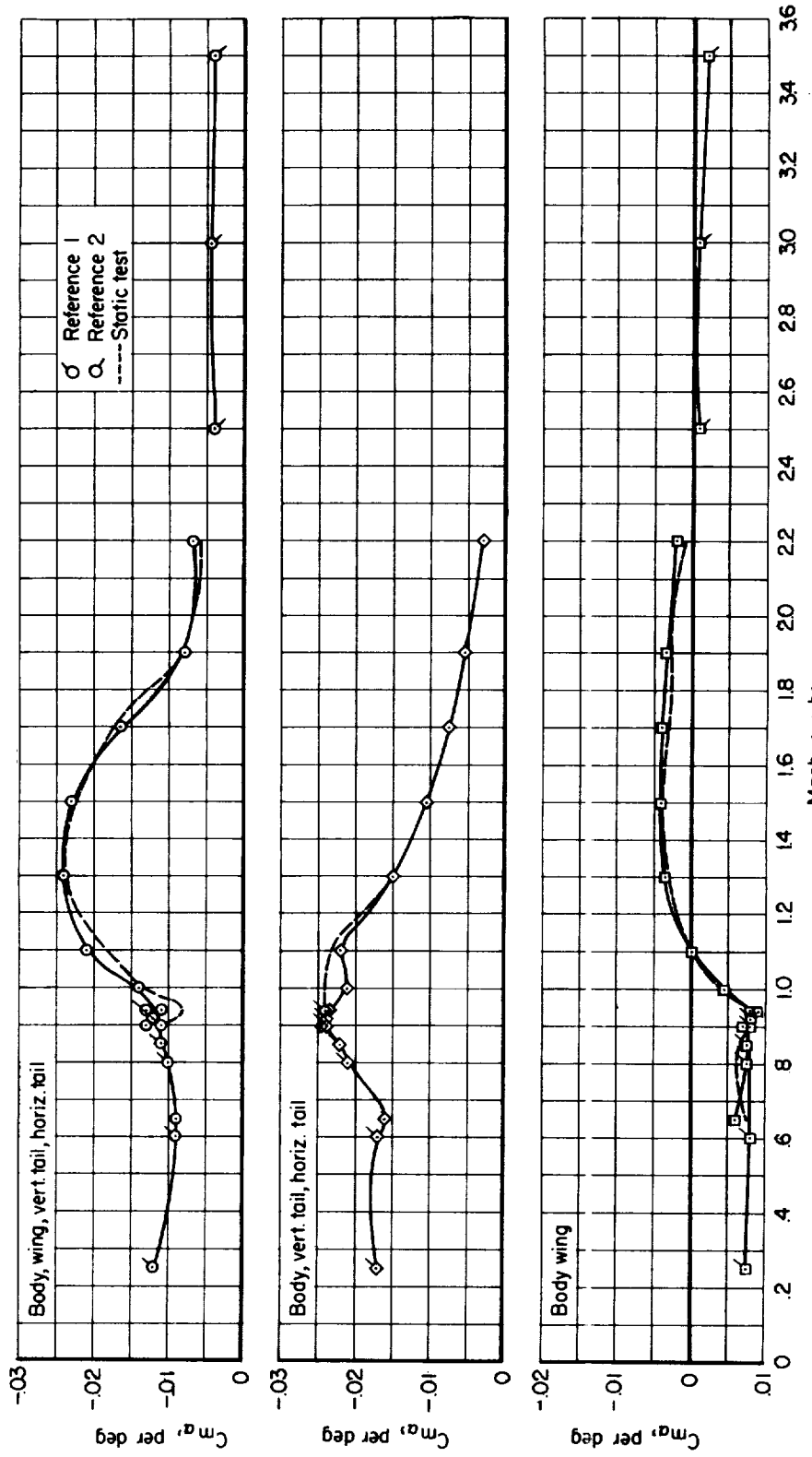

Figure 8.- The variation of C_{m_α} with Mach number. Data from figure 7 are for angles of attack closest to zero.

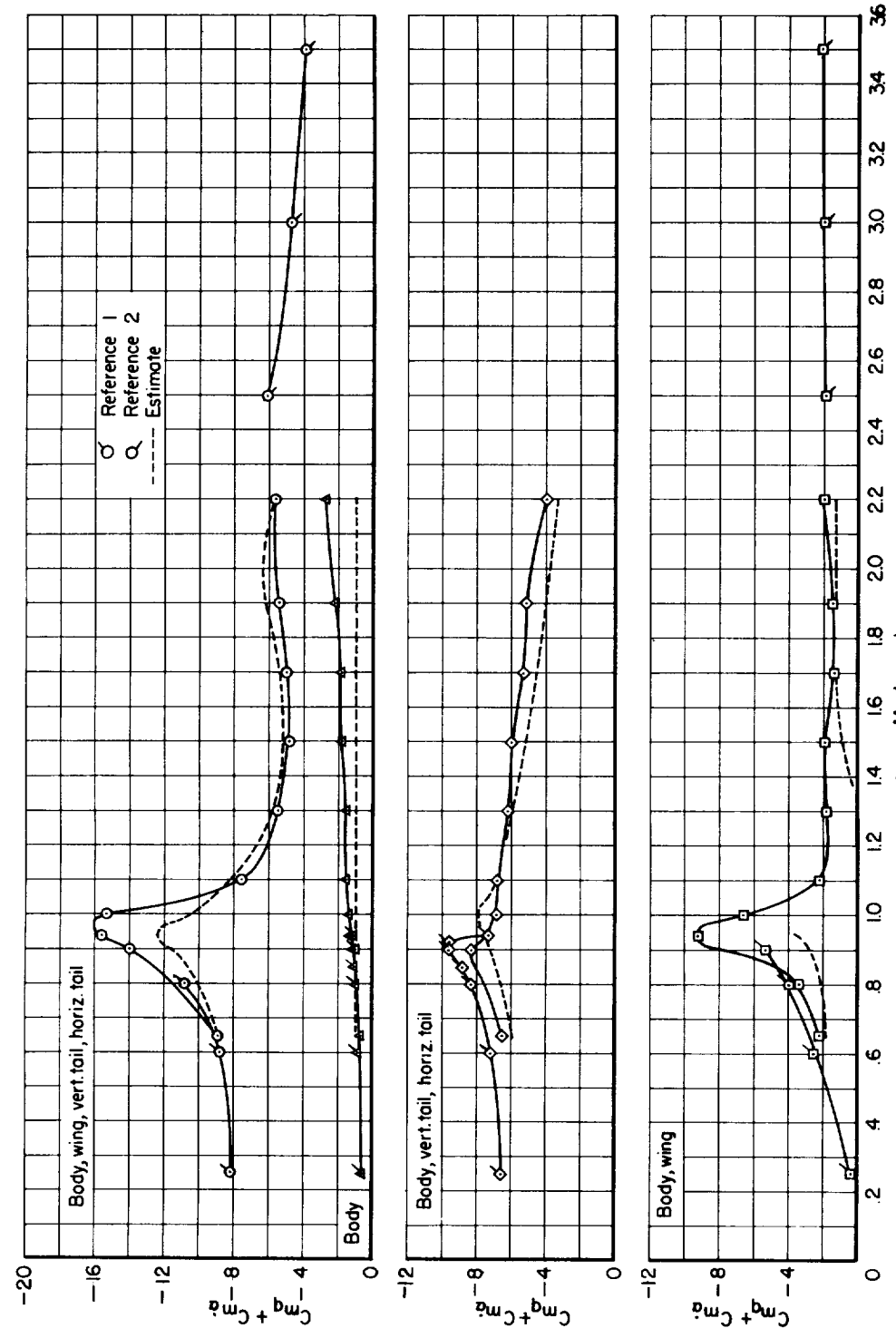

Figure 9.- The variation of $C_{m_q} + C_{m_{\dot{\alpha}}}$ with Mach number. For complete configuration data from figure 7, $\alpha = 0^{\circ}$; data for other component combinations from figure 7 are for angles of attack closest to zero.

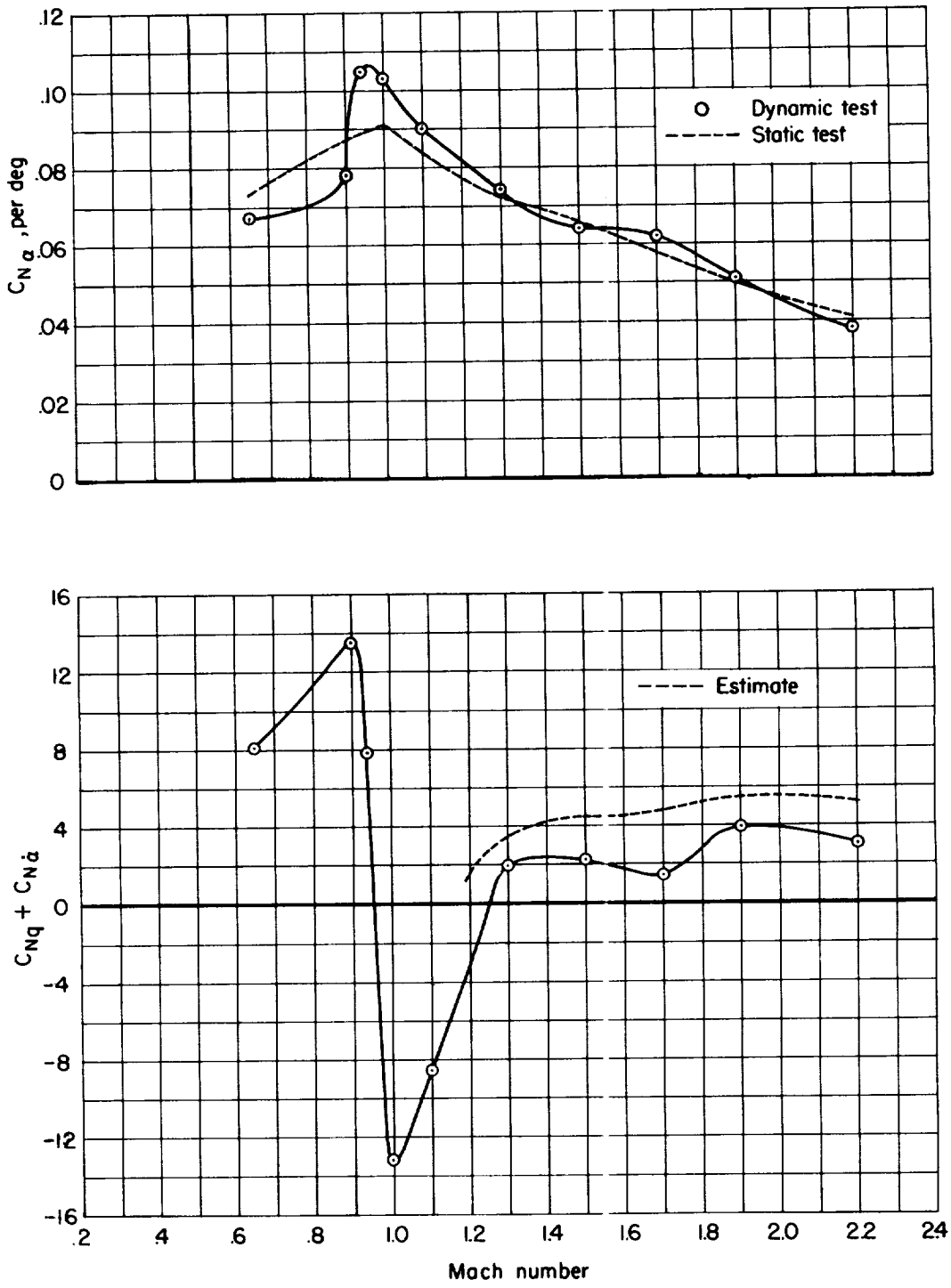

Figure 10.- The variation of C_{N_α} and $C_{N_q} + C_{N_{\dot{\alpha}}}$ with Mach number; complete configuration, $\delta = 0.1^\circ$.

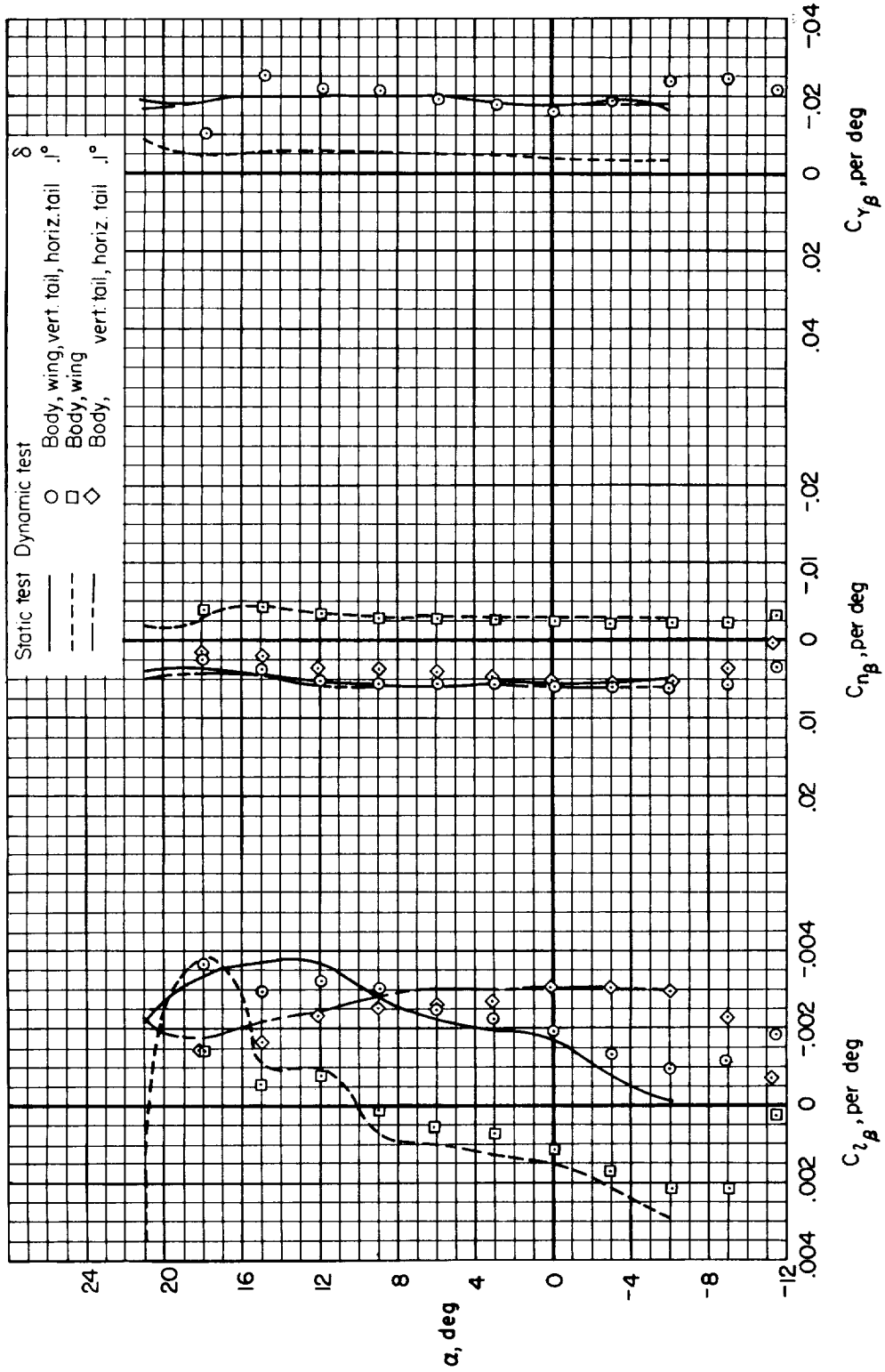

(a) M = 0.65

Figure 11.- The variation of C_{l_β}, C_{n_β}, C_{Y_β} with angle of attack.

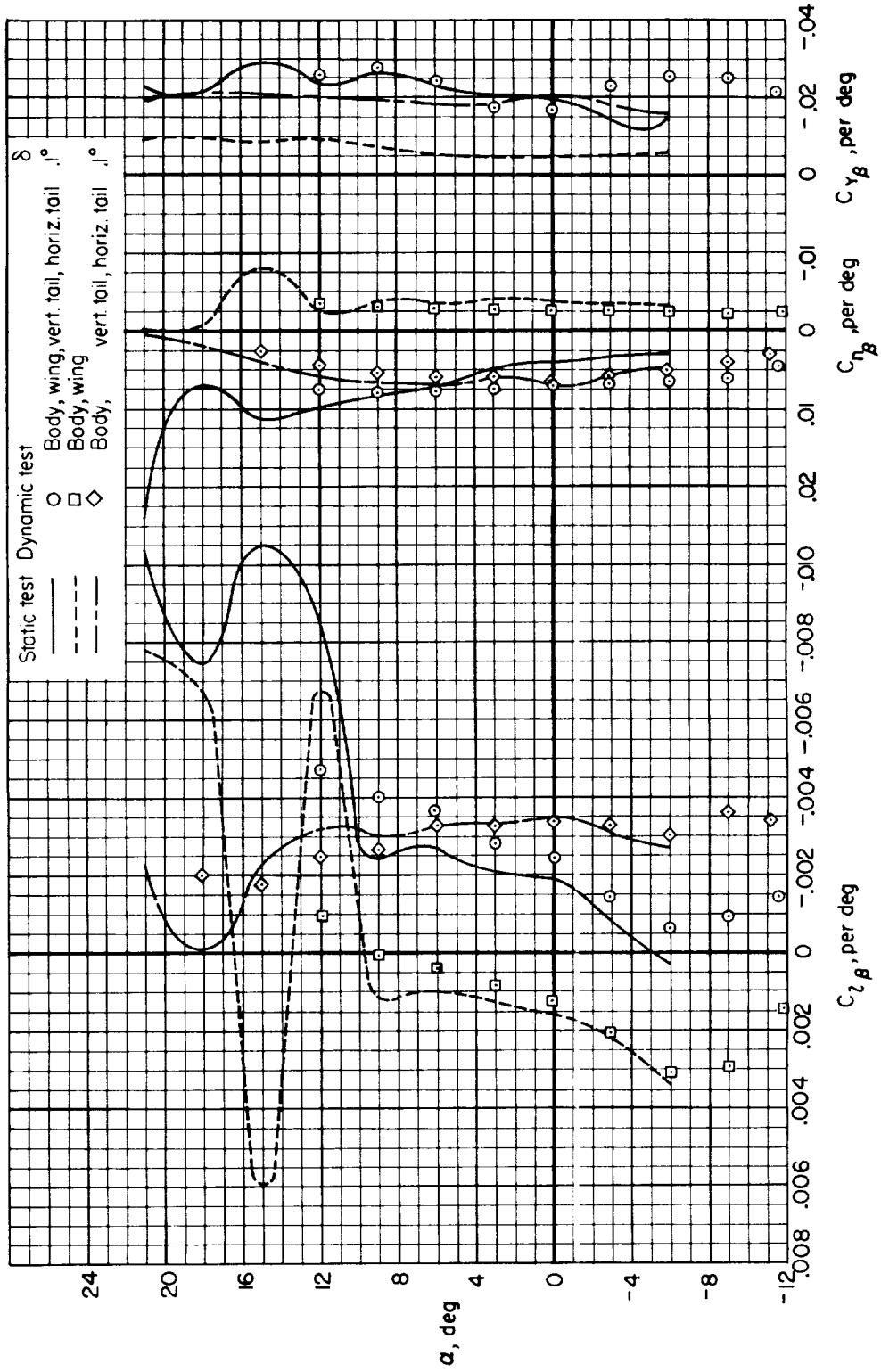

(b) M = 0.90

Figure 11.- Continued.

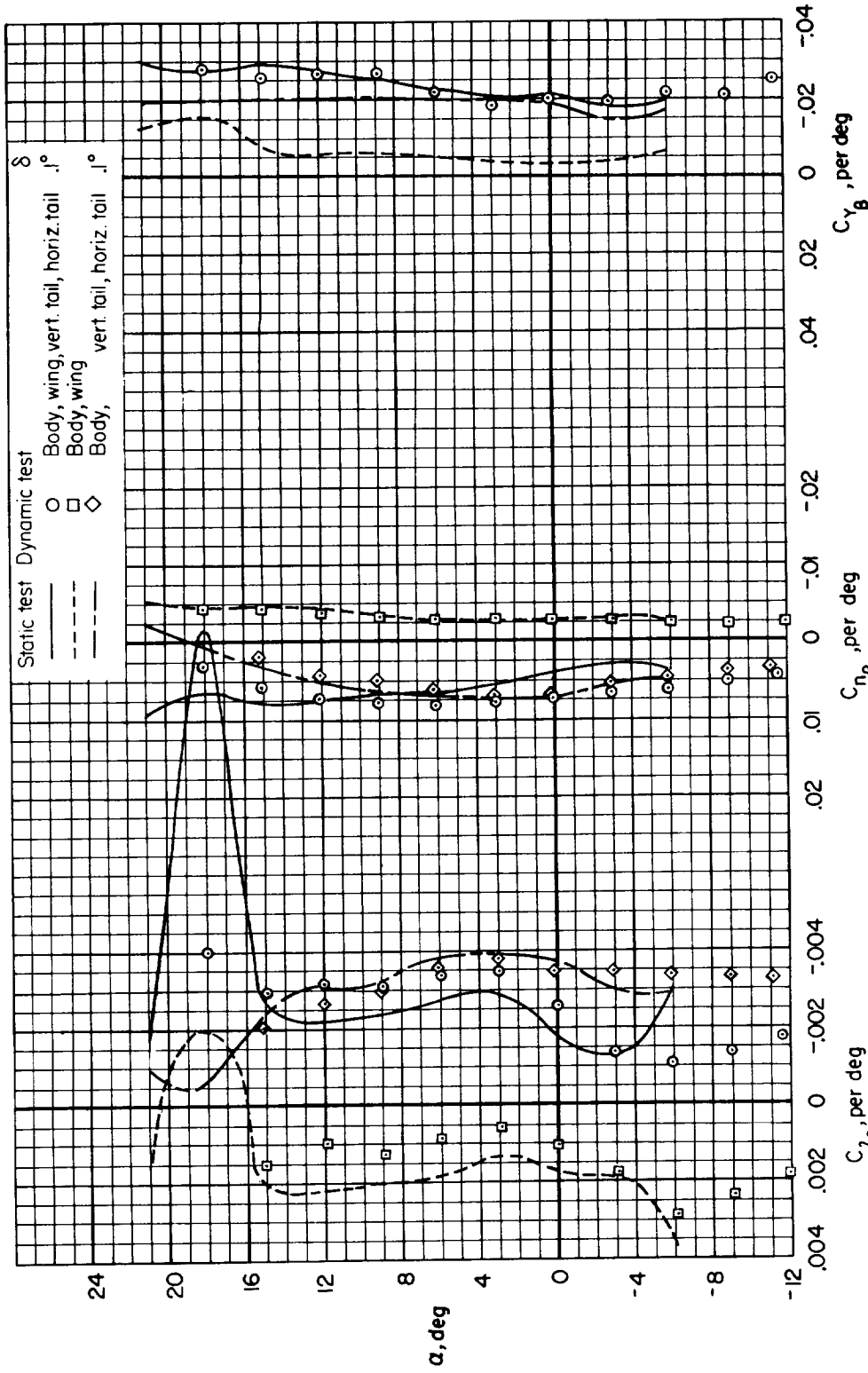

(c) M = 0.94

Figure 11.- Continued.

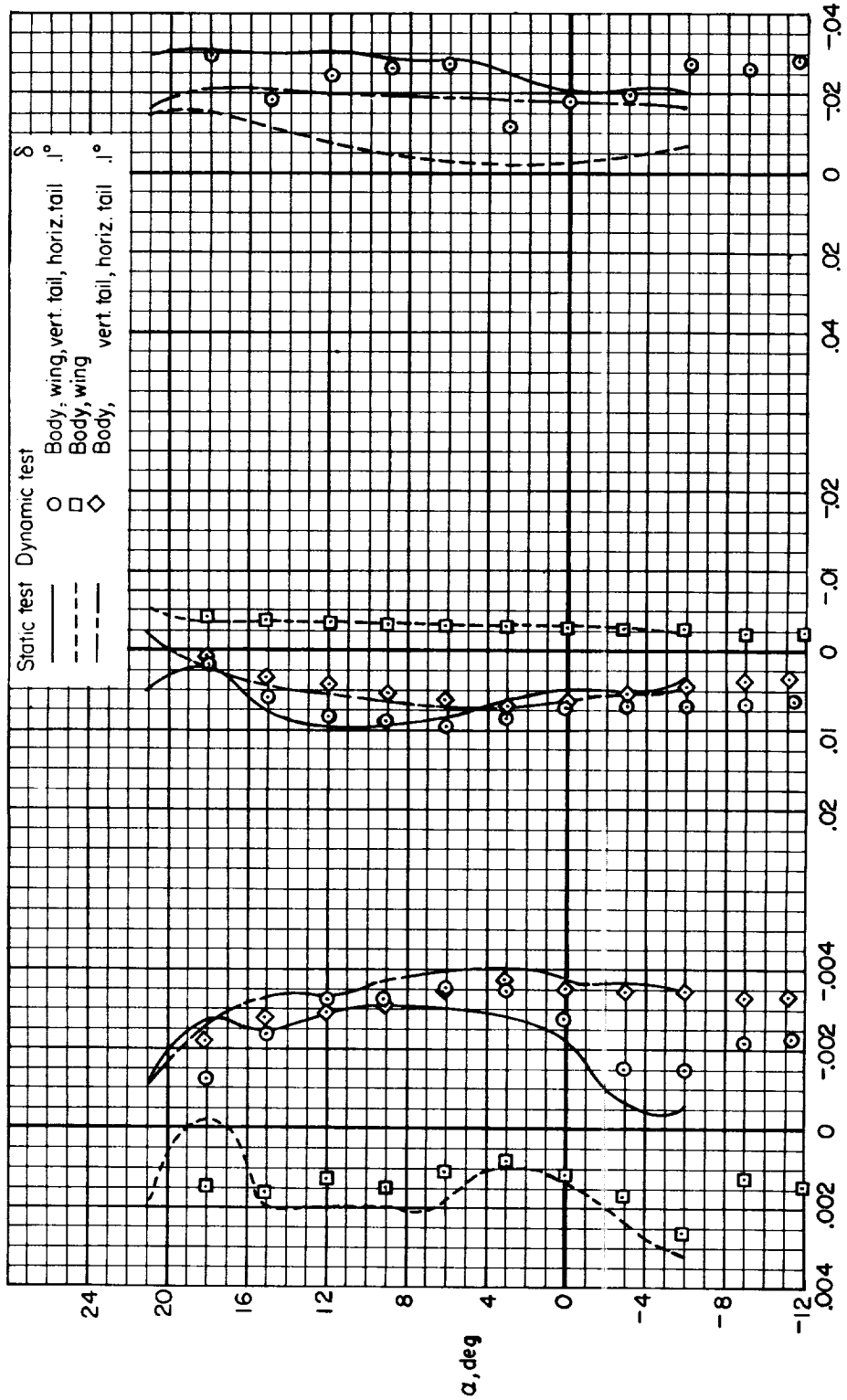

(d) M = 1.0

Figure 11.- Continued.

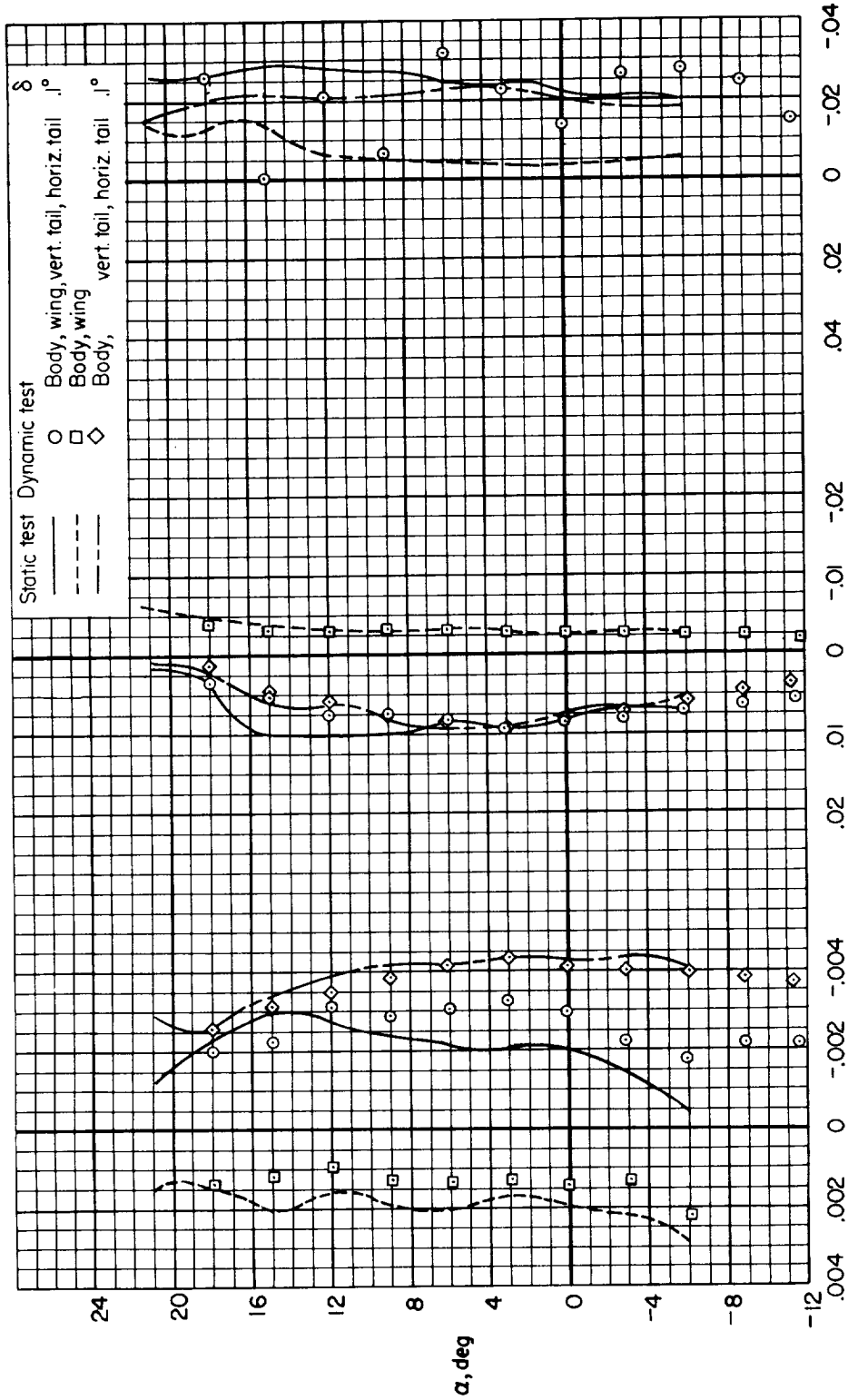

(e) M = 1.1

Figure 11.- Continued.

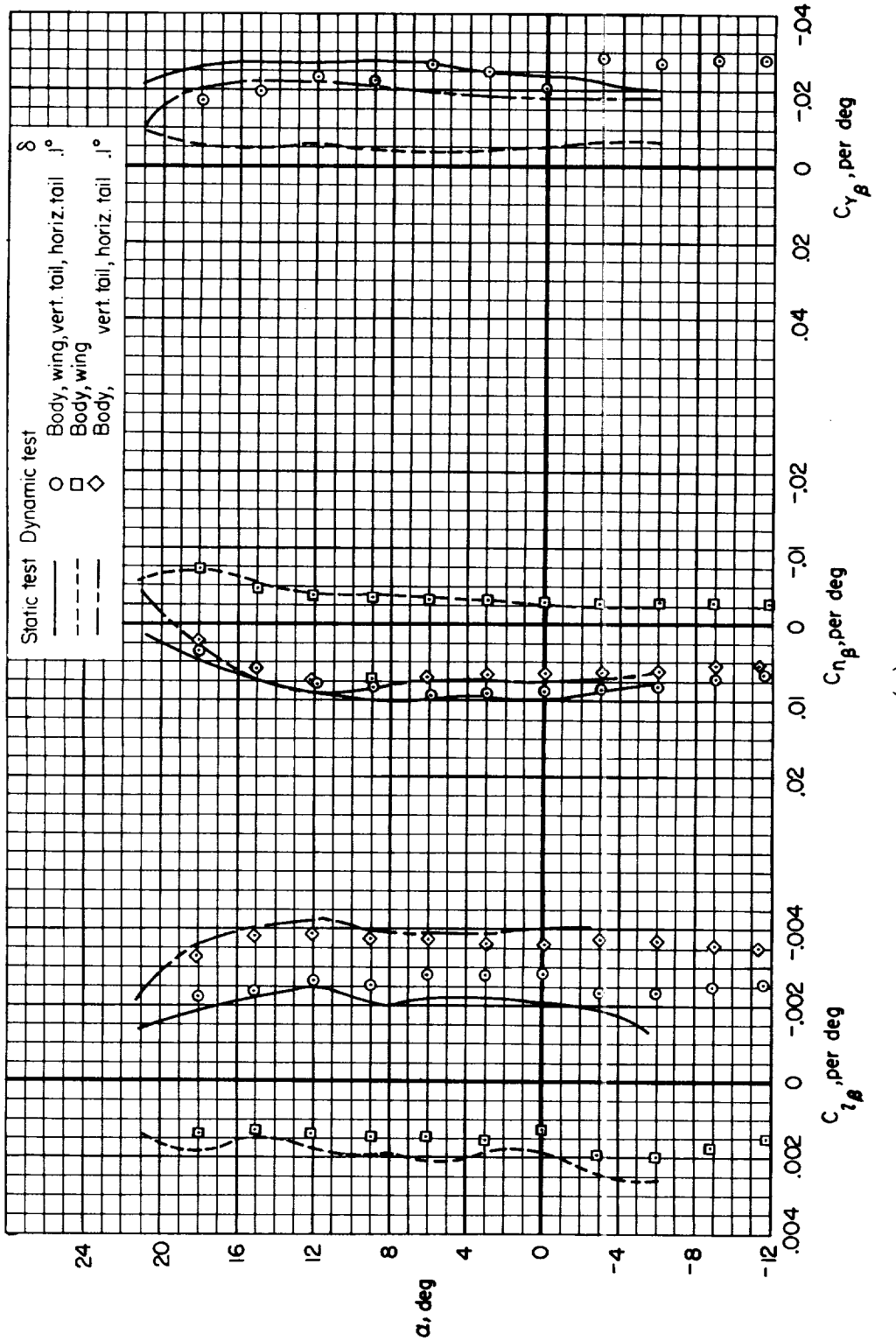

(f) M = 1.3

Figure 11.- Continued.

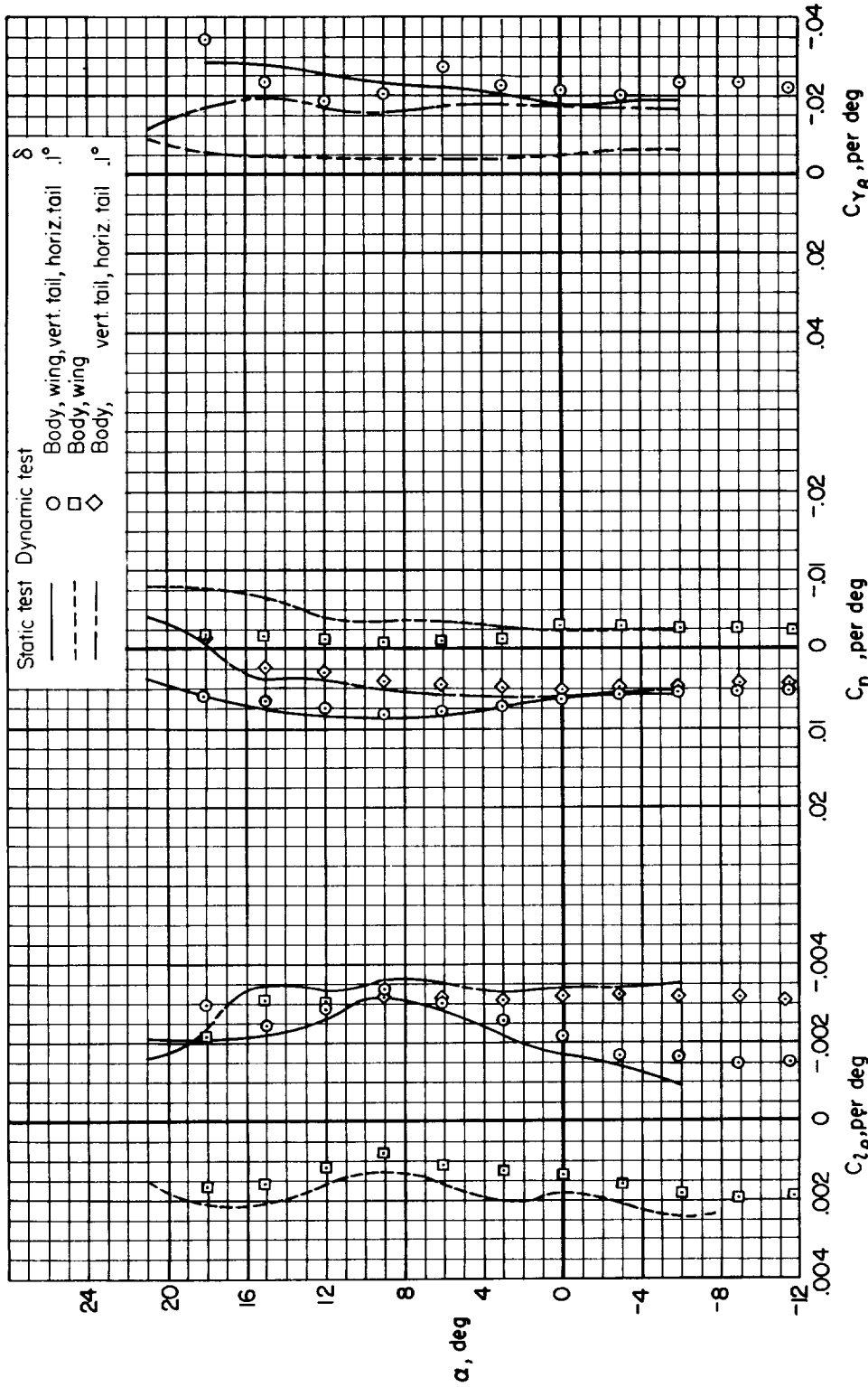

(g) M = 1.5

Figure 11.- Continued.

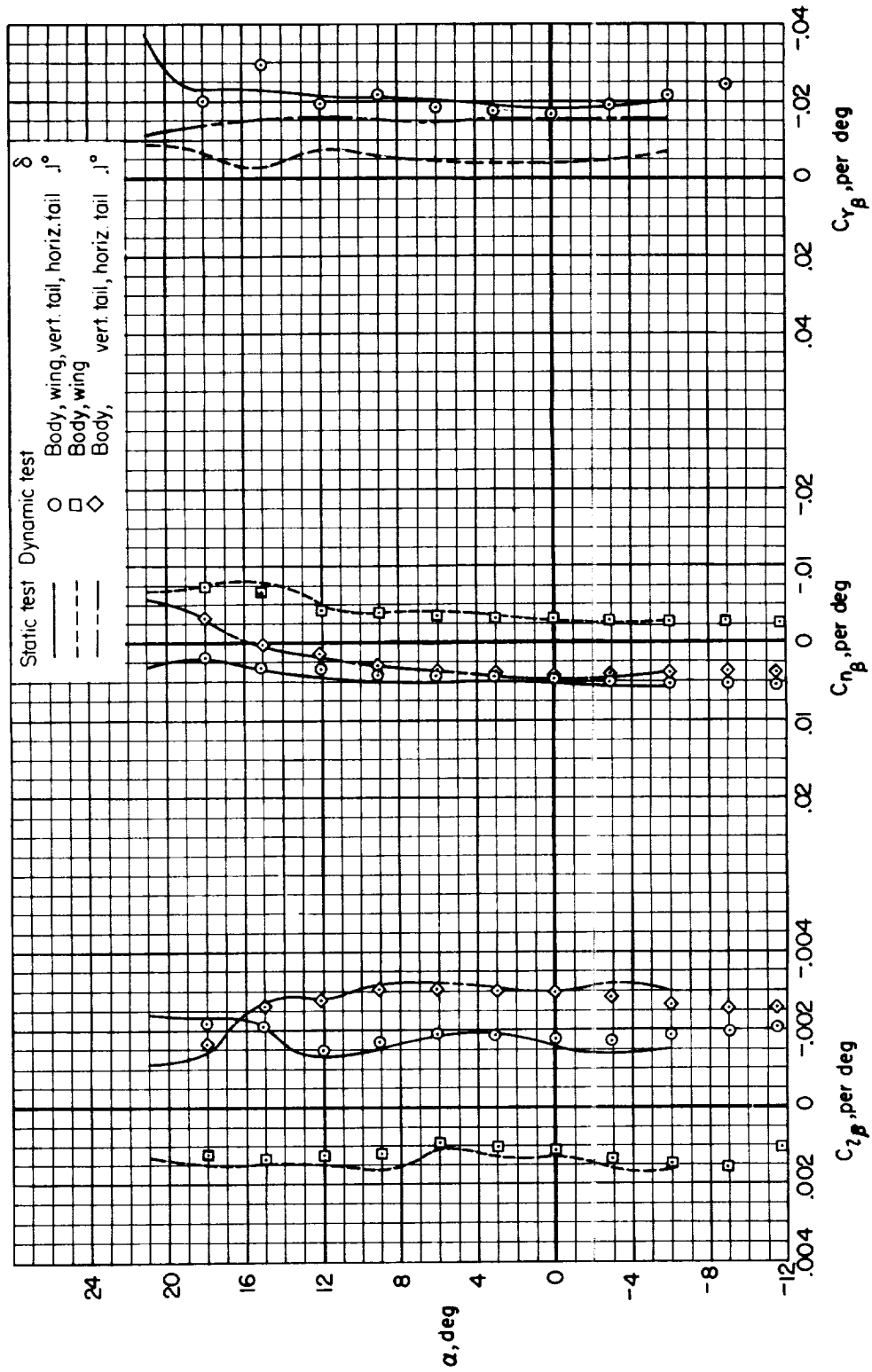

(h) M = 1.7

Figure 11.- Continued.

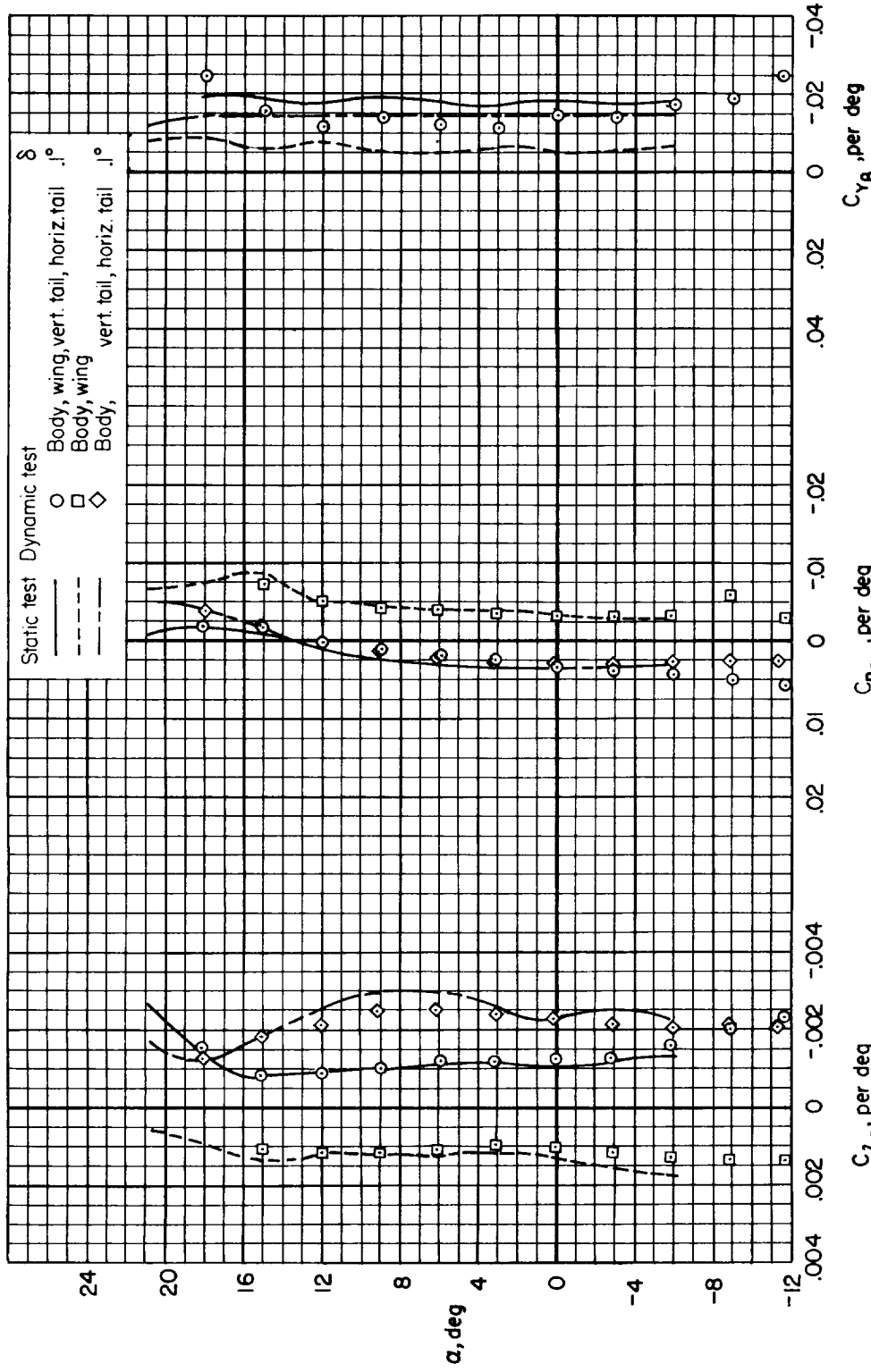

(i) $\bar{M} = 1.9$

Figure 11.- Continued.

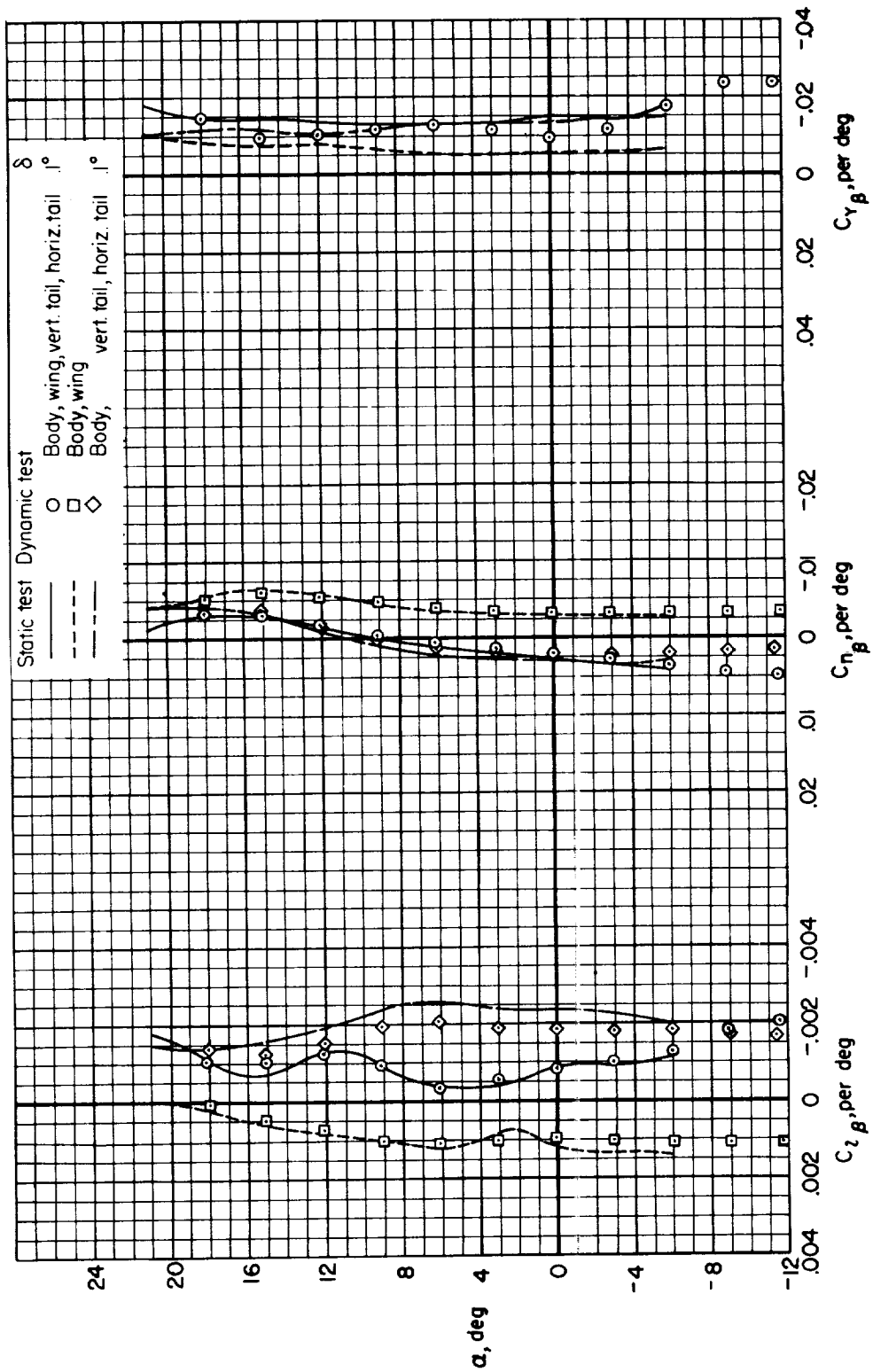

(j) M = 2.2

Figure 11.- Concluded.

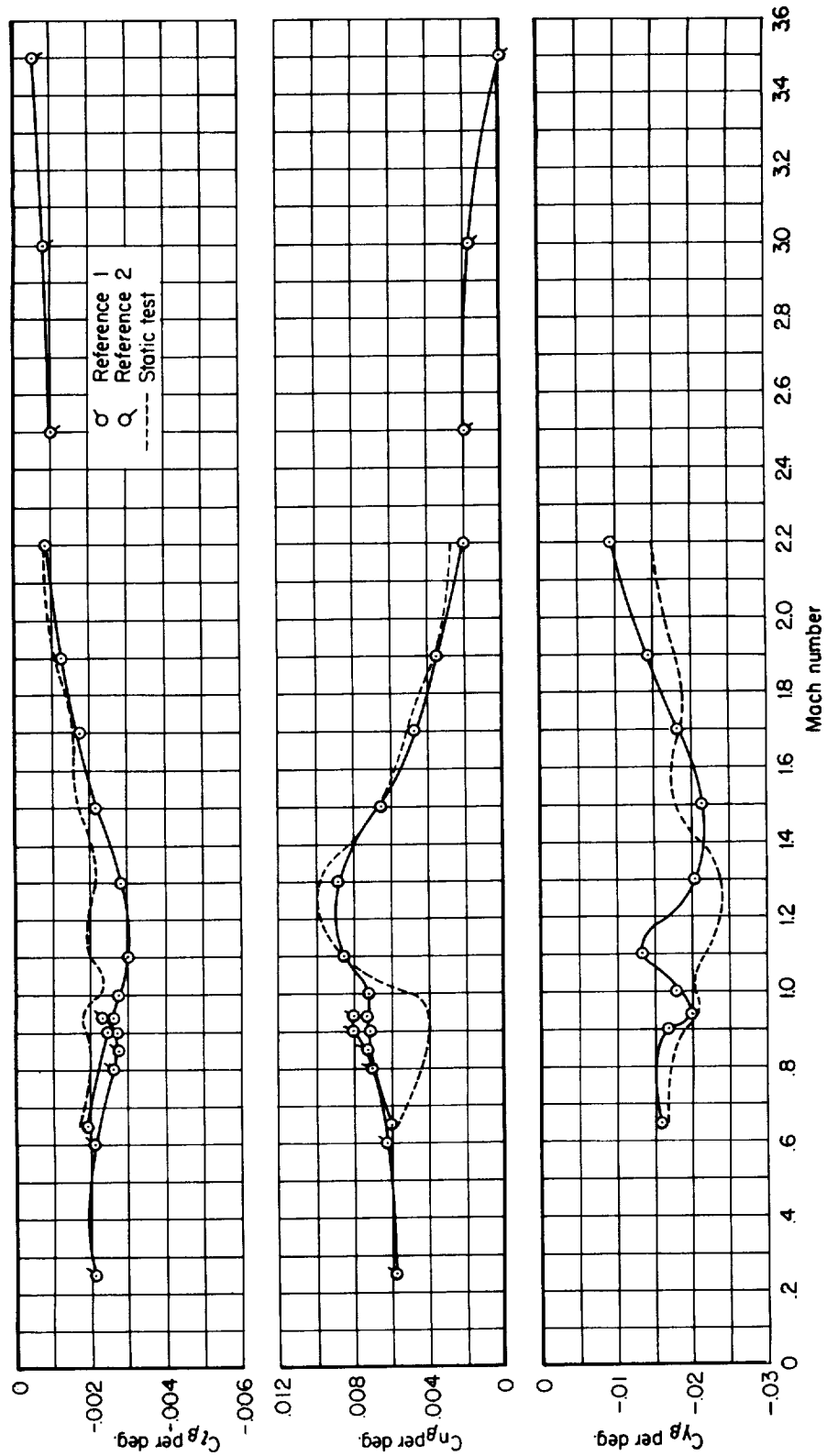

Figure 12.- The variation of C_{l_β}, C_{n_β}, C_{Y_β} with Mach number. Complete configuration, $\delta = 0.1^\circ$, $\alpha = 0^\circ$.

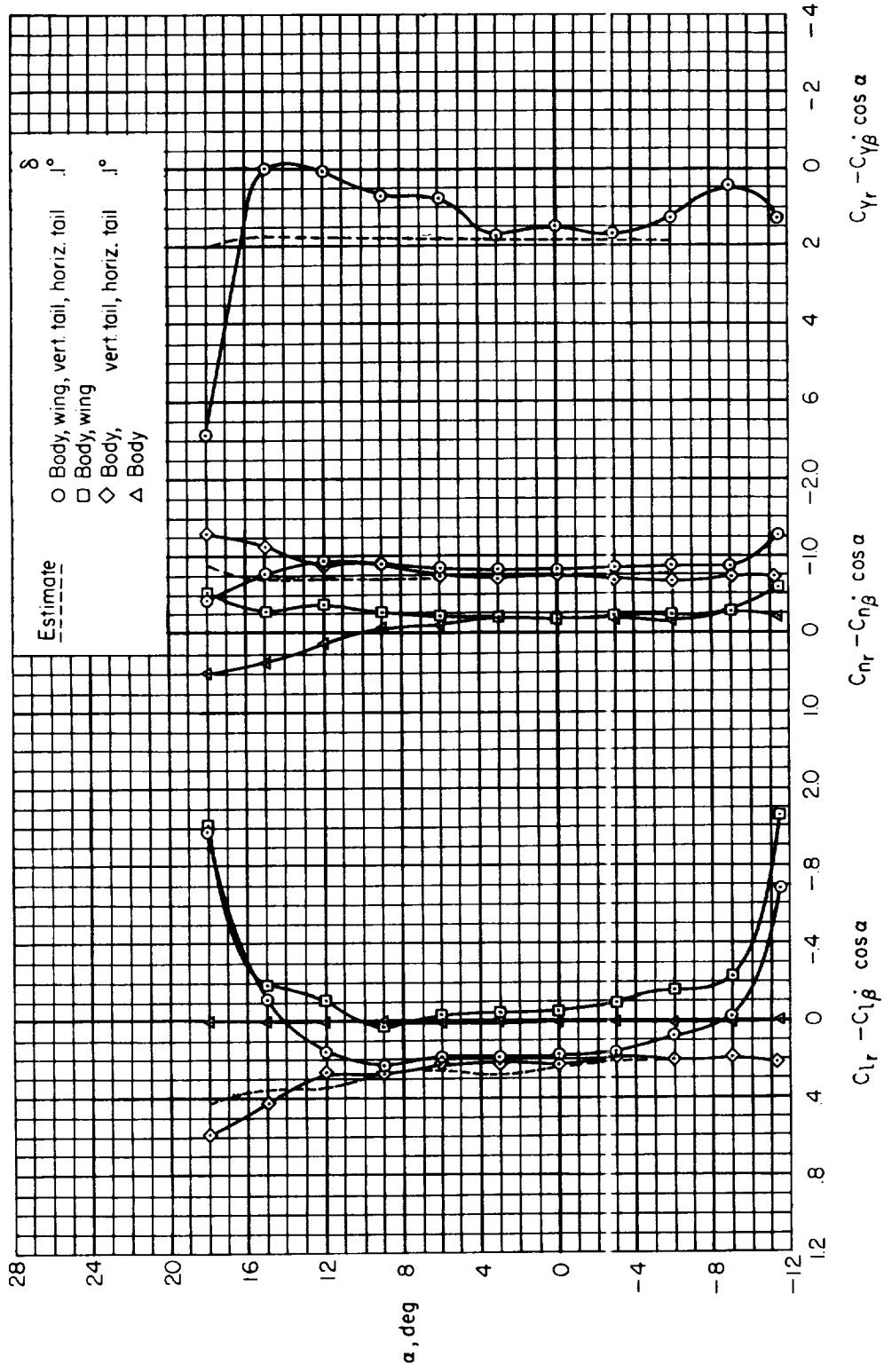

(a) M = 0.65

Figure 13.- The variation of $C_{l_r} - C_{l_{\dot{\beta}}} \cos\alpha$, $C_{n_r} - C_{n_{\dot{\beta}}} \cos\alpha$, $C_{Y_r} - C_{Y_{\dot{\beta}}} \cos\alpha$ with angle of attack.

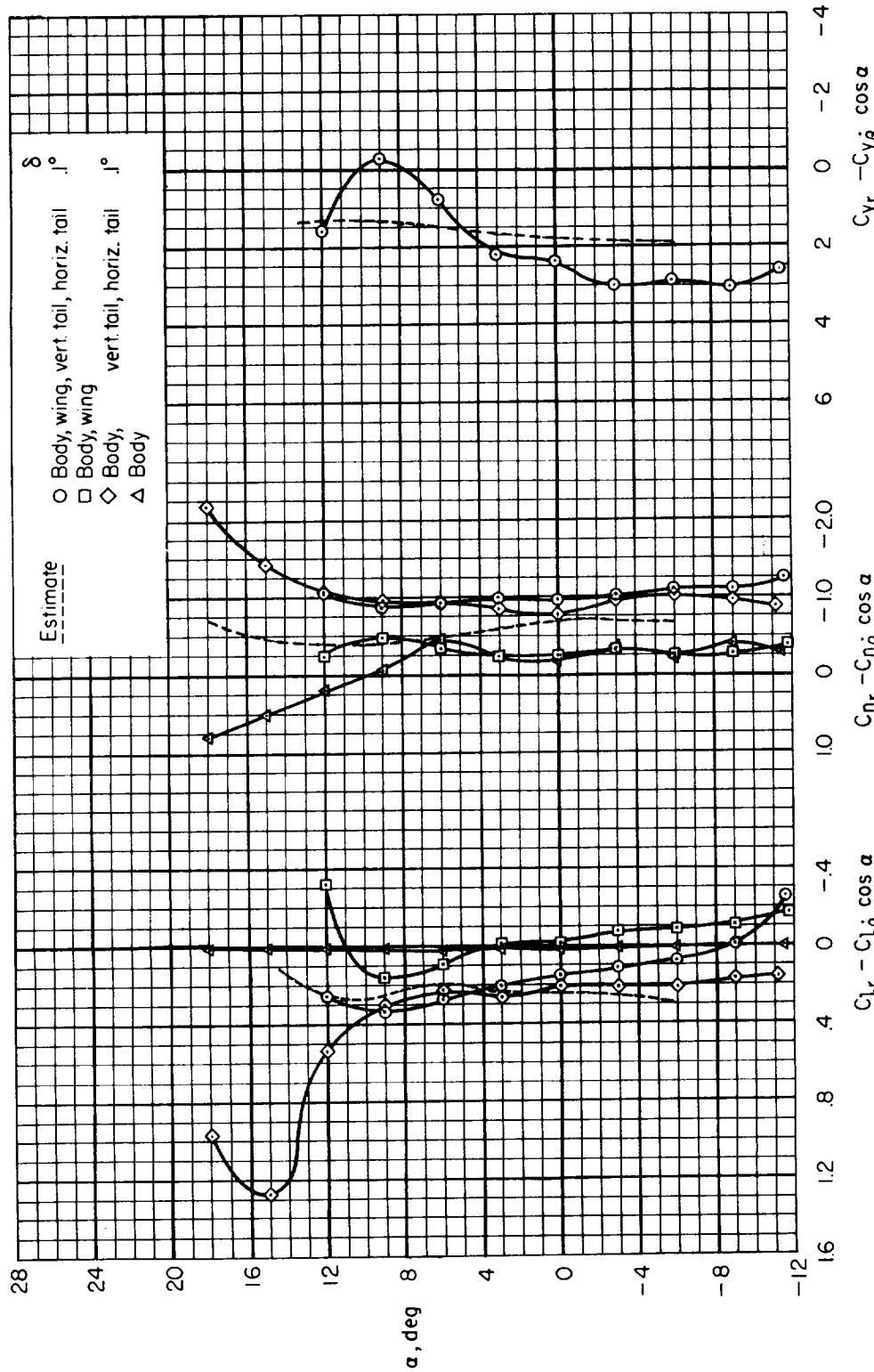

(b) M = 0.90

Figure 13.- Continued.

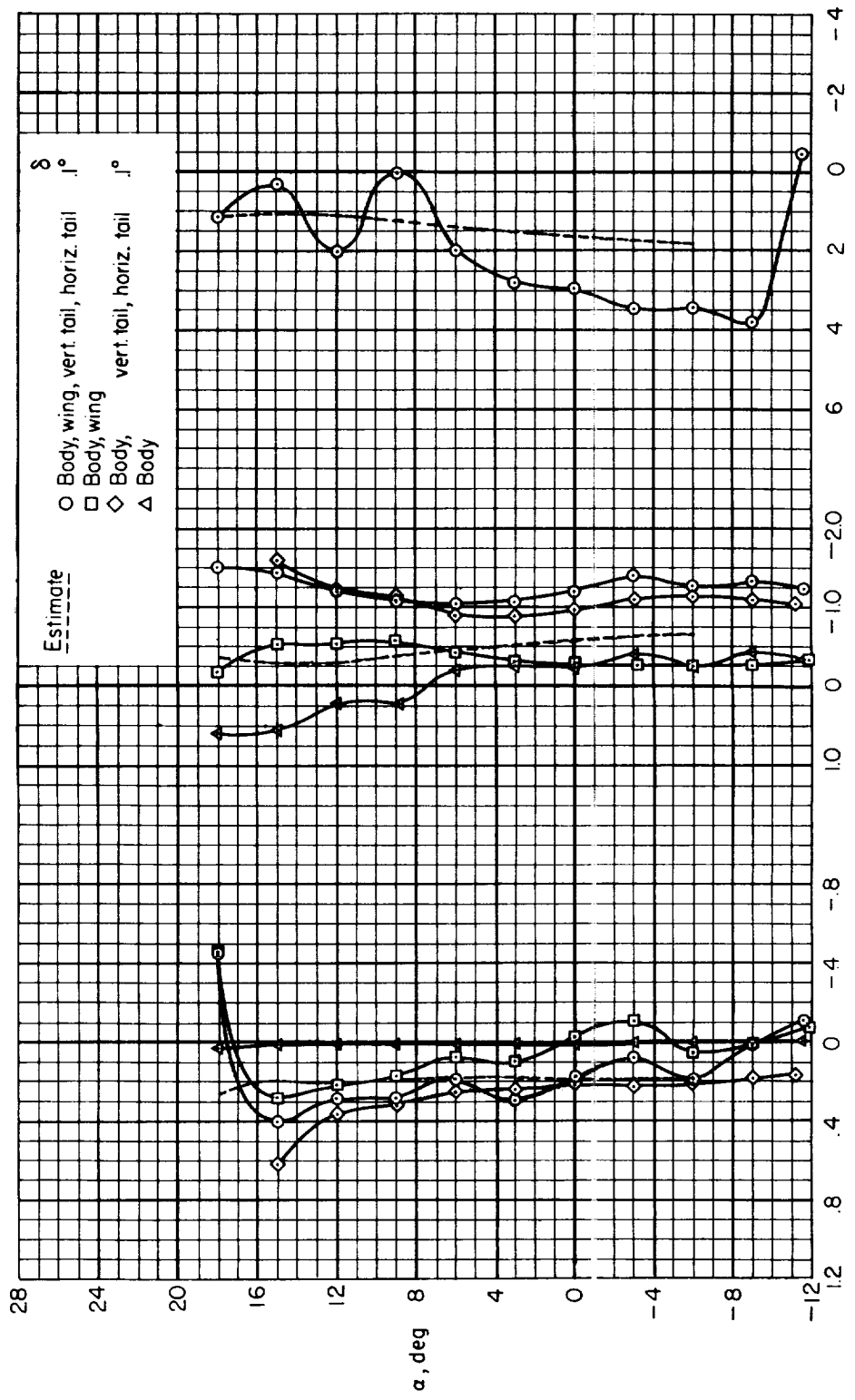

(c) M = 0.94

Figure 13.- Continued.

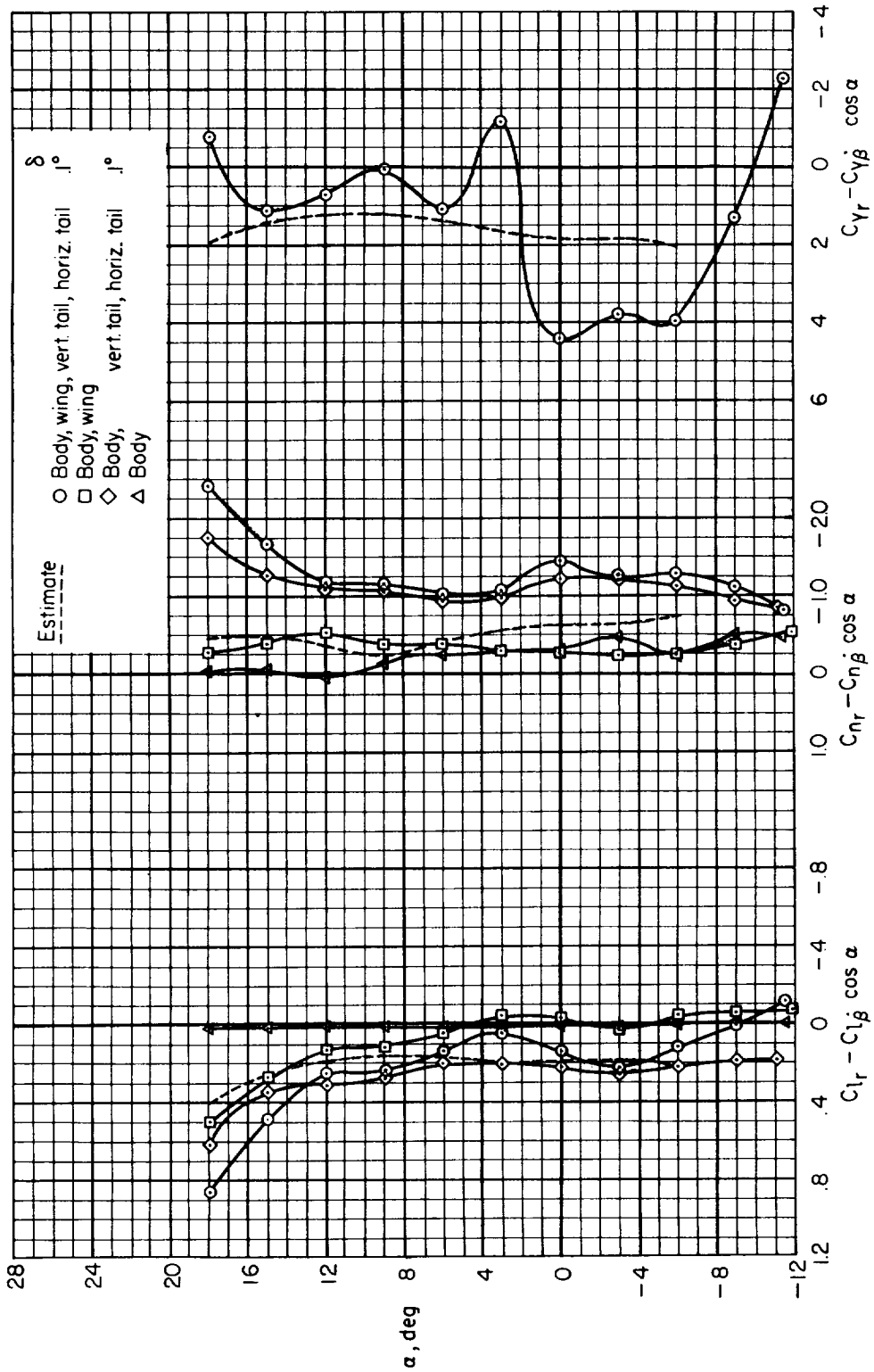

(d) M = 1.0

Figure 13.- Continued.

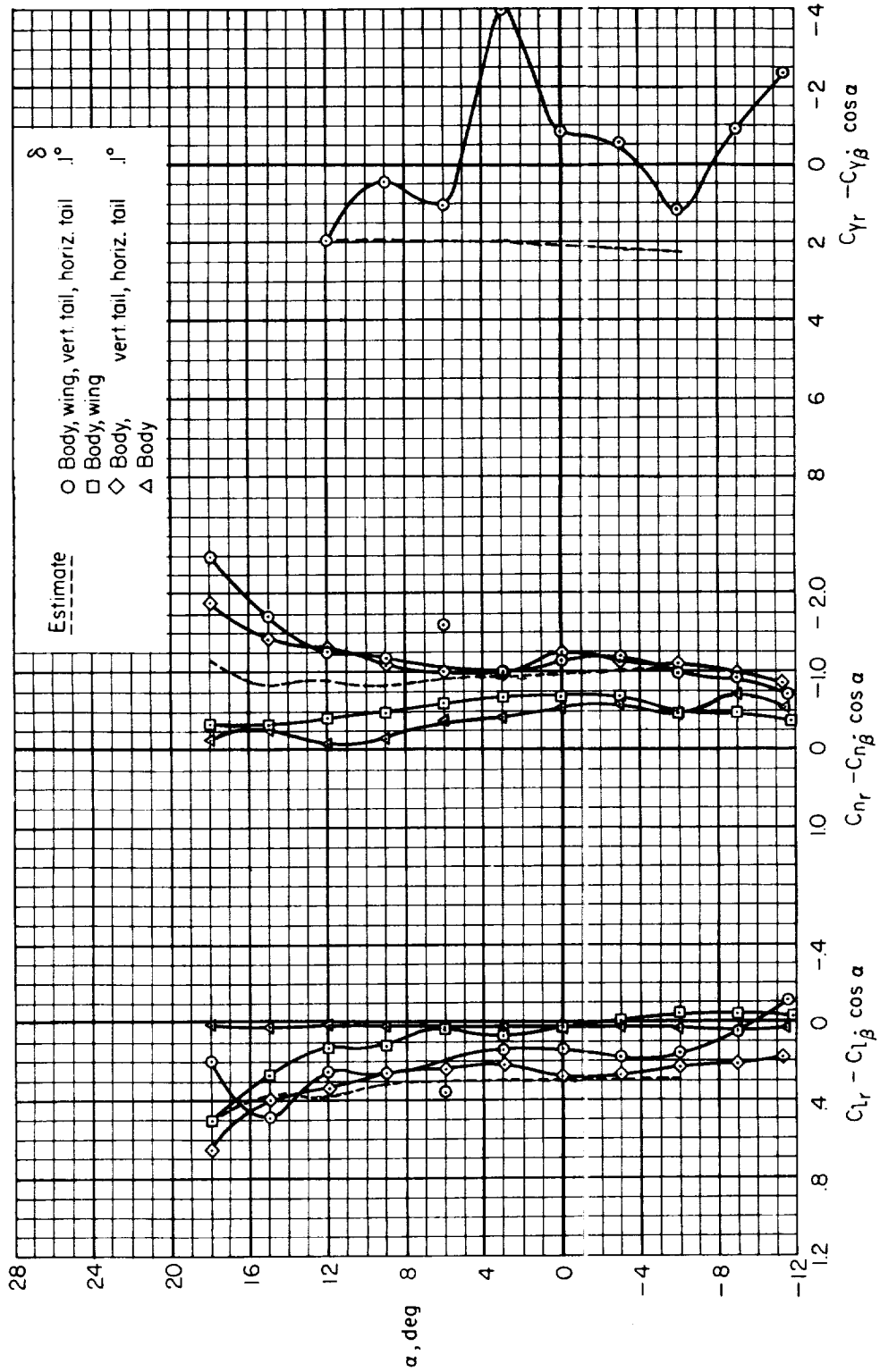

(e) M = 1.1

Figure 13.- Continued.

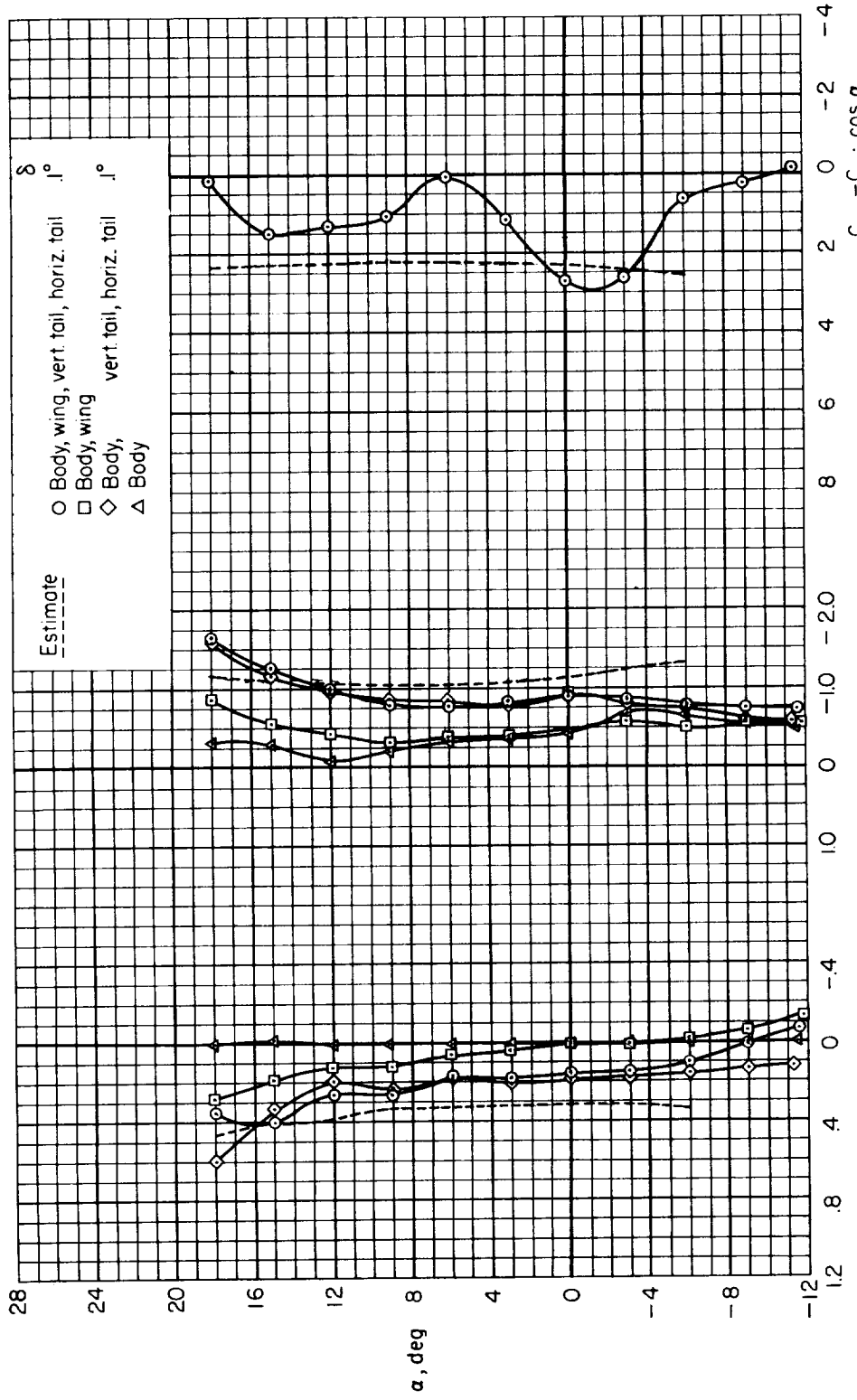

(f) M = 1.3

Figure 13.- Continued.

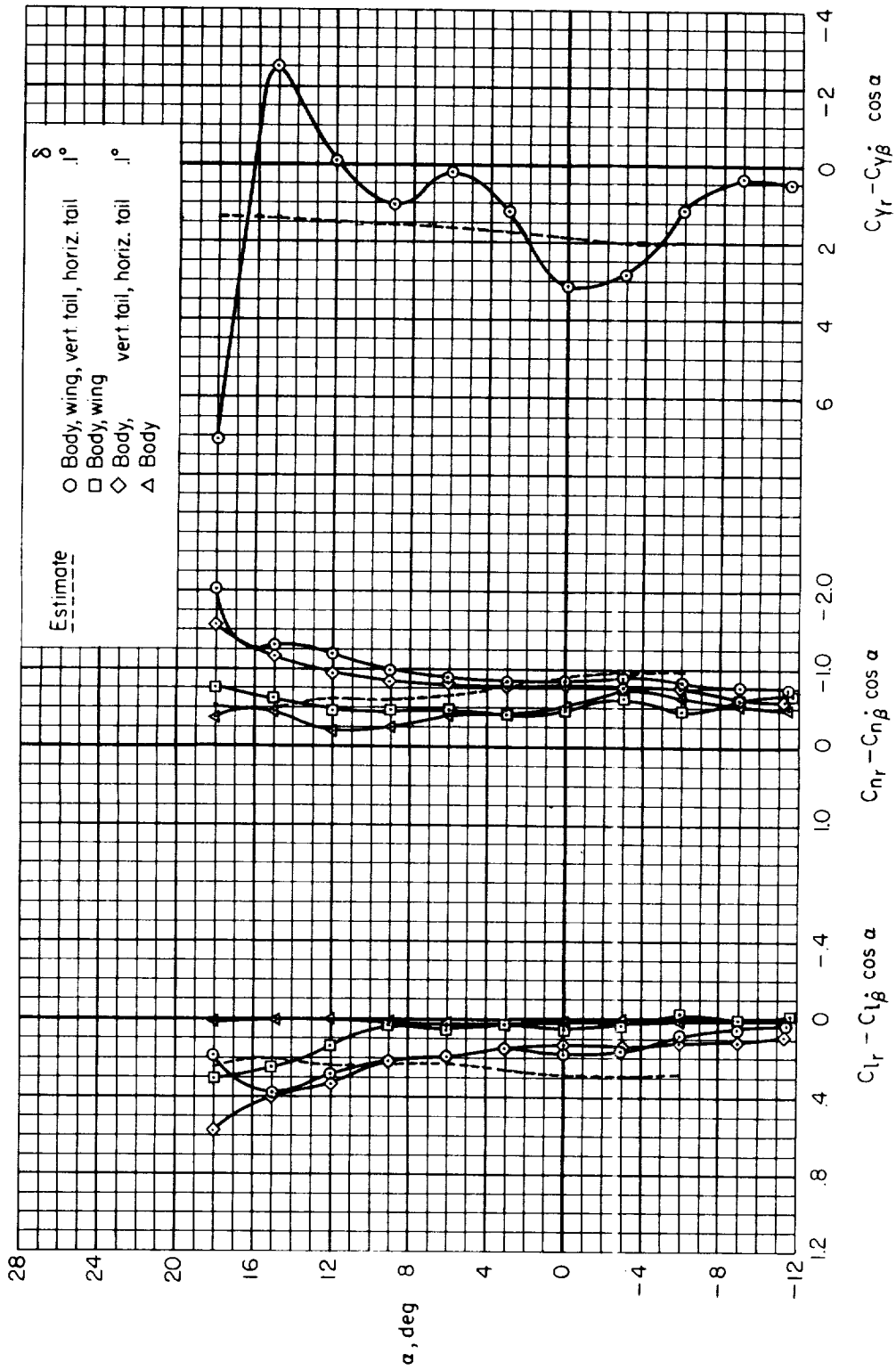

(g) M = 1.5

Figure 13.- Continued.

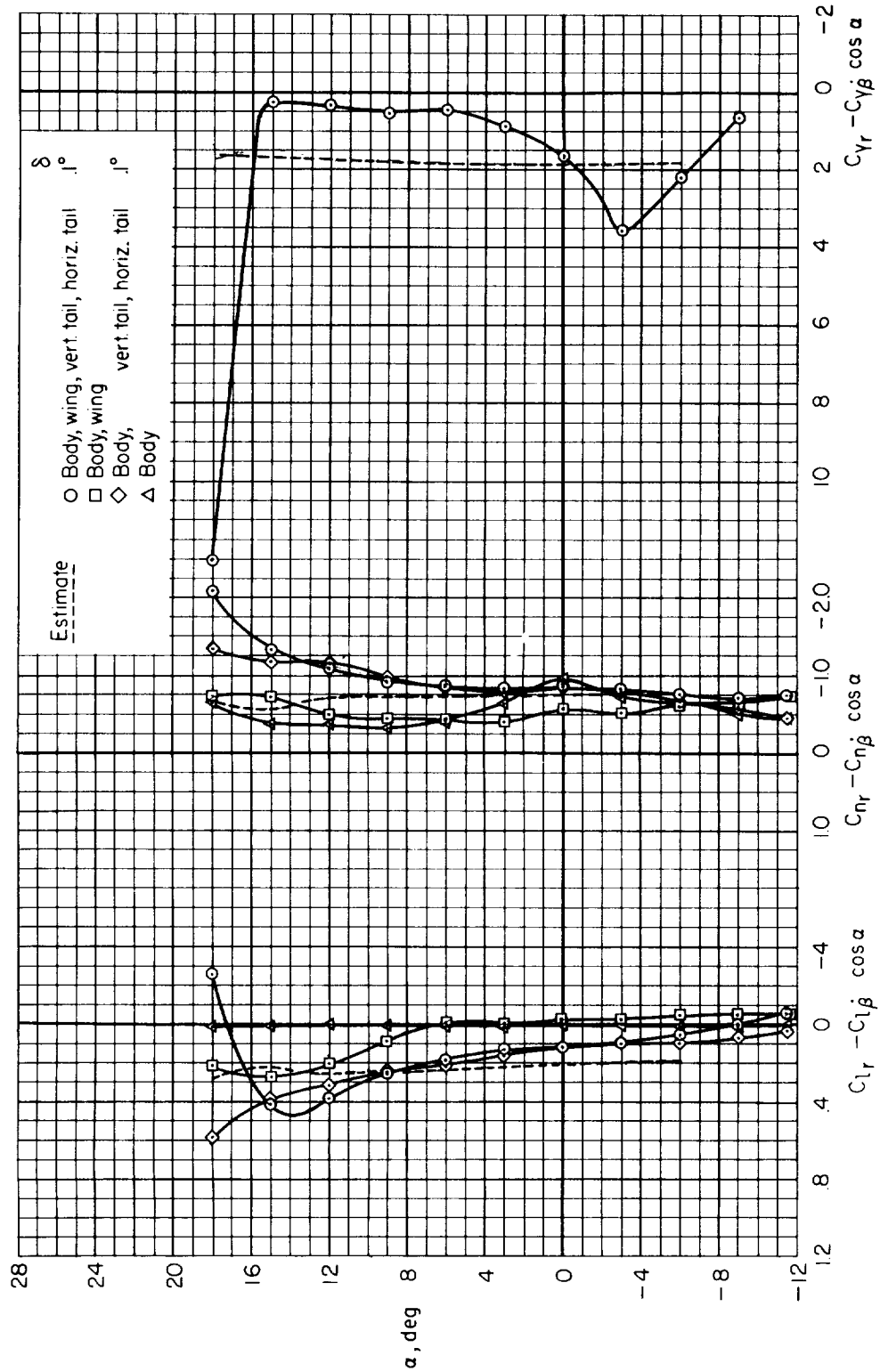

(h) M = 1.7

Figure 13.- Continued.

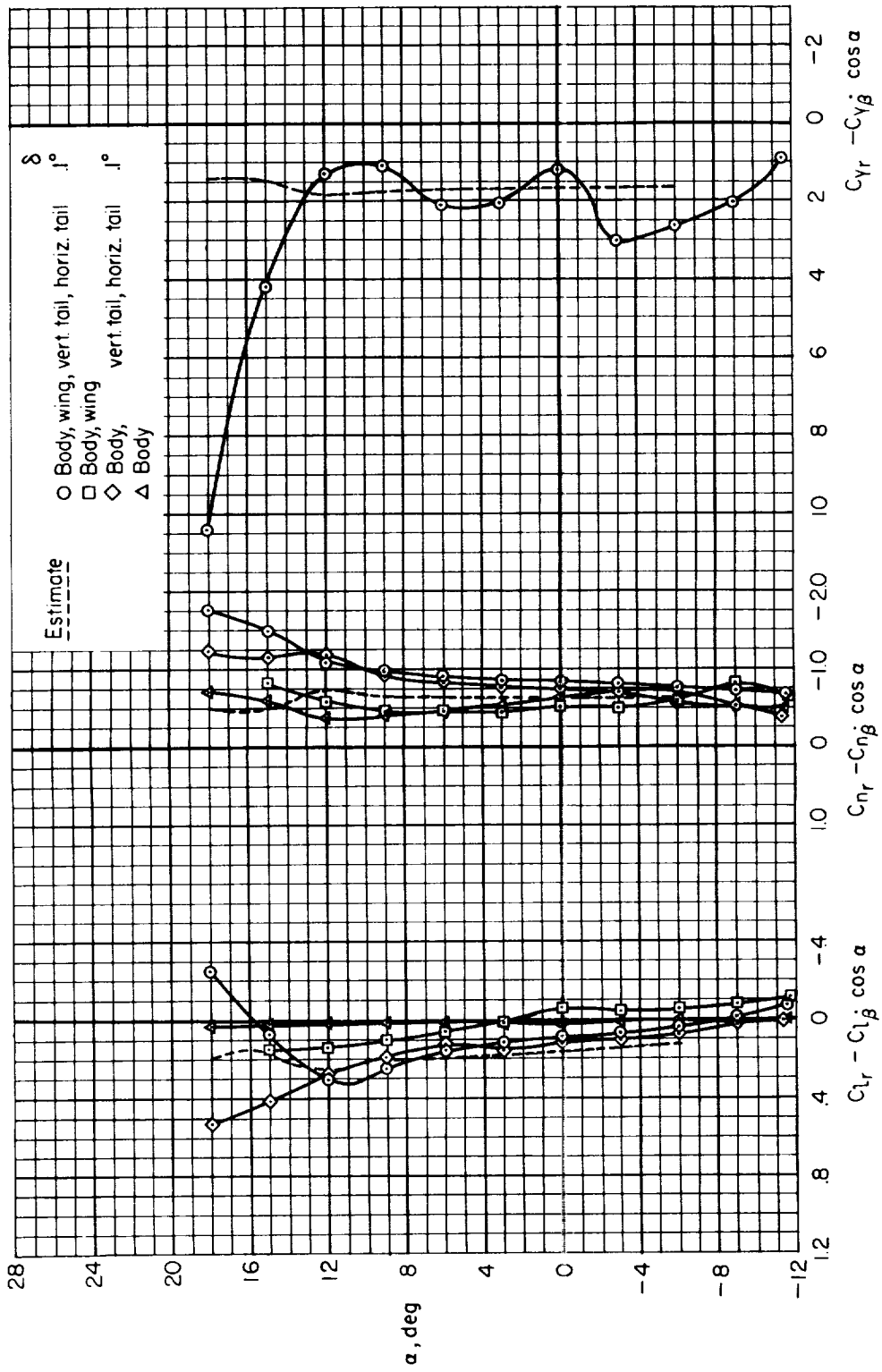

(i) M = 1.9

Figure 13.- Continued.

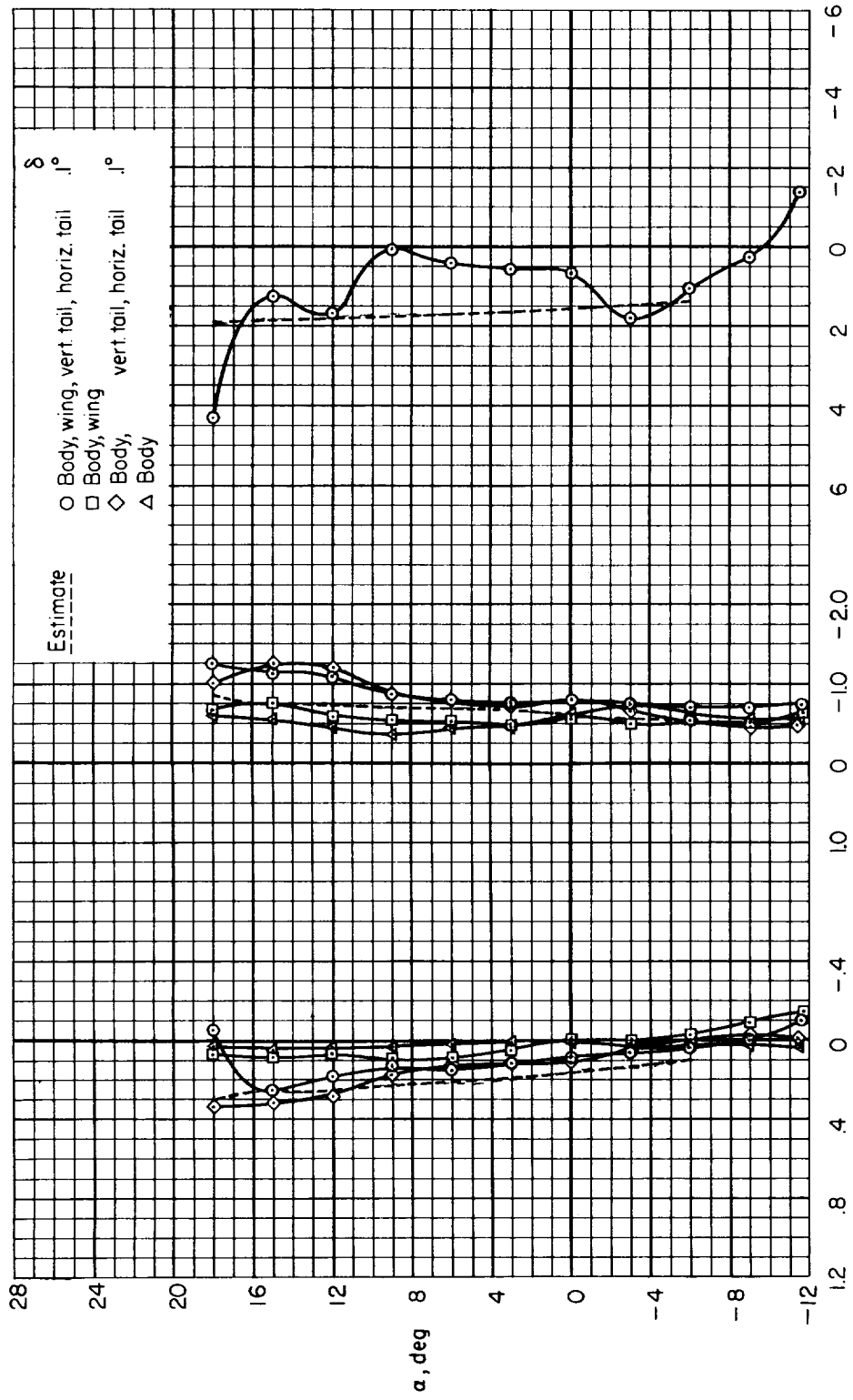

(j) M = 2.2

Figure 13.- Concluded.

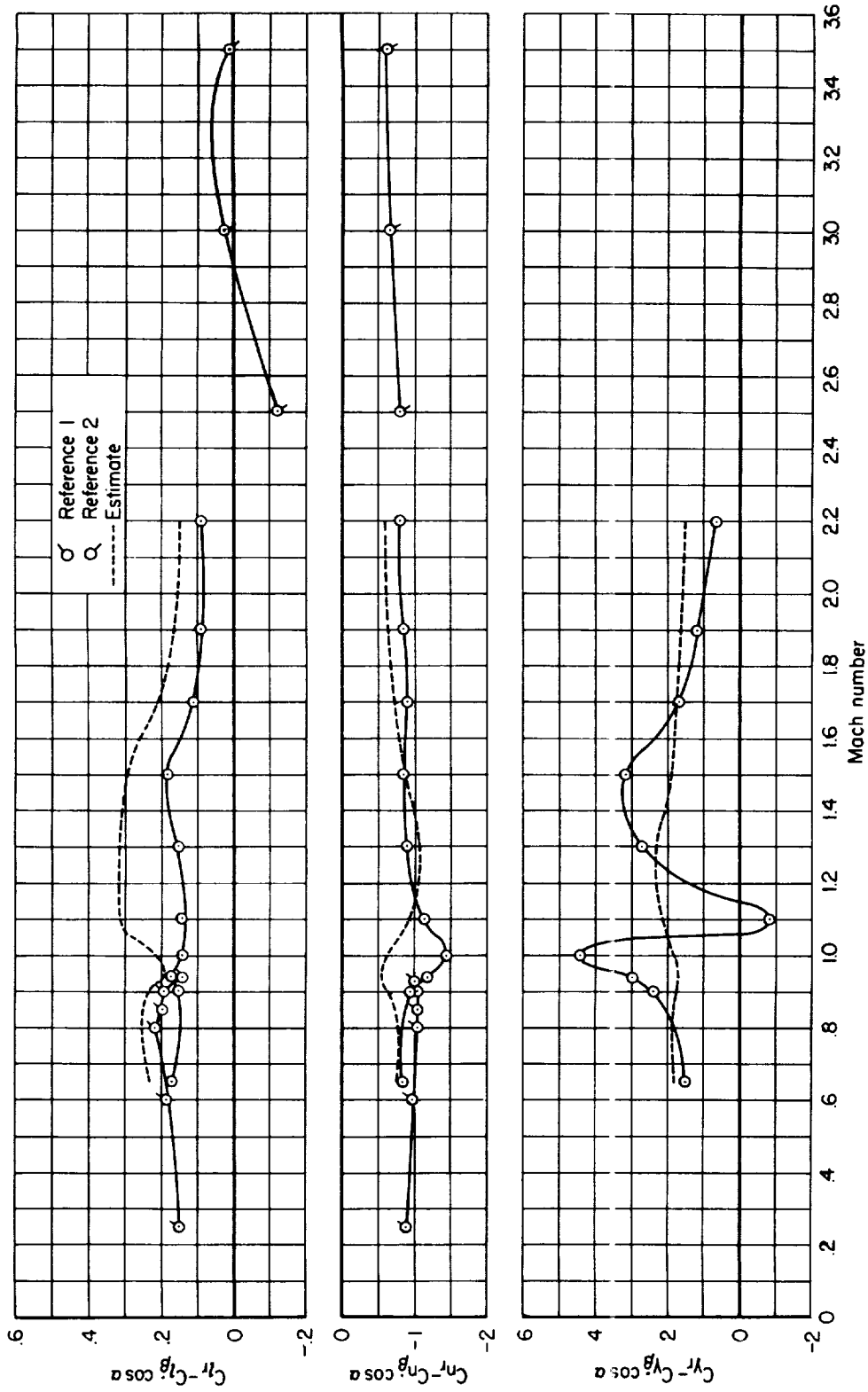

Figure 14.- The variation of $C_{l_r} - C_{l_{\dot{\beta}}} \cos \alpha$, $C_{n_r} - C_{n_{\dot{\beta}}} \cos \alpha$, $C_{Y_r} - C_{Y_{\dot{\beta}}} \cos \alpha$ with Mach number; complete configuration, $\delta = 0.1^{\circ}$, $\alpha = 0^{\circ}$.

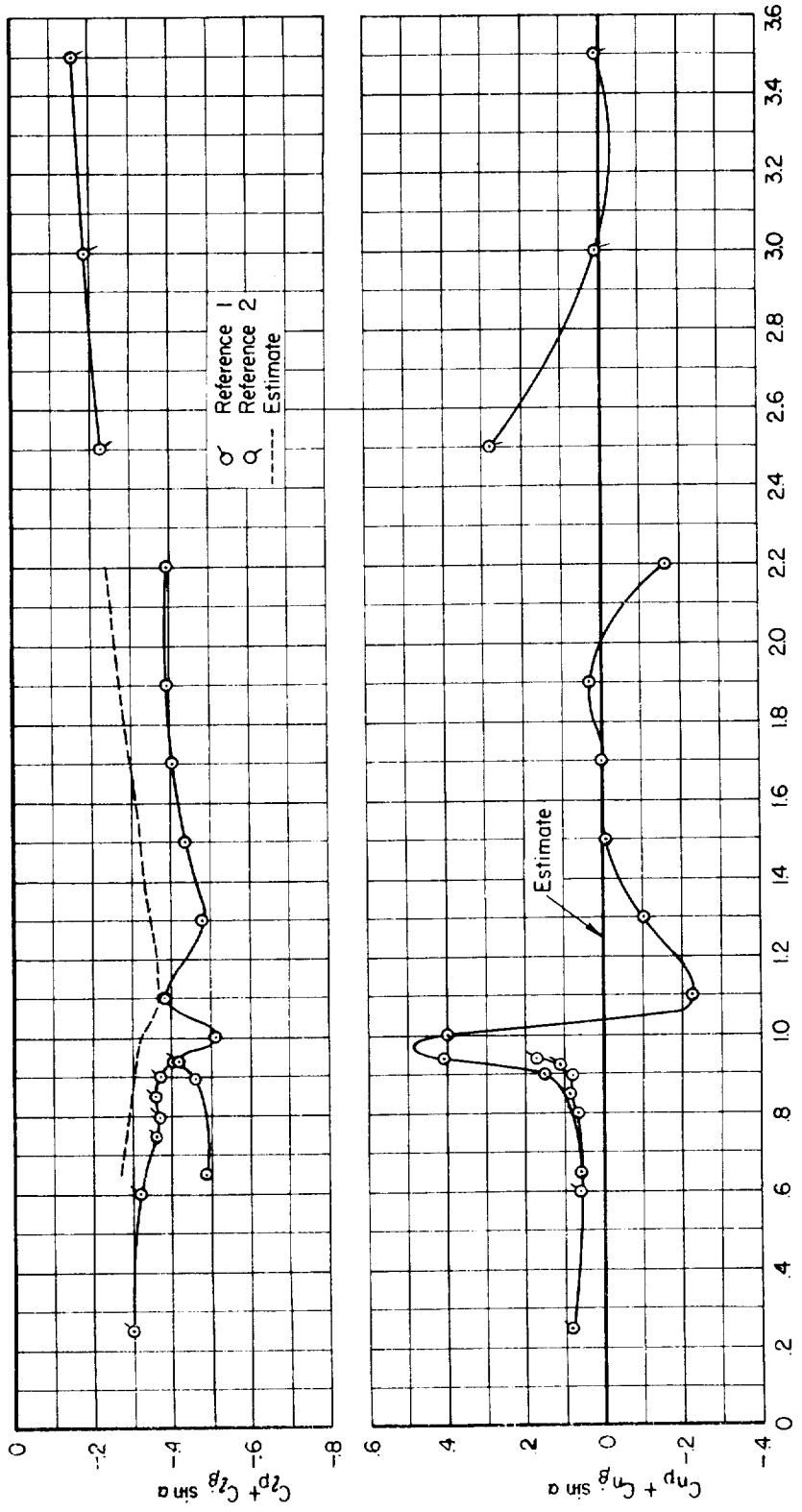

Figure 15.- The variation of $C_{l_p} + C_{l_\beta} \sin\alpha$, $C_{n_p} + C_{n_\beta} \sin\alpha$ with Mach number; complete configuration, $\delta = 0.1^\circ$, $\alpha = 0^\circ$.